

For Reference

NOT TO BE TAKEN FROM THIS ROOM

University of Alberta,
Edmonton, Alberta, Canada.

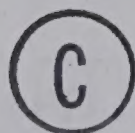
EX LIBRIS
UNIVERSITATIS
ALBERTAENSIS



THE UNIVERSITY OF ALBERTA

MEASUREMENTS OF THE LONGITUDINAL SOUND VELOCITY
IN SINGLE CRYSTALS OF SOLID HELIUM

by



RENE WANNER

A THESIS

SUBMITTED TO THE FACULTY OF GRADUATE STUDIES
IN PARTIAL FULFILMENT OF THE REQUIREMENTS FOR THE DEGREE
OF DOCTOR OF PHILOSOPHY

DEPARTMENT OF PHYSICS

EDMONTON, ALBERTA

FALL, 1970

Thesis
1970 F
87 D

UNIVERSITY OF ALBERTA

FACULTY OF GRADUATE STUDIES

Measurements of the longitudinal sound velocity v_l in hcp He^4 single crystals were made as a function of direction relative to the hexagonal axis for molar volumes between 20.3 and 17.3 cm^3/mole . The direction was determined by measuring the birefringence of the crystals along the sound path. The variation of v_l with molar volume is much stronger than predicted by theory but agrees with neutron scattering data. Agreement is also found with theoretical predictions for the anisotropy of the velocity.

The undersigned certify that they have read, and recommend to the Faculty of Graduate Studies for acceptance, a thesis entitled "MEASUREMENTS OF THE LONGITUDINAL SOUND VELOCITY IN SINGLE CRYSTALS OF SOLID HELIUM", submitted by René Wanner in partial fulfilment of the requirements for the degree of Doctor of Philosophy.

ABSTRACT

Measurements of the longitudinal sound velocity v_1 in hcp He^4 single crystals were made as a function of direction relative to the hexagonal axis for molar volumes between 20.3 and 17.3 cm^3/mole . The direction was determined by measuring the birefringence of the crystals along the sound path. The variation of v_1 with molar volume is much stronger than predicted by theory but agrees with neutron scattering data. Agreement is also found with theoretical predictions for the anisotropy of the velocity.

All five elastic constants were determined from these measurements and from published compressibility data. They are compared with existing theoretical and experimental constants for solid helium.

The temperature dependence of v_1 was measured at a molar volume of 20.42 cm^3/mole and was related to the temperature dependence of the adiabatic compressibility.

ACKNOWLEDGEMENTS

I wish to express my gratitude to my supervisor, Professor J.P. Franck for his constant encouragement and his generous and active support. Thanks are also due to Drs. C.C. Ackerman, R.A. Guyer, D.M.Lee, L.H. Nosanow, J.E. Vos, N.R. Werthamer and many other solid helium workers for discussions and preprints.

Walter Gloor and Allan O'Shea provided expert and dedicated technical help and advice, the Department of Computing Science ample computing time and Mrs. Marilyn Wahl invaluable assistance in the preparation of the thesis.

The award of a Postgraduate Scholarship of the National Research Council of Canada for the last two years is gratefully acknowledged.

I am especially thankful to my wife Anne for her understanding and cooperation.

TABLE OF CONTENTS

	Page
1. INTRODUCTION	1
2. THEORY	5
2.1 Classical lattice dynamics	6
2.2 Lattice dynamics of solid helium	9
2.3 Sound in hexagonal crystals	22
2.4 Related quantities	30
2.5 Elastic constants from unoriented single crystals in the cubic phase	36
3. EXPERIMENT	40
3.1 Low temperature apparatus	40
3.1.1 Cryostat	40
3.1.2 High pressure cell	45
3.1.3 Temperature measurements and control	50
3.1.4 High pressure gas handling system	53
3.1.5 Crystal growth	55
3.2 Optics	62
3.2.1 Birefringence	62

	Page
3.2.2 Optical apparatus	70
3.2.3 Errors in the orientation measurement	75
3.3 Ultrasonics	77
3.3.1 Electronics	77
3.3.2 Matching	80
4. RESULTS AND DISCUSSION	84
4.1 Sound velocity as a function of crystal orientation	84
4.2 Sound velocity as a function of molar volume	95
4.3 The elastic constants of solid helium	107
4.4 Sound velocity as a function of temperature	116
5. CONCLUSIONS	125
6. BIBLIOGRAPHY	127
7. APPENDIX: COMPUTER PROGRAMS	135

LIST OF TABLES

	Page
1. Birefringence of hcp He ⁴	64
2. Experimental parameters for orientation and velocity measurements	84
3. Grüneisen constants of hcp He ⁴	103
4. Ratio of the crystallographic axes c/a for hcp He ⁴	109
5. Experimental and theoretical elastic constants of hcp He ⁴	113
6. Longitudinal, transverse and second sound velocity for different orientations γ	114

LIST OF FIGURES

	Page
1. A helium atom in the Lennard-Jones potential of its nearest neighbours	13
2. Theoretical sound velocity vs. molar volume	21
3. Ground state energy vs. molar volume in bcc He ³	23
4. Velocity surface of hcp He ⁴ according to Gillis et al.	28
5. Propagation of longitudinal and transverse sound beams in hexagonal crystals (schematic)	31
6. Deviation of beam direction and deviation of polarization vector from wave normal vs. orientation γ	32
7. Transverse vs. longitudinal sound velocity in bcc He ⁴ , based on elastic constants from de Wette et al.	39
8. Pumping system	41
9. Cryostat	44
10. Sample chamber 1	46
11. Sample chamber 2	48

	Page
12. Electronic temperature regulator	51
13. High pressure gas handling system	56
14. Temperature at bottom of sample chamber vs. time for a constant growth rate of 2cm/hr.	58
15. Intensity of longitudinal sound echo under repeated temperature cycling	60
16. Birefringent plates	63
17. Ellipticity and axis direction for elliptically polarized light	66
18. Optics for the birefringence measurement	71
19. Electronics for sound velocity measurements	78
20. Sound echos in liquid and solid helium during crystal growth	82
21. Longitudinal sound velocity in hcp He ⁴ , V = 19.28 cm ³ /mole.	86
22. Longitudinal sound velocity in hcp He ⁴ , V = 20.32 cm ³ /mole.	87
23. Anisotropy of sound velocity in hcp He ⁴	88
24. Sound velocity in hcp He ⁴ , according to Lee et al.	92
25. Longitudinal sound velocity in hexagonal crystals	94

26.	Longitudinal sound velocity in hcp He ⁴ vs. molar volume	97
27.	Theoretical and experimental longitudinal sound velocity in the c-direction in hcp He ⁴	105
28.	Theoretical and experimental elastic constants of hcp He ⁴ vs. molar volume	112
29.	Ratio of specific heat at constant volume to specific heat at constant pressure vs. temperature	118
30.	Temperature dependence of sound velocity in solid helium (estimated)	122
31.	Longitudinal sound velocity in hcp He ⁴ vs. temperature	124

1. INTRODUCTION

Solid helium attracts the interest of experimental and theoretical physicist for various reasons. It can be prepared with a chemical and isotopic purity that is impossible in other substances. Its density can be doubled with modest equipment and finally some hope still persists that the spectacular behaviour of liquid helium below a temperature of 2 K would be reflected in some properties of the solid. From a theoretical point of view, the challenge consists in the complete breakdown of classical lattice dynamics when it is applied to solid helium, most drastically demonstrated by the imaginary sound velocities that classical theory predicts.

The activity shown by theorists in the past ten years to remedy the situation has unfortunately not been matched by many experiments on sound propagation. Measurement of the longitudinal sound velocity in solid He^3 and He^4 by Vignos and H. Fairbank (1961, 1966) on polycrystals gave values with a spread of 12%, indicating the presence of large crystallites or possibly single crystals and anisotropies of that order. The experiment covered a pressure range of

26 to 140 atm, but nothing definite could be concluded about the volume dependence of the velocity because the orientation of the crystals was unknown. Shortly afterwards, Lipshultz and Lee (1965) observed transverse sound in He^4 between 26 and 29 atm and found a somewhat larger anisotropy in the hexagonal phase. Longitudinal sound in bcc He^3 was also seen by Abel et al. (1961).

From the theoretical side, Nosanow and Werthamer (1965) found an anisotropy in the longitudinal velocity that was larger than the observed 12% and also a smaller volume dependence. At that time it was thought that an improved theory (Gillis et al. (1968)) would be accurate to within a few percent. A meaningful comparison with experiment requires therefore that the sound velocity is measured as a function of orientation so that it can be clearly decided whether any discrepancies are real or simply due to anisotropy.

Another incentive was provided by a theoretical paper by Guyer (1966) on sound absorption in solid helium, which led to the observation of second sound by Ackerman et al. (1966). It predicted two peaks in the sound absorption as a function of temperature, one associated with normal processes, the other with umklapp processes. To observe sound attenuation turned out to be difficult and no reproducible

results have been obtained so far (apart from the rule that the absorption increases with decreasing temperature). We found it therefore advisable to first gain more experience in ultrasonics and in preparing single crystals of solid helium. The present work should therefore be regarded as a first step in a project to measure sound absorption. Shortly after starting it, the birefringence of hexagonal close packed (hcp) He^4 was measured by Vos et al. (1967) and by Heybey and Lee (1967). This offered a convenient method of finding the orientation of helium crystals. At the same time I realized that the sound velocity in hexagonal crystals depends only on the angle between the crystallographic c-axis and the propagation direction. Therefore, one does not have to know the direction of all the crystallographic axes but only the c-direction relative to the direction of sound propagation, and this is exactly what the birefringence technique provides.

The impact of these facts led me to abandon the absorption measurements and to measure the longitudinal sound velocity as a function of orientation and later also as a function of pressure and temperature. Simultaneously but independently, the orientation dependence of both longitudinal and transverse velocity was measured by a group working under

Professor D. M. Lee at Cornell University. They grew the crystals from superfluid helium and also use the birefringence technique to find the crystal orientation (Heybey and Lee (1968), Crepeau et al. (1968), Lee et al. (1969)).

Preliminary results of our work have already been reported elsewhere (Franck (1968), Franck and Wanner (1969), Wanner and Franck (1970)).

2. THEORY

Much theoretical work has been done both on sound propagation, lattice dynamics and solid helium, so much in fact that even of the review papers only a small portion will be mentioned here.

Classical lattice dynamics is covered extensively in Born and Huang's book (1962) and by Maradudin, Montroll and Weiss (1963), but I have found Leibfried's handbook article (1955) the clearest introduction to the subject. Anharmonic effects are treated by Leibfried and Ludwig (1961). About 30 papers on lattice dynamics of solid helium have been published since 1962 and are reviewed by Werthamer (1969). I have made heavy use of this paper in the paragraph on solid helium theory. The latest review of experimental data is in Wilks book (1967) and in Keller's book (1969). An introduction to elastic constants that I have often used is the article by Huntington (1958) and the books of the series "Physical Acoustics" edited by Mason.

2.1 Classical lattice dynamics

The problem in lattice dynamics is to calculate the macroscopic elastic and thermal behaviour of a solid from the given microscopic properties of the particles from which it is formed. We will see later that this problem cannot be solved in the case of solid helium using classical mechanics alone, but since some steps are identical in a classical and a quantum mechanical treatment I will give a short outline of classical lattice dynamics, based on Ziman (1965).

To find the equations of motion of each atom we write down the kinetic energy of the whole crystal

$$T = \frac{1}{2}m \sum_{\underline{l}} \dot{\underline{u}}_{\underline{l}}^2 \quad 2.1$$

where m is the mass of one atom and $\underline{u}_{\underline{l}}$ the displacement of the atom from its equilibrium position \underline{l} . The potential energy of the crystal is expanded in terms of the cartesian components $u_{\underline{l}}^j$ of the displacements

$$V = V_0 + \sum_{\underline{l}, j} u_{\underline{l}}^j \frac{\partial V}{\partial u_{\underline{l}}^j} + \sum_{\underline{l}, \underline{l}', j, j'} u_{\underline{l}}^j u_{\underline{l}'}^{j'} \frac{\partial^2 V}{\partial u_{\underline{l}}^j \partial u_{\underline{l}'}^{j'}} + \dots \quad 2.2$$

If the approximation is terminated after the second term it is called a harmonic approximation. The equations of motion

are found using the Lagrangian formulas

$$m\ddot{u}_{\underline{l}}^j = - \sum_{\underline{l}', j'} \frac{\partial^2 V}{\partial u_{\underline{l}}^j \partial u_{\underline{l}'}^{j'}} \cdot u_{\underline{l}'}^{j'} \quad 2.3$$

or written in tensor form

$$m\ddot{u}_{\underline{l}} = - \sum_{\underline{l}'} G_{\underline{l}\underline{l}'} \cdot u_{\underline{l}'} \quad 2.4$$

where

$$G_{\underline{l}\underline{l}'}^{jj'} = \frac{\partial^2 V}{\partial u_{\underline{l}}^j \partial u_{\underline{l}'}^{j'}} \quad 2.5$$

The right hand terms are the forces acting on atom \underline{l} due to the displacement of atom \underline{l}' and can be evaluated if the potential between these atoms is given as was assumed in the beginning. They clearly depend only on the relative position $\underline{h} = \underline{l} - \underline{l}'$ of these atoms.

The periodicity of the lattice reduces the number of equations and restricts the solutions to waves because Bloch's theorem relates the motion of the atoms at different sites

$$u_{\underline{l}} = u_{\underline{l}'} e^{i\mathbf{q}\cdot\mathbf{h}} \quad 2.6$$

\underline{q} is the wave vector of a particular solution of the equations of motion. The equation of motion for that particular solution and a particular atom is then

$$m\ddot{\underline{u}}(\underline{q}) = \left(\sum_{\underline{h}} G(\underline{h}) e^{i\underline{q}\cdot\underline{h}} \right) \underline{u}(\underline{q}) \equiv G(\underline{q}) \underline{u}(\underline{q}) \quad 2.7$$

$G(\underline{q})$ is called the dynamical matrix and is simply the Fourier transform of the force constant tensor $G(\underline{h})$. To solve that equation, we try a solution of the form

$$\underline{u}(\underline{q}) = \underline{u}_0 e^{i\omega t} \quad 2.8$$

plug it into 2.7 and get 3 simultaneous equations for the components u_0^j (depending on the wave vector \underline{q})

$$\sum_{j=1}^3 (G^{jj'}(\underline{q}) - \omega^2 m \delta_{jj'}) u_0^{j'}(\underline{q}) = 0 \quad 2.9$$

The secular equation (that is the condition that the determinant of the system of equations is zero) will give 3 solutions for $\omega(\underline{q})$, corresponding to the three different polarizations of the waves.

In principle then, this is the recipe for calculating sound velocities from interparticle potentials: First write down the tensor $G(\underline{h})$, involving the second derivative of the

interparticle potentials of as many neighbours as is necessary. Next calculate the Fourier transform $G(\mathbf{q})$ for that wave vector \mathbf{q} for which the sound velocity is desired. The secular determinant of that matrix gives a cubic equation for the frequency ω . The sound velocity for the wave in the direction \mathbf{q} is $v = \omega / |\mathbf{q}|$.

It is customary to restrict the use of the word "sound" to the limiting case $\mathbf{q} \rightarrow 0$, that is to long wavelengths (long compared with the lattice spacing) and to speak of phonons for general \mathbf{q} . The elements of the dynamical matrix in the long wave length limit are intimately related to the elastic constants c_{ik} (see equation 2.28).

2.2 Lattice dynamics of solid helium

The classical theory of lattice dynamics fails dramatically for solid helium. Using a Lennard-Jones potential

$$V(r) = 4\epsilon \left((\sigma/r)^{12} - (\sigma/r)^6 \right) \quad 2.10$$

for the attraction between two He atoms with parameters ϵ and σ derived from measured virial coefficients of helium gas it predicts a molar volume of 10 cm^3 which is too small by a factor 2, a compressibility too small by a factor 30 and sound

velocities too high by a factor 4 if compared to experimental values at $T = 0\text{K}$ and at $p = 26\text{ bar}$, the minimum pressure required to solidify He^4 .

An attempt by de Wette and Nijboer (1965) to calculate the phonon frequencies classically yielded imaginary frequencies and sound velocities for volumes larger than $12\text{ cm}^3/\text{mole}$, although the lattice is stable for volumes up to $21\text{ cm}^3/\text{mole}$.

The reason for this unusual behaviour is that the helium atoms have a large kinetic energy from the zero-point motion, an energy comparable or larger than the potential energy which has only a very shallow attractive well due to the tightly bound electronic shell. This zero-point energy can be estimated using the uncertainty principle. Confining an atom to its lattice site will define its position with an uncertainty of the order of the lattice constant a which will lead to an uncertainty in momentum and thereby to a kinetic energy per atom of

$$\frac{E_z}{2} \approx \frac{(\Delta p)^2}{2m} \approx \frac{\hbar^2}{2ma^2} \quad . \quad 2.11$$

Because of that motion the atom will no longer be at the minimum of the potential well and the lattice will expand to such an extent that helium solidifies only under pressure, even at 0 K .

Using these arguments F. London (1954) has calculated the molar volume of the solid at 0 K and found agreement to within 15% of the measured value and his simple theory reproduces the volume dependence of the groundstate energy or the compressibility remarkably well.

A more detailed theory of solid helium faces a number of problems. Because of the large vibration amplitudes the forces on an atom will be highly anharmonic. Figure 1 shows a He atom in the potential of its two nearest neighbours in a simple, one dimensional model. Instead of being at a minimum, the central atom sits at a maximum and assumed vibrations around this position will be unstable since the second derivative of the potential is negative and the vibration frequencies therefore imaginary. This is the explanation for the imaginary phonon frequencies obtained by de Wette and Nijboer (1965). The problem is therefore that the anharmonic terms are so large that the quasi harmonic approximation does not exist any longer.

How to introduce into the theory the correlation between the movement of neighbouring atoms, the so-called short-range or dynamic correlations poses another question: One might expect that the large amplitude vibration of the atom would lead to many collisions between neighbouring atoms,

involving the strong hardcore repulsion, but in fact the atoms will correlate their movements to avoid such collisions. Nosanow (1966) points out that correlation lowers both the kinetic energy by increasing the radius of the effective potential well and the potential energy by increasing the probability that two particles are at a distance r_{\min} corresponding to the minimum in the Lennard-Jones potential.

Finally, if the theory is formulated in terms of phonons it is not obvious a priori whether the large anharmonicity will not lead to unreasonably short phonon lifetimes, that is whether phonons do exist in solid helium or not (Gillis and Werthamer (1968)).

Two different approaches have been tried to deal with these problems. One is formulated in terms of single particle wave functions while the other describes the crystal in terms of phonons.

The basic idea of the single particle picture (Nosanow (1964), Fredkin and Werthamer (1965)) is to do a time dependent Hartree calculation assuming a trial wave function of the so called Jastrow form (Jastrow (1955))

$$\Psi(r_1 \dots r_n) = \prod_i \phi_0(r_i - l_i) \prod_{j,k} f(r_j - r_k) \quad 2.12$$

FIGURE 1

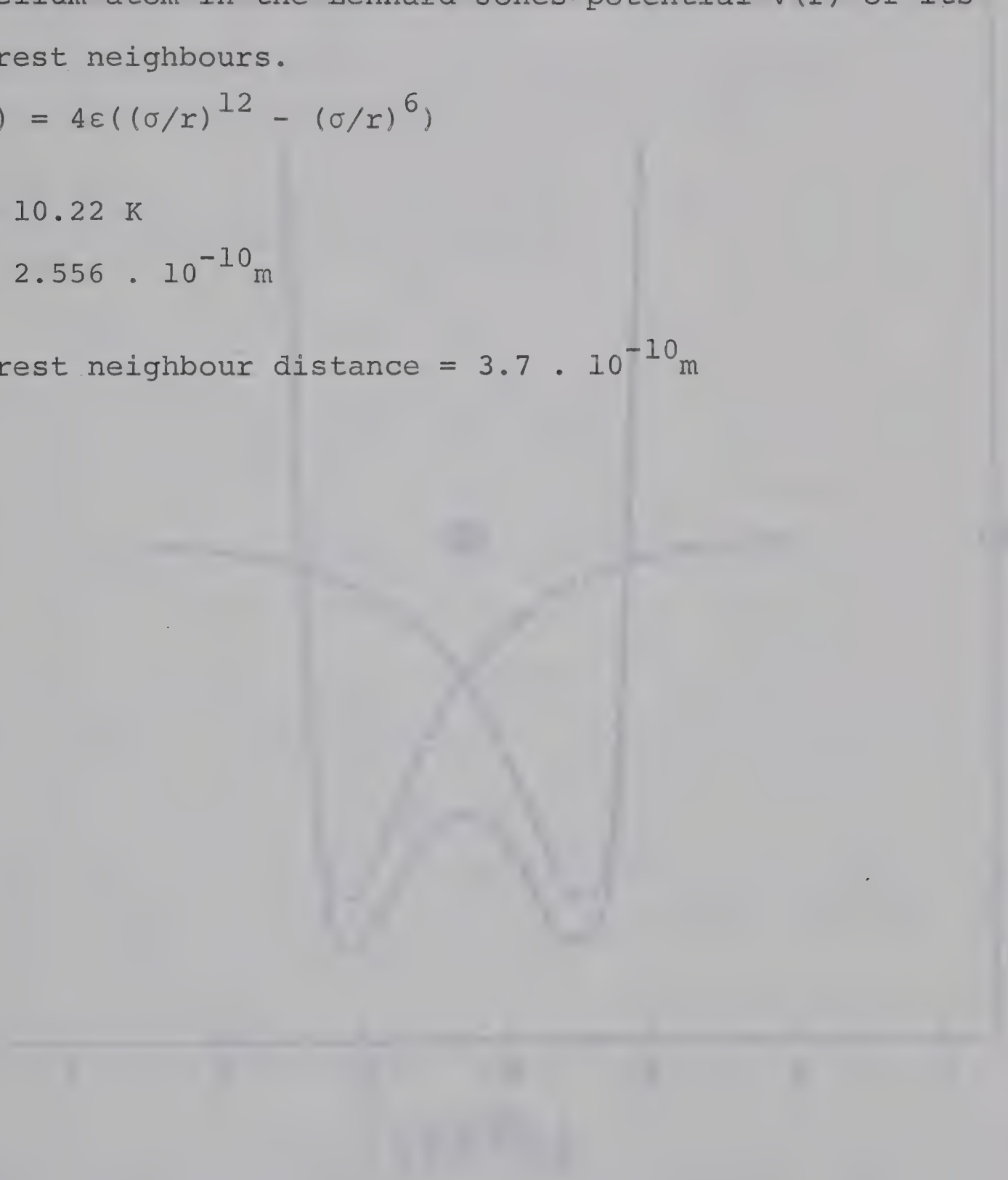
A helium atom in the Lennard-Jones potential $V(r)$ of its nearest neighbours.

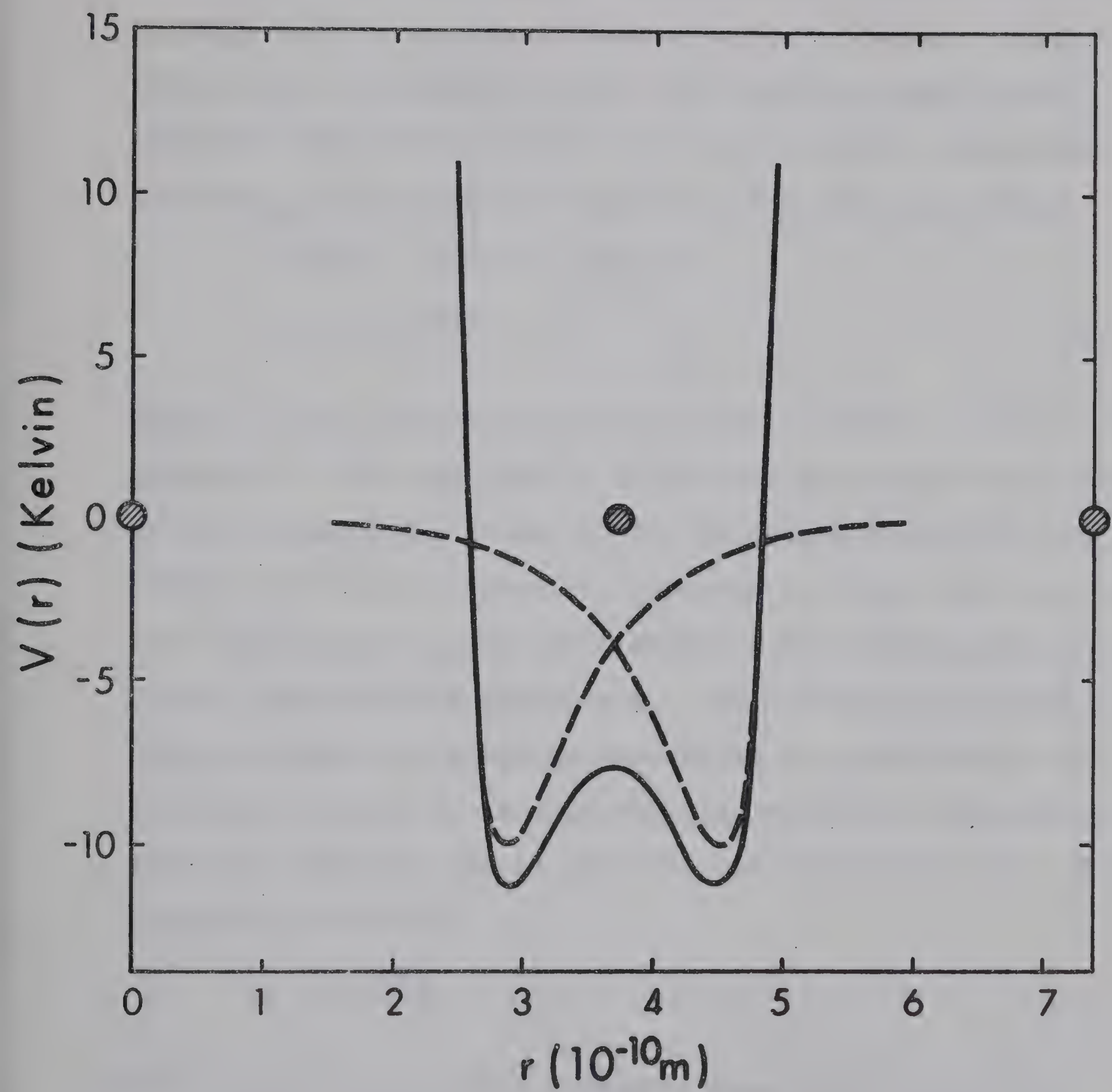
$$V(r) = 4\epsilon((\sigma/r)^{12} - (\sigma/r)^6)$$

$$\epsilon = 10.22 \text{ K}$$

$$\sigma = 2.556 \cdot 10^{-10} \text{ m}$$

$$\text{Nearest neighbour distance} = 3.7 \cdot 10^{-10} \text{ m}$$





The ϕ_0 are single particle wave functions localized around the lattice sites l_i while $f(r_j - r_k)$ describes the correlations between particle j and k . The correlation function $f(r)$ should go to zero for r smaller than the hardcore radius, thereby decreasing the probability that two particles come closer together and should be unity for large particle separation because ϕ_0 will not be influenced by far away particles.

A useful analytic form is

$$f(r) = e^{-KV(r)} \quad 2.13$$

where $V(r)$ is the Lennard-Jones potential and K a variational parameter. The next step is to express the expectation value of the ground state energy E_0 for an assumed value of K in terms of a cluster expansion, truncate it after the first term and then minimize E_0 to get a differential equation for the single particle wave function ϕ_0 . This equation is solved and the ground state energy calculated as a function of K . It turns out that ϕ_0 is approximated well by a spherically symmetric Gaussian (as is the case for the ground state of the harmonic oscillator)

$$\phi_0 = e^{-Ar^2/2} \quad 2.14$$

where A is a variational parameter that minimizes E_0 for a

given K . Finally, the ground state energy is minimized by varying K . The whole procedure is formally equivalent to a Hartree calculation with no correlations in which the Lennard-Jones potential is replaced by an effective potential

$$V_{\text{eff}}(r) = [V(r) + \frac{\hbar^2 K}{m} \cdot \nabla^2 V(r)] \cdot e^{-2KV(r)} \quad 2.15$$

This effective potential has a softer core than the Lennard-Jones potential. Using manybody techniques, Fredkin and Werthamer (1965) have shown how to calculate the phonon frequencies from these single particle excitations. They find for the eigenvalue equation at $T = 0$ K

$$m\omega^2 \cdot \underline{u}(\underline{q}) = \sum_{\underline{h}} (1 - e^{-i\underline{q}\underline{h}}) \frac{\partial^2}{\partial \underline{u}_1 \partial \underline{u}_1'} \langle 0 | V_{\text{eff}}(\underline{r} - \underline{r}' + \underline{h}) | 0 \rangle \underline{u}(\underline{q}) \quad 2.16$$

The above equation is very similar to the eigenvalue equation 2.9 of classical lattice dynamics with the exception that the interparticle potential has been replaced by an average with respect to the mean position probability of the two particles

$$\langle 0 | V_{\text{eff}} | 0 \rangle. \quad 2.17$$

From here on the equations of classical lattice dynamics (Leibfried and Ludwig 1961) apply. This is also a plausible

theoretical explanation why helium is in many respects a solid like any other which has long been established experimentally.

The single particle picture has been refined in various ways but all numerical calculations were done for the bcc structure only. Hetherington et al (1967) extended the cluster expansion to include 3-body terms. They find that the expansion converges indeed sufficiently fast for a correlation of the form 2.13. Another expansion given by Brueckner and Froberg (1965) however seems to converge less well. The ground state energy was also computed by Hansen and Levesque (1965) with a Monte Carlo Method using a different correlation function. Etters (1968) considers the dynamical behaviour of a pair of particles in the averaged field of all other particles.

Another improvement especially in the volume dependence of the calculated quantities is expected from a better correlation function f . The usefulness of the particular choice 2.13 for f is mainly in the rapid convergence of the cluster expansion. Brueckner and Froberg (1965) and recently Mullin et al. (1969) have tried different correlation functions obtained by numerically solving a differential equation for f . To find a better correlation function is difficult because the cluster expansion converges only for a restricted class of

functions f and not all variational parameters are suitable variational parameters. Massey and Woo (1968) use an effective potential V_{eff} that includes liquid like correlations while in Meissners formulation (1968a, 1968b) both long and short range correlations are included. No numerical results have yet been published for sound velocities in hcp helium based on these improved correlation functions.

The theories mentioned so far emphasize the single particle aspect of the problem and the phonons are constructed from the normal modes of response of the crystal to an externally applied disturbance.

The so-called self consistent phonon theories (Hooton (1958), Boccara and Sarma (1965), Ranninger (1965), Koehler (1967, 1968), Choquard (1967)) consider the phonons as the basic coordinates for describing the crystal (thereby assuming that they exist in solid helium) and describe the motion of the individual atoms through the occupation number of the different phonon modes. While the two different approaches give similar results (Koehler (1967)) at $T = 0$ K, the collective theories seem to be more suitable for numerical calculations. In Koehlers work, this was achieved by expanding the crystal potential in Hermite polynomials (being the eigenfunctions of the harmonic oscillator) instead of a Taylor series.

The idea underlying the collective theories is the following (Koehler (1968)):

The true crystal Hamiltonian H_c

$$H_c = - \frac{\hbar^2}{2m} \sum_i \nabla_i^2 + \sum_{ij} V_{ij} \quad 2.18$$

is approximated by a harmonic Hamiltonian H_h

$$H_h = - \frac{\hbar^2}{2m} \sum_i \nabla_i^2 + V_0 + \frac{1}{2} \sum_{\underline{1}\underline{1}'} u_{\underline{1}}^j G_{\underline{1}\underline{1}'}^{jj'} u_{\underline{1}'}^{j'} \quad 2.19$$

where the entire set of spring constants G is to be determined variationally. Koehler finds that the choice of G that minimizes the energy is

$$G_{\underline{1}\underline{1}'}^{jj'} = \langle 0 | \nabla_{\underline{1}}^j \nabla_{\underline{1}'}^{j'} | 0 \rangle \quad 2.20$$

and that the ground state eigenfunction of the harmonic Hamiltonian is

$$|0\rangle = \exp\left(-\frac{1}{2} \sum_{\underline{1}\underline{1}'} u_{\underline{1}}^j F_{\underline{1}\underline{1}'}^{jj'} u_{\underline{1}'}^{j'}\right) \quad 2.21$$

where

$$F^2 = (m/\hbar^2) \cdot G \quad 2.22$$

The similarity with the single particle picture is apparent and the main difference is that instead of averaging with

respect to single particle distributions, the average is here with respect to the phonon groundstate. The theory is self-consistent because the spring constants G depend on the eigenfunctions $|0\rangle$ which in turn depend on G .

As in the single particle theory, a Jastrow factor has to be introduced to deal with correlations.

Horner (1967) uses a diagrammatic technique which in lowest order is equivalent to the selfconsistent phonon-approximation and also includes finite lifetime corrections, which affect the sound velocity via the Kramers-Kronig relations. This effect is also included in the papers by Ranninger (1965), Choquard (1967) and Werthamer (1967).

Unfortunately, only two papers (Nosanow and Werthamer (1965), Gillis, Koehler and Werthamer (1968)) contain numerical values for sound velocities in hcp He^4 . Nosanow and Werthamer's (1965) calculation is based on a single particle theory with a Jastrow factor of the form 2.13 and a Lennard-Jones inter-particle potential with $\epsilon = 10.22$ K and $\sigma = 2.556$ Å. The cluster expansion of the groundstate energy is truncated after the two body terms and the energy estimated to be accurate within a few percent.

Within the framework of the selfconsistent phonon theory Gillis, Koehler and Werthamer (1968) have calculated the

phononspectrum at two different densities and the sound velocities at the density of $19.2\text{cm}^3/\text{mole}$, using the same data for the interparticle potential and the same Jastrow-factor as Nosanow and Werthamer. The internal energy is lowered by about 17 cal/mole in comparison with values given by the single particle theory (Nosanow(1966), Hetherington et al.(1967)).

Figure 2 shows the two theoretical results for the sound velocities in different crystal directions. They will be compared with experimental data in sections 4.1 to 4.3.

Sound propagation in hexagonal crystals will be discussed in section 2.3 and the elastic constants obtained from the data of Gillis et al.will be used as an example to illustrate the concepts.

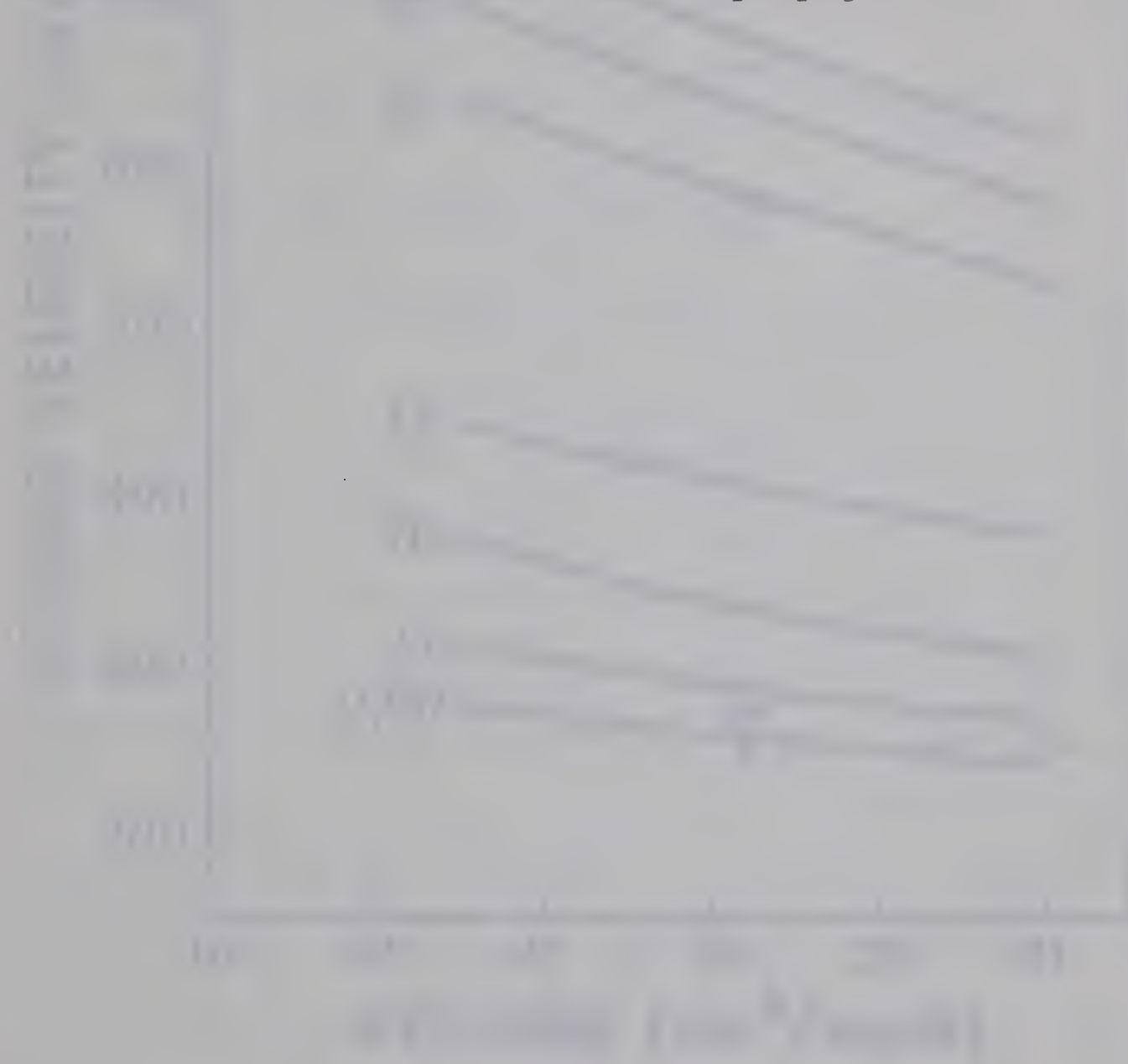
In order to give an impression of the performance of the other theories I show in figure 3 the internal energy E_0 at absolute zero for bcc He^3 for which most numerical calculations have been done. The reason for this is that the cubic structure is simpler than the hexagonal, and only in He^3 does this structure exist at absolute zero and over a sizable volume range. The experimental points are from Pandorf and Edwards (1968).

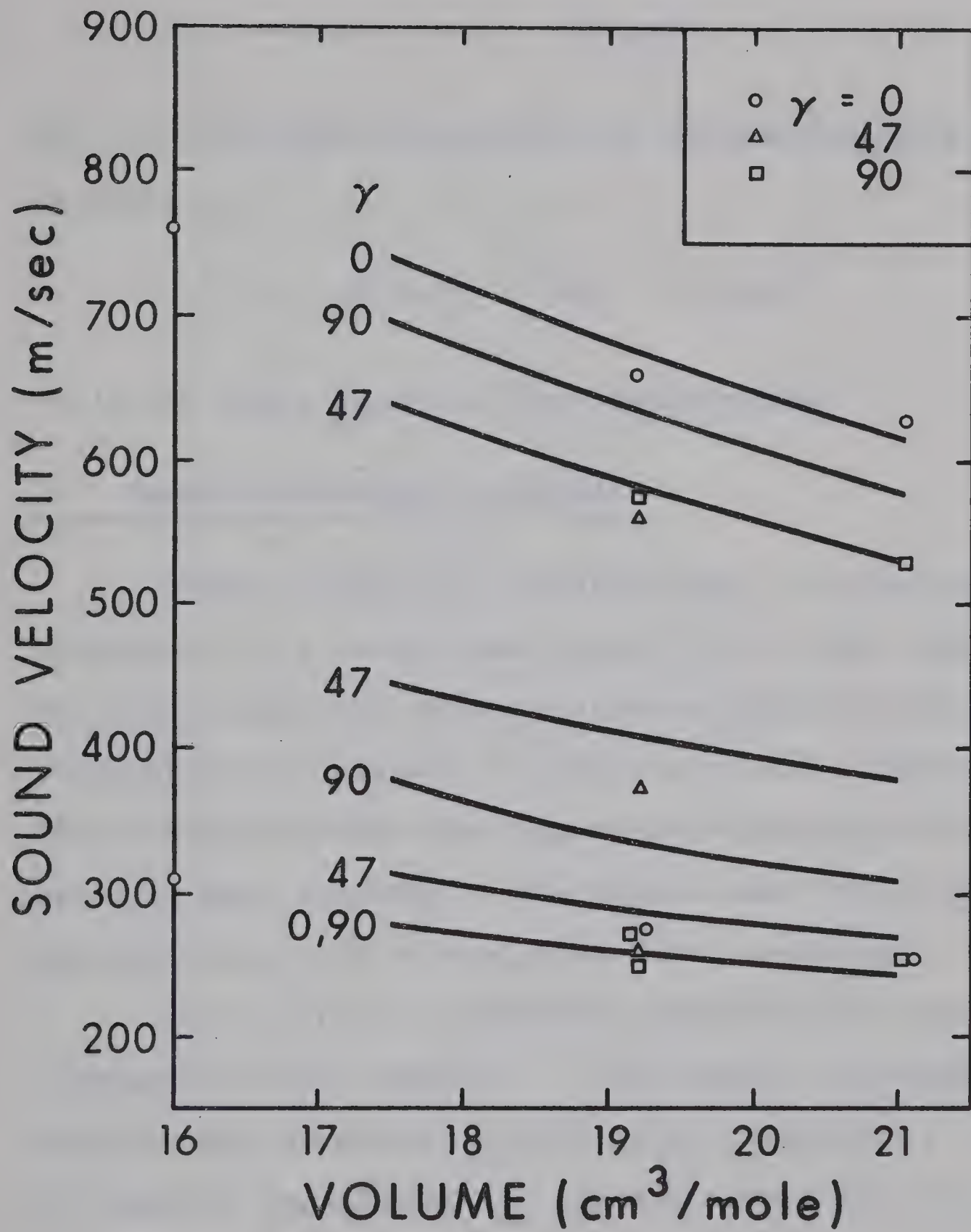
From $E_0(V)$ we obtain the pressure p

$$p = -dE_0/dV$$

FIGURE 2

Theoretical sound velocity vs. molar volume, according to Nosanow and Werthamer (1965) (solid lines), and Gillis et al. (1968) (circles, triangles and squares). γ is the angle between c-axis and direction of propagation.





the Bulk modulus B

$$B = -V dp/dV = V \cdot d^2 E_0 / dV^2 \quad 2.24$$

and an approximate expression for the longitudinal sound velocity v_e

$$v_1^2 \approx B \cdot V/M = (V^2/M) \cdot d^2 E_0 / dV^2 \quad 2.25$$

(V is the molar volume, M the atomic weight).

2.3 Sound in hexagonal crystals

Before measuring the anisotropy of the sound velocities in a crystal one would like to know something in principle about the velocity surface which consists of the three surfaces obtained by plotting in each direction the longitudinal and the two transverse velocities. They must have the same symmetry as the crystal and I will show that in addition they have to meet some other conditions.

The surface is described completely by the elastic constants and the density. The elastic constants c_{ijkl} describe the stresses σ_{ij} in various directions in the crystal in terms of the strains ϵ_{kl} applied in various other directions:

$$\sigma_{ij} = \sum_{k,l} c_{ijkl} \cdot \epsilon_{kl} \quad 2.26$$

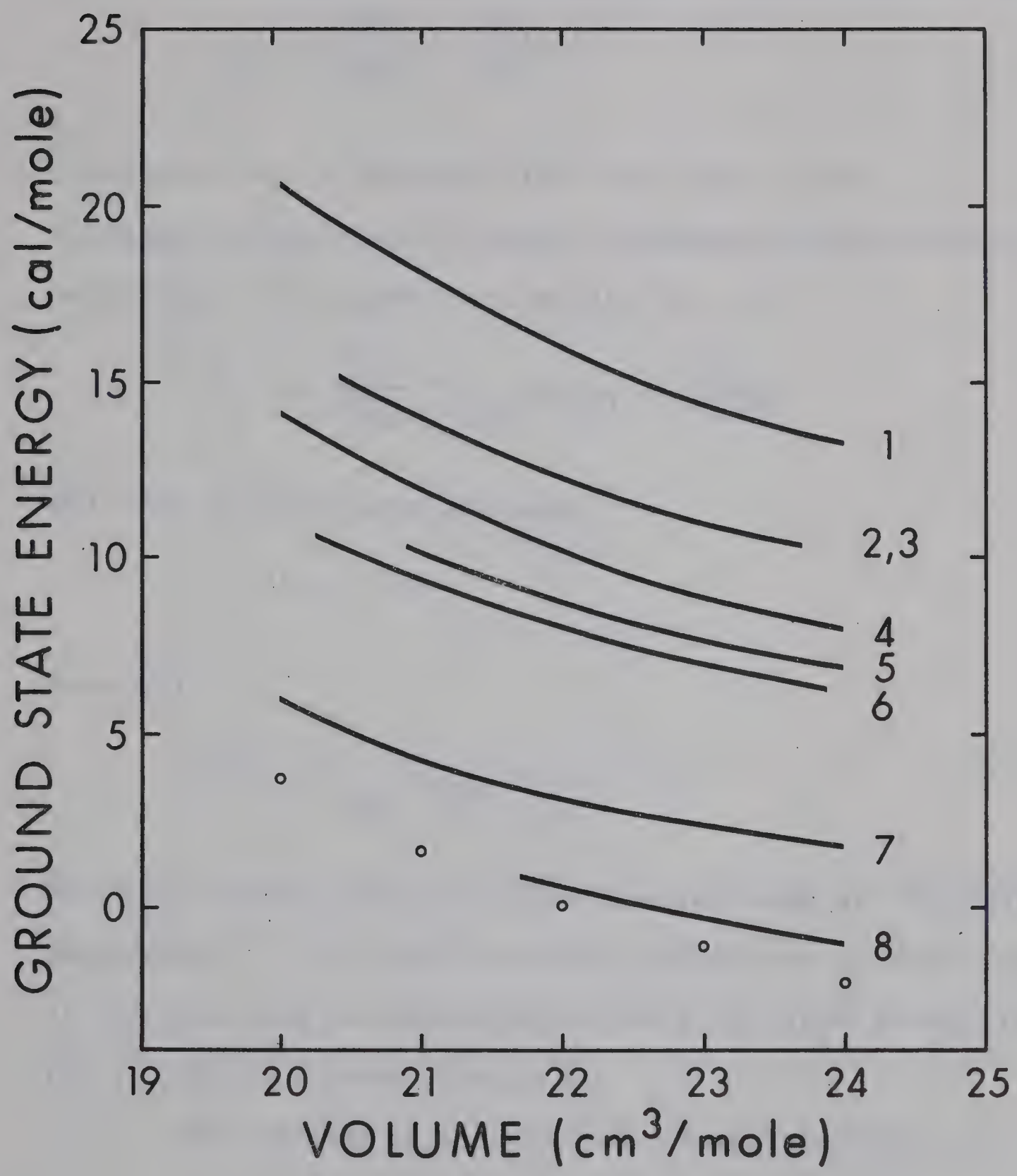
FIGURE 3

Ground state energy E_0 vs. molar volume V in bcc He^3

The curves represent calculations by

1. London (1954, p. 24)
2. Nosanow (1966)
3. Hetherington et al. (1967)
4. Mullin et al. (1969)
5. Horner (1967)
6. Koehler (1967)
7. Hansen and Levesque (1968)
8. Iwamoto and Namaizawa (1966)

The circles are measurements by Pandorf and Edwards (1968).



σ_{ij} is the force acting on plane i in direction j and the strain ϵ_{kl} is defined in terms of the displacement \bar{u} as

$$\epsilon_{kl} = \frac{1}{2} \left(\frac{du_k}{dx_l} + \frac{du_l}{dx_k} \right) \quad 2.27$$

Equation 2.26 is nothing else than Hook's law.

Knowing the forces on a small elementary cube allows us to write down the equation of motion for it

$$\rho \ddot{u}_i = \sum_j \frac{d\sigma_{ij}}{dx_j} = \sum_{jkl} c_{ijkl} \cdot \frac{d^2 u_k}{dx_j dx_l} \quad 2.28$$

This has a plane wave solution

$$\underline{u} e^{i(\underline{q} \cdot \underline{r} - \omega t)} \quad 2.29$$

from which

$$\rho \omega^2 u_i = \sum_{jlk} c_{ijkl} q_j q_l \cdot u_k \quad 2.30$$

which is nothing else than the leading term in the Fourier expansion 2.7. To get the sound velocities we then proceed in the same way as before by solving the secular equation for the desired wave vectors \underline{q} .

The number of independent elastic constants is greatly

reduced using symmetry and thermodynamic arguments and only 5 remain for hexagonal crystals namely c_{11} , c_{12} , c_{13} , c_{33} and c_{44} (we have used the shorted notation of Voigt $c_{1111} = c_{11}$, $c_{1122} = c_{12}$, $c_{1133} = c_{13}$, $c_{3333} = c_{33}$, $c_{2323} = c_{44}$) and the matrix c_{ik} for hexagonal symmetry is

$$c_{ik} = \begin{vmatrix} c_{11} & c_{12} & c_{13} & 0 & 0 & 0 \\ c_{12} & c_{11} & c_{13} & 0 & 0 & 0 \\ c_{13} & c_{13} & c_{33} & 0 & 0 & 0 \\ 0 & 0 & 0 & c_{44} & 0 & 0 \\ 0 & 0 & 0 & 0 & c_{44} & 0 \\ 0 & 0 & 0 & 0 & 0 & \frac{1}{2}(c_{11}-c_{12}) \end{vmatrix} \quad 2.31$$

Several authors (Zener (1936), Gold (1950), Musgrave (1954)) have explicitly solved the secular equation for hexagonal crystals and find that for this symmetry (and no other) the cubic equation factors into a quadratic and a linear equation for all directions and the sound velocity can therefore be expressed explicitly as a function of the direction cosines of the wave vector \underline{q} . Another result which is of decisive importance for the design of the experiment is that the velocity surface has a cylindrical symmetry around the

c-axis, which means that the sound velocities depend only on the angle γ between wave vector and c-axis.

The expressions for the sound velocities are:

$$\begin{aligned} v_1 &= (c_1/\rho)^{\frac{1}{2}} \\ v_{t_1} &= (c_{t_1}/\rho)^{\frac{1}{2}} \\ v_{t_2} &= (c_{t_2}/\rho)^{\frac{1}{2}} \end{aligned} \quad 2.32$$

with

$$\begin{aligned} c_1 &= \frac{1}{2}[(c_{11} + c_{44}) \sin^2 \gamma + (c_{33} + c_{44}) \cos^2 \gamma + \phi(\gamma)] \\ c_{t_1} &= \frac{1}{2}(c_{11} - c_{12}) \sin^2 \gamma + c_{44} \cos^2 \gamma \\ c_{t_2} &= \frac{1}{2}[(c_{11} + c_{44}) \sin^2 \gamma + (c_{33} + c_{44}) \cos^2 \gamma - \phi(\gamma)] \\ \phi^2 &= (c_{11} - c_{44})^2 \sin^4 \gamma + (c_{33} - c_{44})^2 \cos^4 \gamma + \\ &+ 2 \sin^2 \gamma \cos^2 \gamma [(c_{11} - c_{44})(c_{44} - c_{33}) + 2(c_{13} + c_{44})^2] \end{aligned} \quad 2.33$$

For propagation along the c-axis ($\gamma = 0$)

$$c_1 = c_{33}$$

$$c_{t_1} = c_{t_2} = c_{44}$$

and for propagation in the basal plane ($\gamma = 90^\circ$)

$$c_l = c_{11}$$

$$c_{t_1} = \frac{1}{2}(c_{11} - c_{12})$$

$$c_{t_2} = c_{44}$$

A computer program for calculating velocities from elastic constants is found in the appendix.

If the sound velocities are known as a function of the angle γ , the elastic constants of the solid can be calculated. The most convenient set of values are the velocities along the c-axis, perpendicular to the c-axis and for a direction in between (which is necessary to obtain c_{13}).

A section through a velocity surface based on theoretical sound velocities published by Gillis et al. (1968) is shown in figure 4. The corresponding elastic constants are given in section 4.3.

Some peculiarities about sound propagation in crystals are worth mentioning here. One of them is that in general the direction of propagation of a sound beam does not coincide with the wave normal so that we have the situation shown in figure 5. The formula for the angle Δ_i between beam direction

FIGURE 4

Velocity surface of hcp He^4 according to Gillis et al. (1968)



c - axis

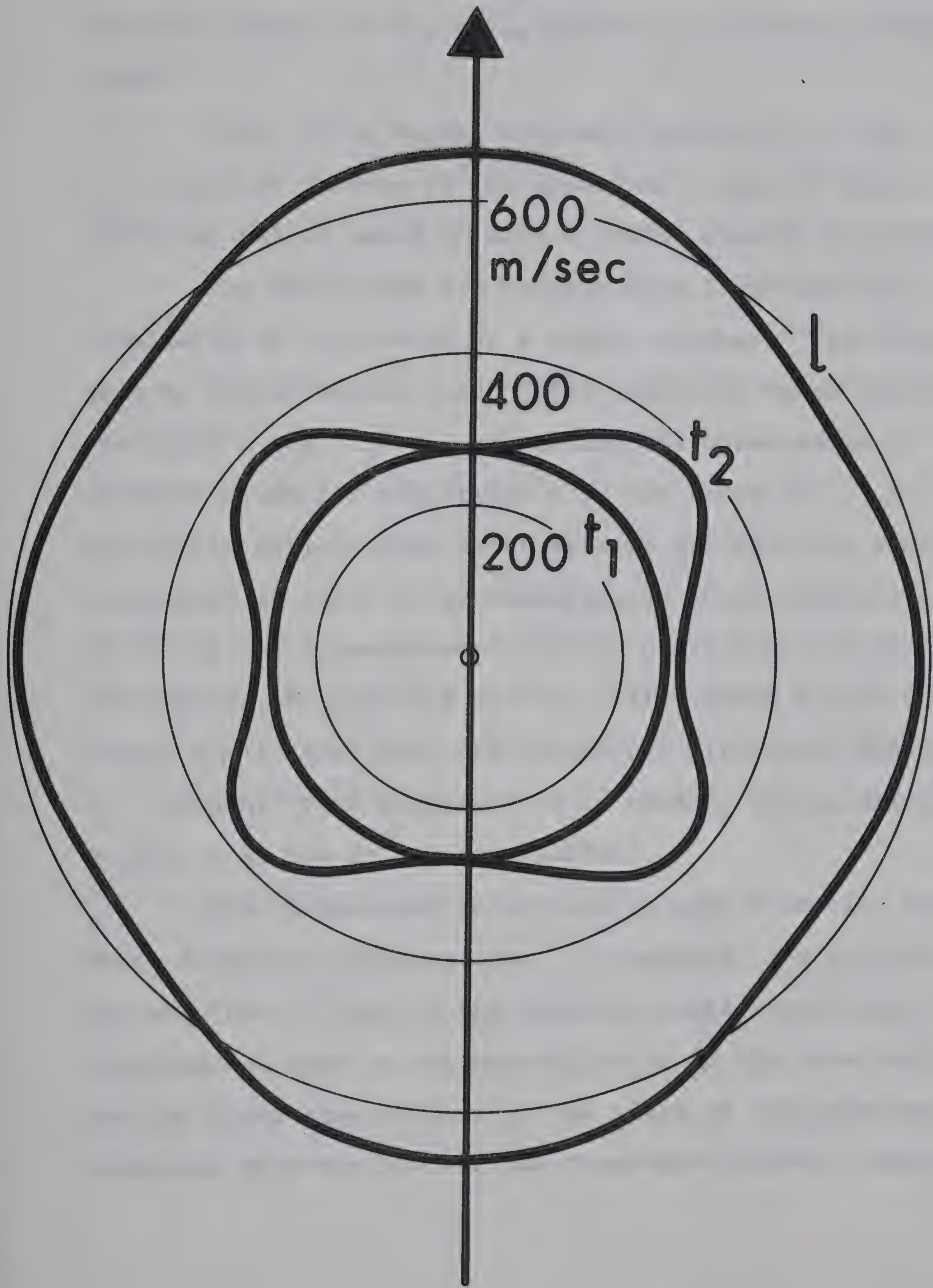
600
m/sec

400

200 t_1

t_2

l



and wave normal for the polarization i is given by Musgrave (1954).

Since it is rather lengthy I present it in the form of a computer program in the appendix. Figure 6 shows numerical values based on Gillis (1968) elastic constants.

The deviations are surprisingly large and have to be considered in the design of a sample chamber. The chamber used by Vignos and Fairbank (1966) cuts off beams completely for which $\Delta \geq 10^\circ$ thereby preventing the observation of longitudinal sound for directions γ in the range $20 \dots 45^\circ$. This may partly explain that their data do not show the same large anisotropy as found in my measurements where deviations Δ up to 30° can be accommodated. Similar considerations apply to the chamber of Lipshultz and Lee (1965) which allows a deviation $\Delta \leq 16^\circ$ that cuts off almost all directions for the t_2 - branch. This property can be used to obtain elastic constants in bcc He^3 (Wanner (1970)).

The three sound velocities in each direction have three different polarizations. In general, the polarizations are not "pure", that is the particle displacement for the longitudinal mode is not perpendicular to the wavefront, nor are the transverse motions in the plane of the wavefront. In hexagonal crystals however one transverse branch (usually

labelled t_1) is always pure due to the rotational symmetry of the velocity surface. Its polarization is perpendicular to the c-axis and the propagation vector and it usually has the lowest anisotropy of all branches. The other transverse branch t_2 and the longitudinal branch l deviate by an angle δ (figure 6) but the 3 polarization vectors are mutually perpendicular.

The motion of a transducer surface will therefore be split into 3 components, and the transducer will in general excite all three branches with an amplitude proportional to the corresponding component along the polarization vector.

It is difficult to observe the transverse components when exciting with a longitudinal transducer because the first transverse echos often coincide with the second longitudinal, but longitudinal sound coming from transverse transducers has occasionally been seen both by us and Lee et al (1969).

2.4 Related Quantities

If the transverse and longitudinal velocities are known for a sufficient number of directions, the elastic constants can be determined. From known elastic constants several other quantities such as the Debye temperature θ_0

FIGURE 5

Propagation of longitudinal and transverse sound beams in hexagonal crystals (schematic).



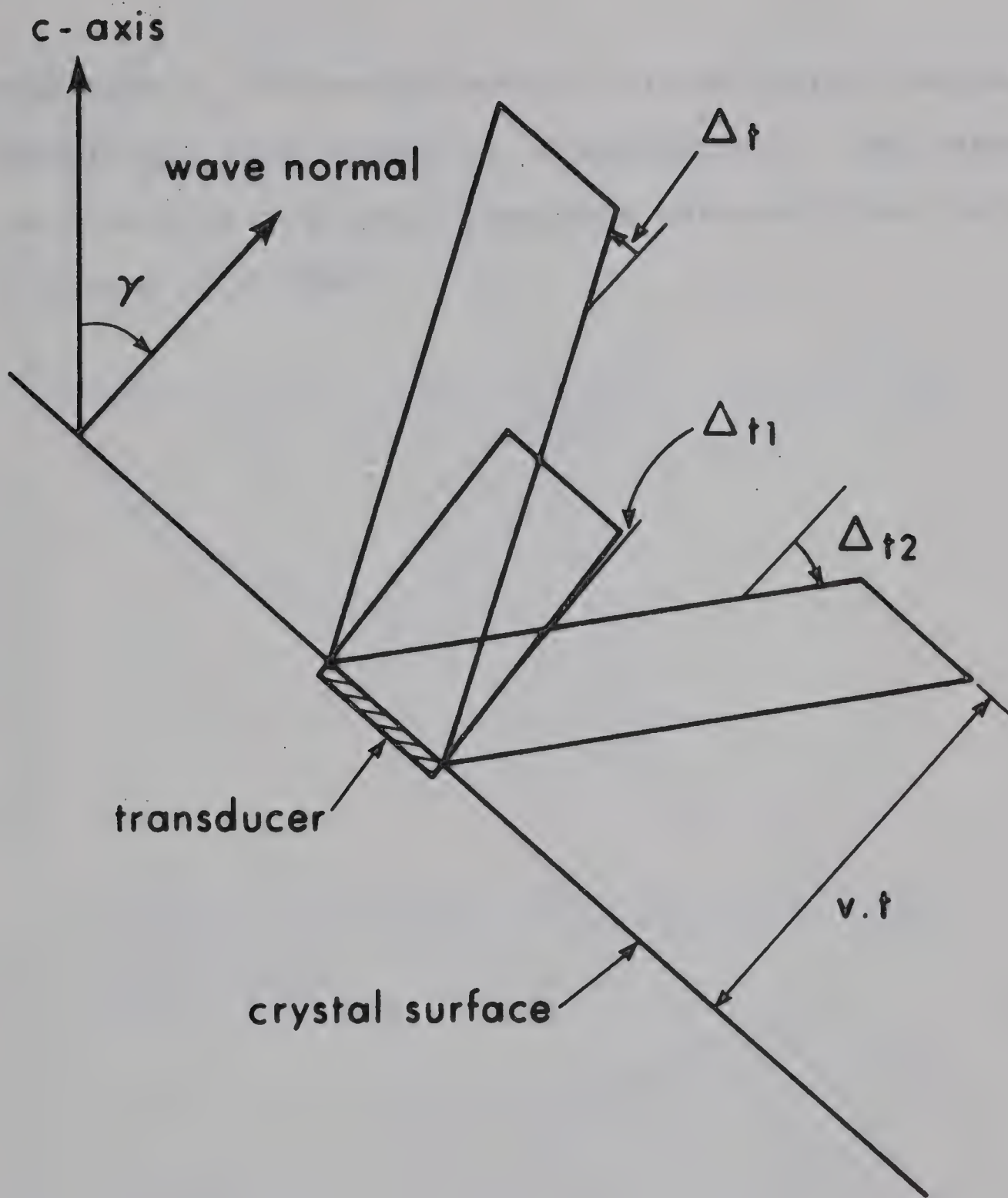
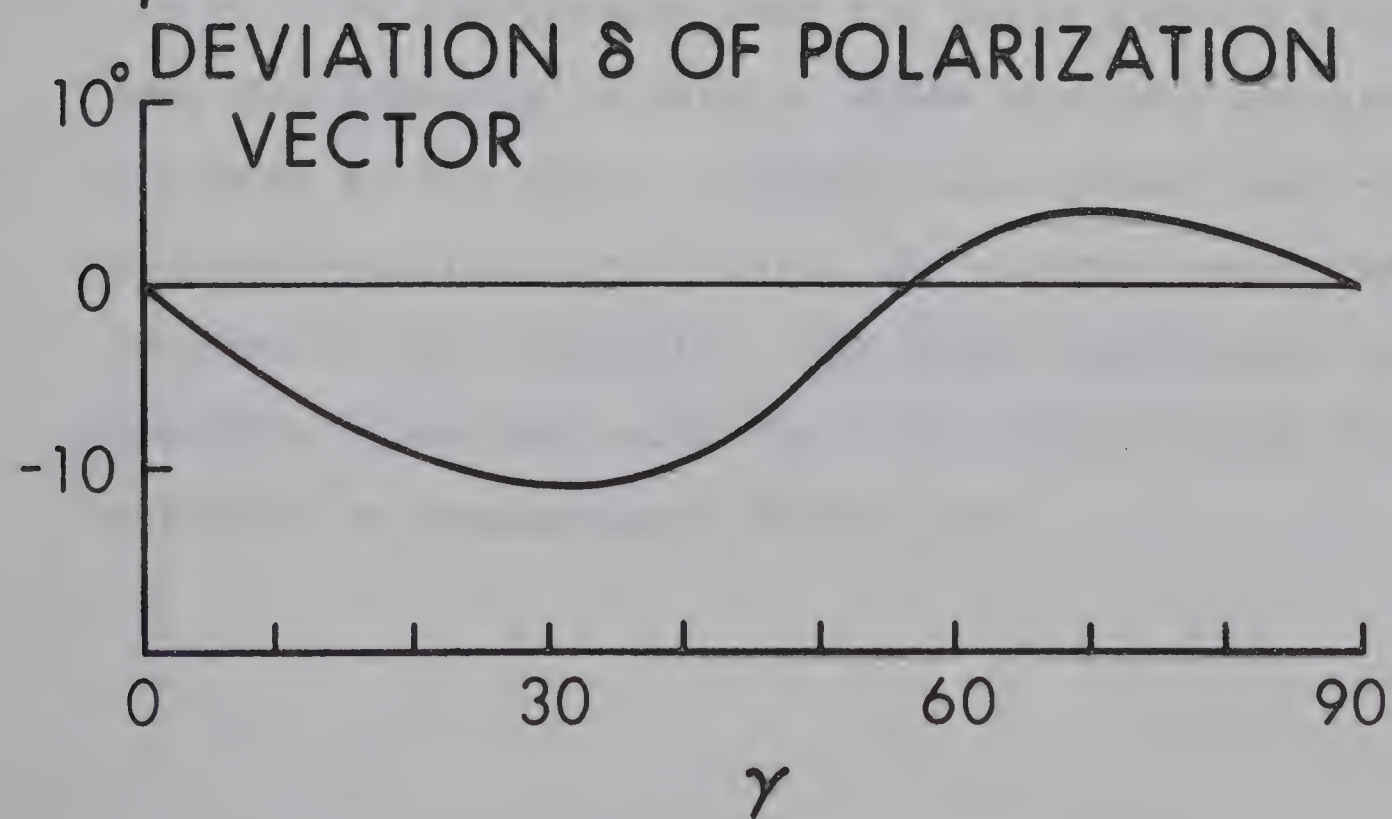
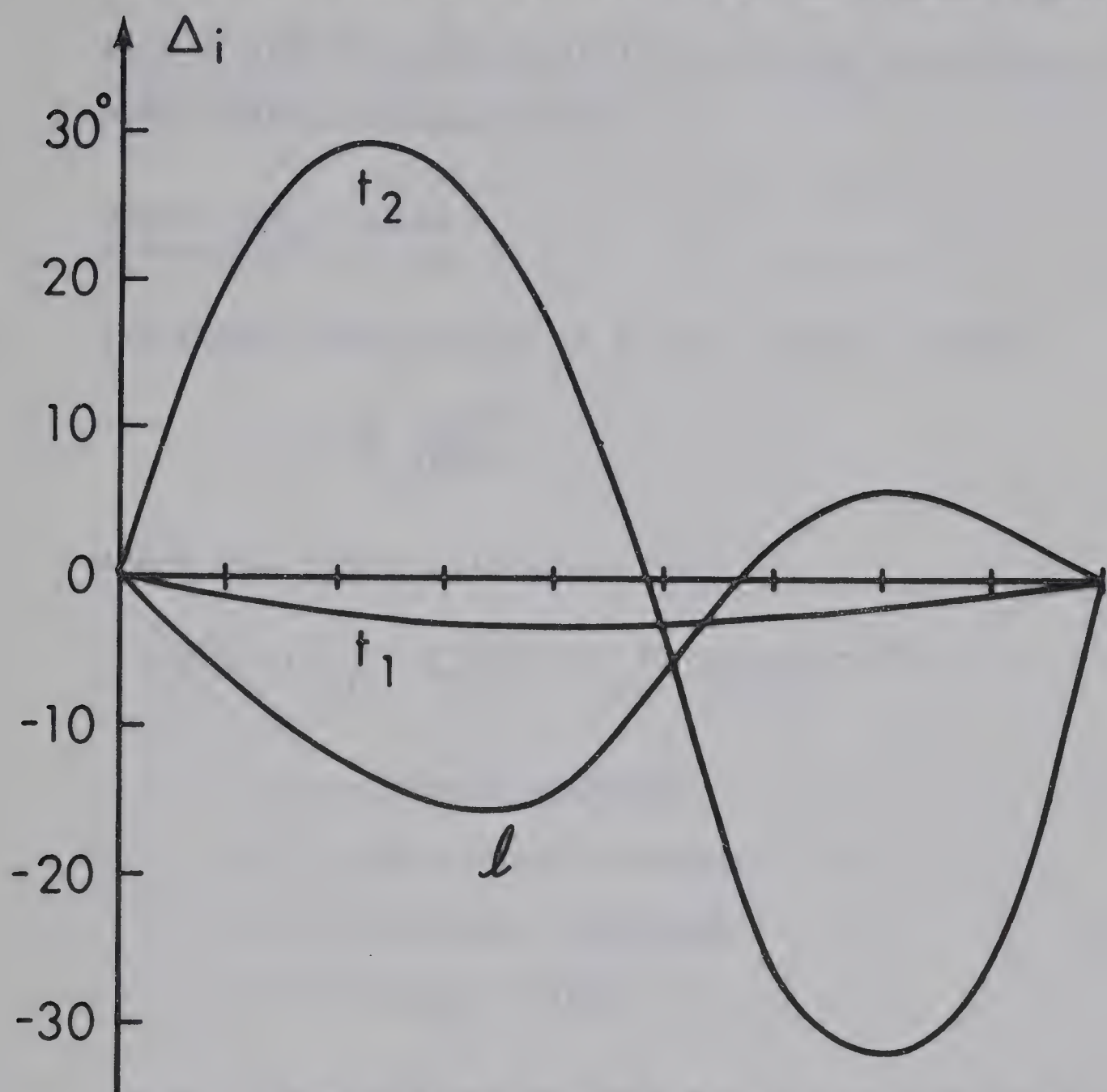


FIGURE 6

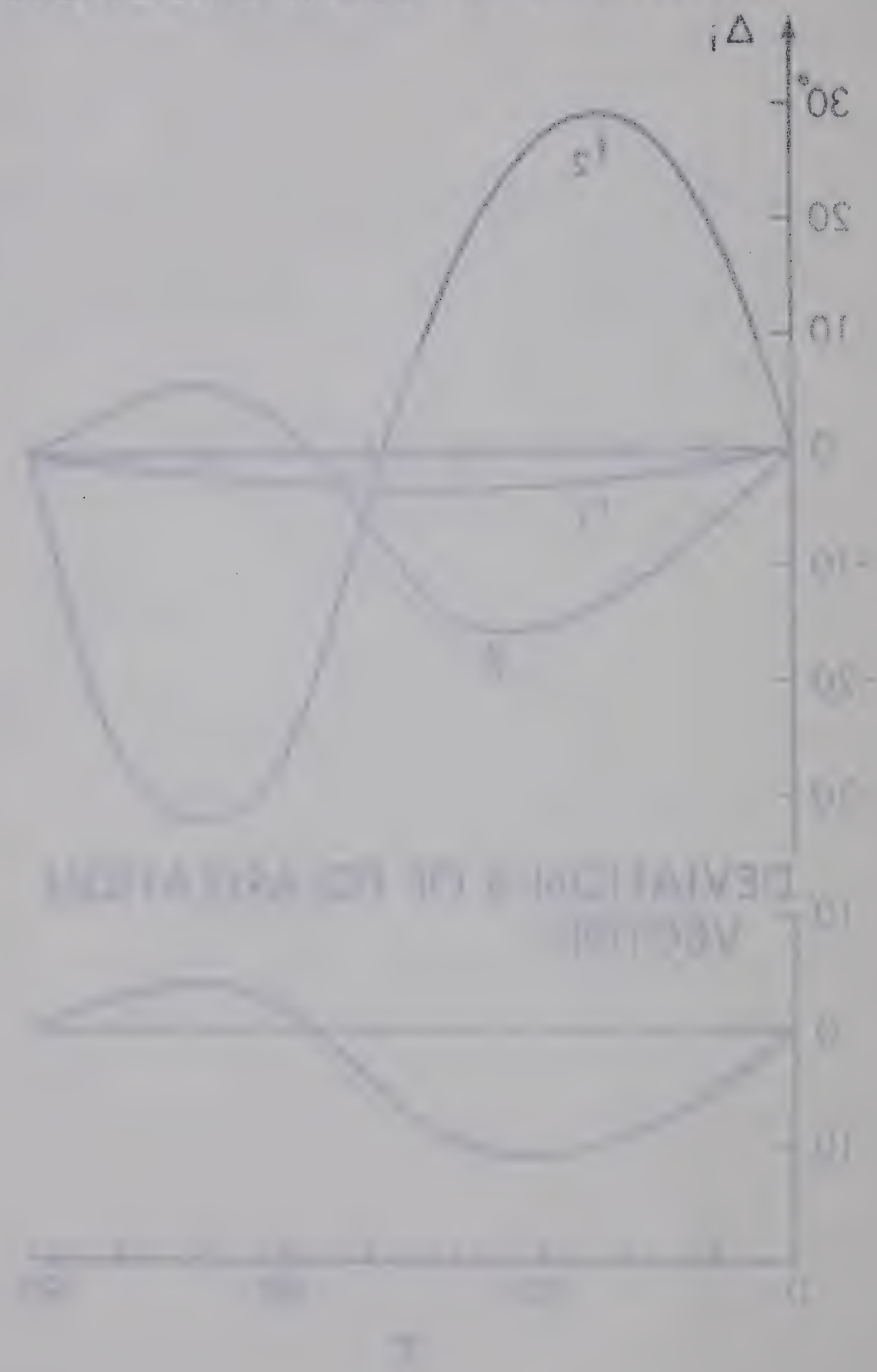
Deviation Δ_1 of beam direction and deviation δ of polarization vector from wave normal vs. orientation γ . The curves are calculated from elastic constants obtained from the work of Gillis et al. (1968).



DEVIATION OF BEAM DIRECTION



DEVIATION OF BEAM DIRECTION



at 0 K and the compressibility can be calculated and compared with thermal measurements.

Debye temperature θ_0

The Debye temperature at 0 K is (Akers (1965))

$$\theta_0 = \frac{h}{k} \left(\frac{3N}{4\pi V} \right)^{\frac{1}{3}} \cdot v \quad 2.34$$

where the Debye velocity v is

$$v = \left(\int (v_l^{-3} + v_{t_1}^{-3} + v_{t_2}^{-3}) d\Omega / 12\pi \right)^{-1/3} \quad 2.35$$

h = Planck constant

k = Boltzmann constant

N = Avogadro constant

V = molar volume

The integration over the solid angle Ω is particularly easy for hexagonal crystals, where the only integration variable is the angle γ between wave vector and c-axis. A computer program for θ_0 using the elastic constants as input is given in the appendix. The Debye temperature so obtained should be identical with the calorimetric Debye temperature measured at temperatures below $\theta_0/50$.

Compressibility, isothermal and adiabatic elastic constants

For hexagonal crystals the isothermal compressibility $K = -(\partial V / \partial p) / V$ in terms of the isothermal elastic constants is (Nye (1946), p. 146)

$$K = \frac{c_{11} + c_{12} - 4c_{13} + 2c_{33}}{c_{11}c_{33} + c_{12}c_{33} - 2c_{13}^2}, \quad 2.36$$

To compare the compressibility obtained by thermodynamic measurements with the compressibility calculated from sound velocity data one has to keep in mind that the former are static measurements giving the isothermal compressibility while the sound velocities give adiabatic elastic constants and compressibility. The difference $c_{ik}^s - c_{ik}^t$ depends on the particular elastic constant and is of the order (Bhatia (1967) p. 40)

$$\frac{c_{ik}^s - c_{ik}^t}{c_{ik}^t} \approx \frac{C_p - C_v}{C_v} \quad 2.37$$

(C_p , C_v heat capacities at constant pressure, volume).

Further comments on this point are found in section 4.4.

Phonon spectrum

The sound velocity is equal to the phase velocity of phonons

$$v = \left. \frac{\omega}{q} \right|_{q \ll q_{\max}} \quad 2.38$$

(ω = phonon energy, q = wave vector, q_{\max} = wave vector at zone boundary) in the limit of long wavelengths Leibfried and Ludwig (1961, p. 426) argue that the above definition may give isothermal sound velocities rather than adiabatic velocities, but leave the question open. In neutron scattering experiments, the excited phonons have usually rather high frequencies compared with ultrasonic frequencies and elastic constants calculated from 2.38 are therefore isothermal constants (see section 4.4). I have purposely avoided the notation " $q \rightarrow 0$ ", since this, taken literally, would give adiabatic constants.

Second sound

Assuming an isotropic material, the velocity of second sound is (Ackerman and Guyer (1968))

$$v_{II}^2 = \frac{1}{3} (v_l^{-3} + 2v_t^{-3}) / (v_l^{-5} + 2v_t^{-5}) \quad 2.39$$

Cauchy relations

If every atom in the crystal is a centre of inversion symmetry and if there are only central forces between a pair of atoms the elastic constants obey relations known as Cauchy relations (Born and Huang (1962)). For hexagonal crystals these are

$$c_{44} = c_{13}$$

2.40

$$c_{11} = 3c_{12}$$

In a hexagonal close packed crystal the condition of inversion symmetry is not satisfied, but Leibfried (1955) shows that this affects only the relation $c_{11} = 3c_{12}$. For the case of next nearest neighbour central forces $c_{13} = c_{44}$ remains valid.

2.5 Elastic constants from unoriented single crystals in the cubic phase

Finding the orientation of the crystals with the birefringence technique is possible only for the hexagonal phase. The orientation of cubic crystals is done either with neutron diffraction or with x-rays. It is believed that

neutron diffraction is not a suitable method for He^3 because of the large capture cross section for this isotope and x-ray scattering has so far been applied only to samples of a few millimeter diameter, because the small x-ray scattering cross section of helium requires thin container walls. On the other hand bcc He^3 is of great experimental interest. The large deviation of the specific heat from the Debye theory at low temperatures is as yet unexplained and sound velocity measurements at low temperatures would at least establish the phonon contribution to the specific heat. From a theoretical point of view, this phase and isotope have been studied most extensively. I have therefore investigated the possibility of finding the elastic constants of a cubic crystal using ultrasonic means alone. Assuming that the crystals do not grow in preferred directions, that many crystals can be grown and a substantial fraction of them are single crystals, this should indeed be possible.

The method consists of measuring the longitudinal velocity v_l and at least one transverse velocity v_t along the same path and then plotting them on a (v_l, v_t) -graph. For cubic single crystals the points are restricted to the two shaded areas indicated in figure 7. These areas are topologically identical for all cubic crystals and the co-

ordinates of their prominent features, namely of the corners and extrema can be expressed in terms of the elastic constants. For most cubic elements the figure lies in the (v_l, v_t) - plane as drawn, but for some binary compounds it may be rotated by 180° . The calculations (Nosanow and Werthamer (1965), de Wette et al. (1967)) show that in this respect helium is similar to most of the elemental crystals, but should the figure turn out to be upside down the extension of the analysis would be straight forward.

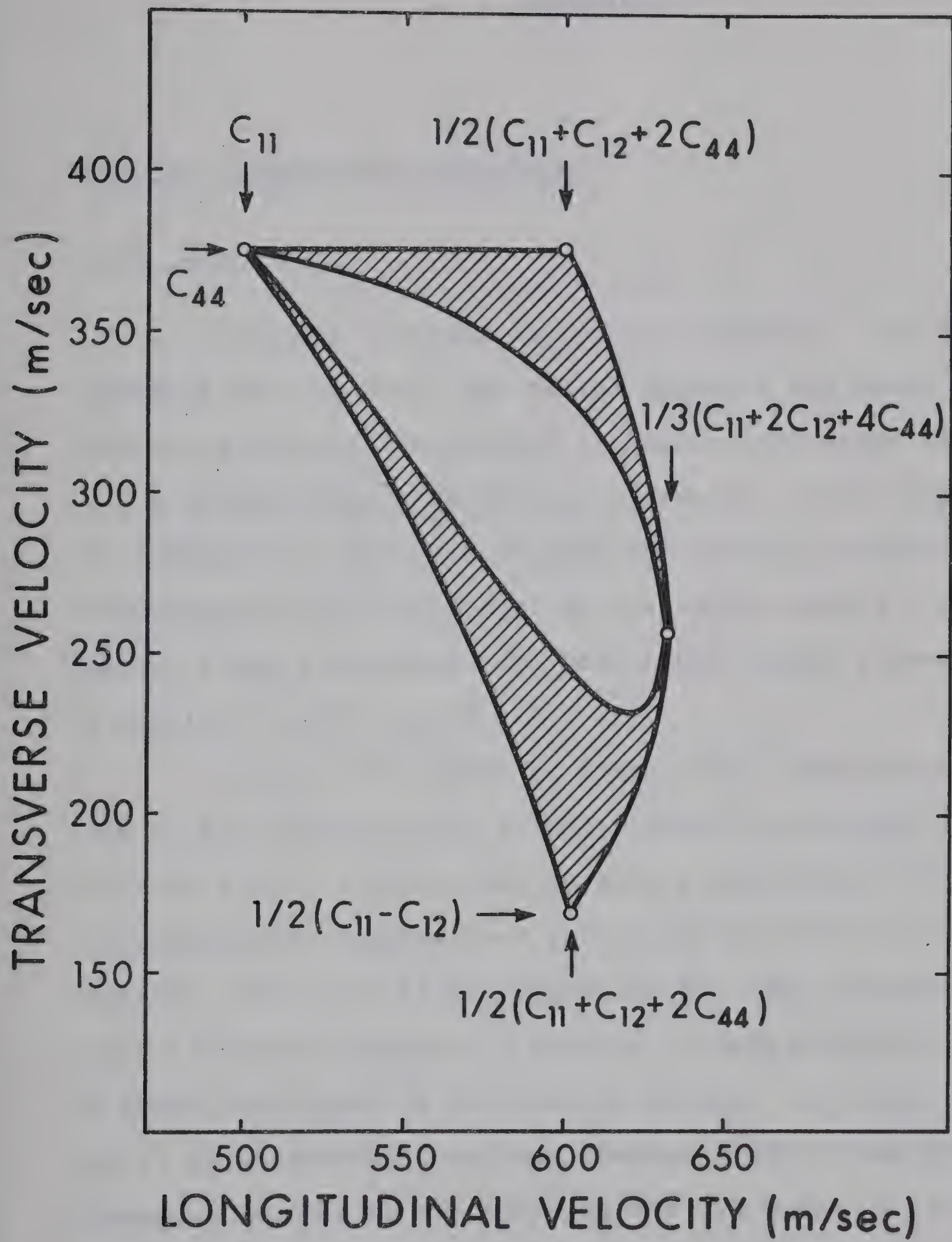
Sound velocities in polycrystals will increase the areas and fill in the forbidden zone in the center but the extremas and corners will not be obscured. With a sufficient number of (v_l, v_t) - points it should be possible to determine their coordinates and calculate the 3 elastic constants from them. Five linear combinations of c_{11} , c_{12} and c_{44} are obtained which allows a check for consistency. This method works also for hexagonal materials, even better than for cubic since the (v_l, v_t) - points are restricted to ly on two curves rather than in two areas.

Once the elastic constants are obtained it is in principle also possible to find the orientation of the crystal from sound velocity measurements alone (Green and Henneke (1967)).

FIGURE 7

Transverse vs. longitudinal sound velocity in bcc He^4 , based on elastic constants from de Wette et al. (1967).





3. EXPERIMENT

3.1 Low temperature apparatus

3.11 Cryostat

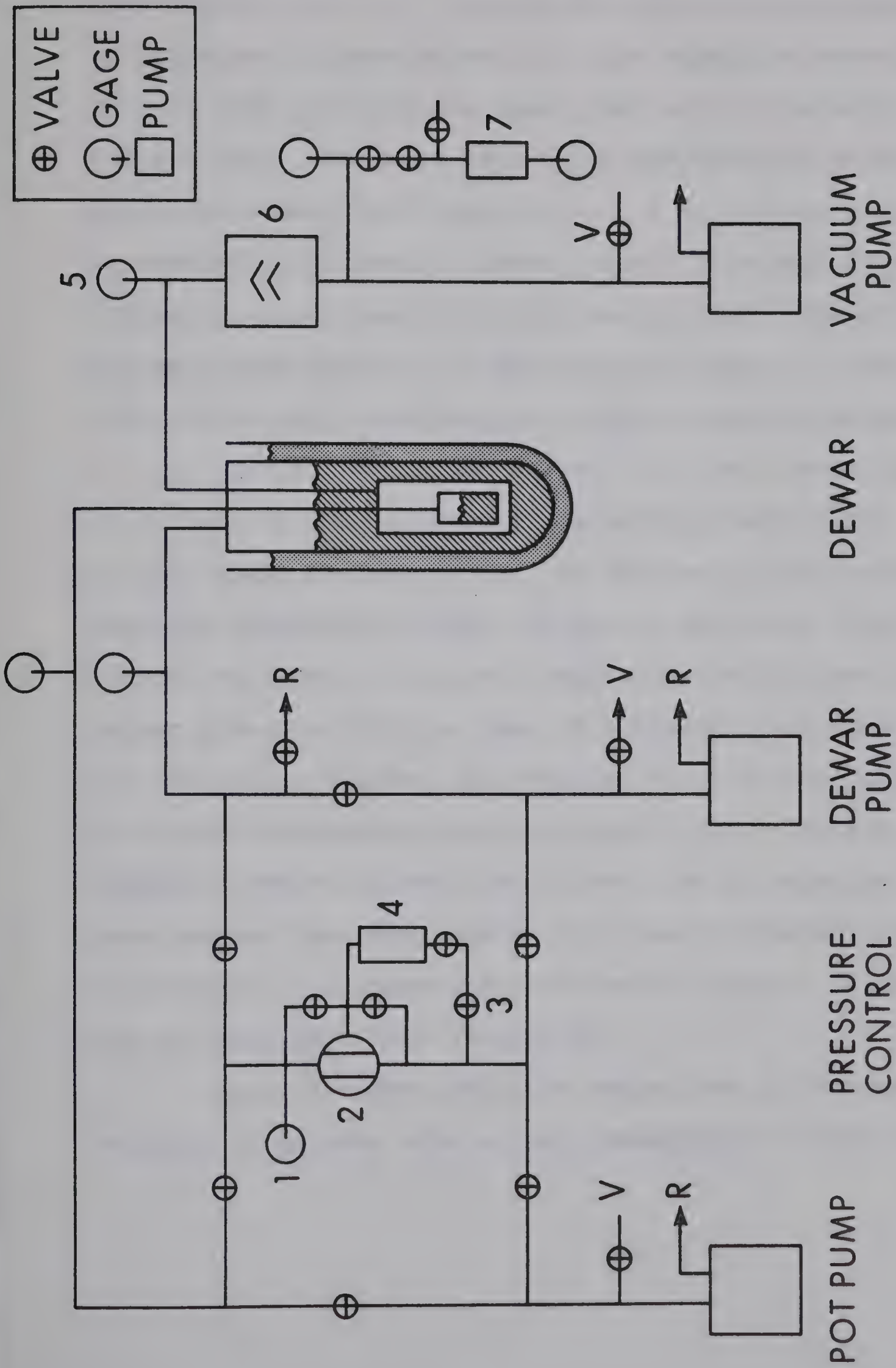
Helium solidifies only under pressure. The high pressure cell in which the helium crystals are grown must therefore contain transducers to measure the sound velocity and a window through which the orientation of the crystal can be determined. In order to grow and anneal a crystal, the temperature of the cell must be controlled during a long time within close tolerances. To meet these design parameters, a special cryostat was built.

Crystals are grown by keeping the temperature at the top of the pressure cell slightly above the melting temperature with an electric heater and by slowly decreasing the bottom temperature by pumping on a helium pot on which the cell is mounted. The cell is in vacuum and the high pressure fill line is vacuum jacketed to prevent it from blocking. Figure 8 shows the layout of the pumping system. An important part of it is a pressure regulator (Walker (1959)) that can be connected either to the pumpline for the dewar or to the

FIGURE 8

Pumping system

1. Wallace - Tiernan precision pressure gage
 2. Walker pressure regulator
 3. Needle valve
 4. Ballast volume
 5. High vacuum gage
 6. Diffusion pump
 7. Exchange gas container
- V Vent valve
- R Connection to helium gas recovery system



pumpline for the pot. Usually the helium in the dewar was at atmospheric pressure and 4 K, the regulator connected to the pot pump line and the dewar pump used in parallel with the pot pump. The regulator holds temperatures within a few mK in the temperature range 1.4 ... 4 K. It can very easily be adapted to automatic crystal growth (Ackerman (1967)) by including a low flow calibrated needle valve through which the reference pressure in the ballast volume is slowly pumped down and the pot temperature therefore slowly decreased.

One filling of the 280 cm³ pot lasts about 16 hours at 2 K and it can be refilled through a needle valve in about 10 min. while pumping on it. In this way it is possible to keep the temperature below 2 K for an arbitrary long time. A rough estimate of the pot temperature is obtained from the vapour pressure which is read on a bourdon gage (Model FA 145, Wallace & Tiernan, Belleville, N.J.) in the pump line. The lowest temperature obtained was 1.23 K. The pot is suspended on two stainless steel tubes, one of which is the pumpline and the other serves as a vapour pressure bulb for calibration of a germanium thermometer which is attached to the pot near that bulb (Figure 9).

Optical access into the copper can is through a vertical 13 mm tube with a room temperature window at the top

of the cryostat. This is a very easy solution from the point of view of cryostat construction but requires a window or prism inside the cryostat and one on top of it to get a horizontal light beam. This complicates the optical problems. A nickel vane inside the vacuum container and at low temperature can be moved from the outside with a magnet to block the optical path so that no room temperature radiation enters. However neither the temperature control of the pot nor the growth of helium crystals was in any way affected by opening or closing this vane.

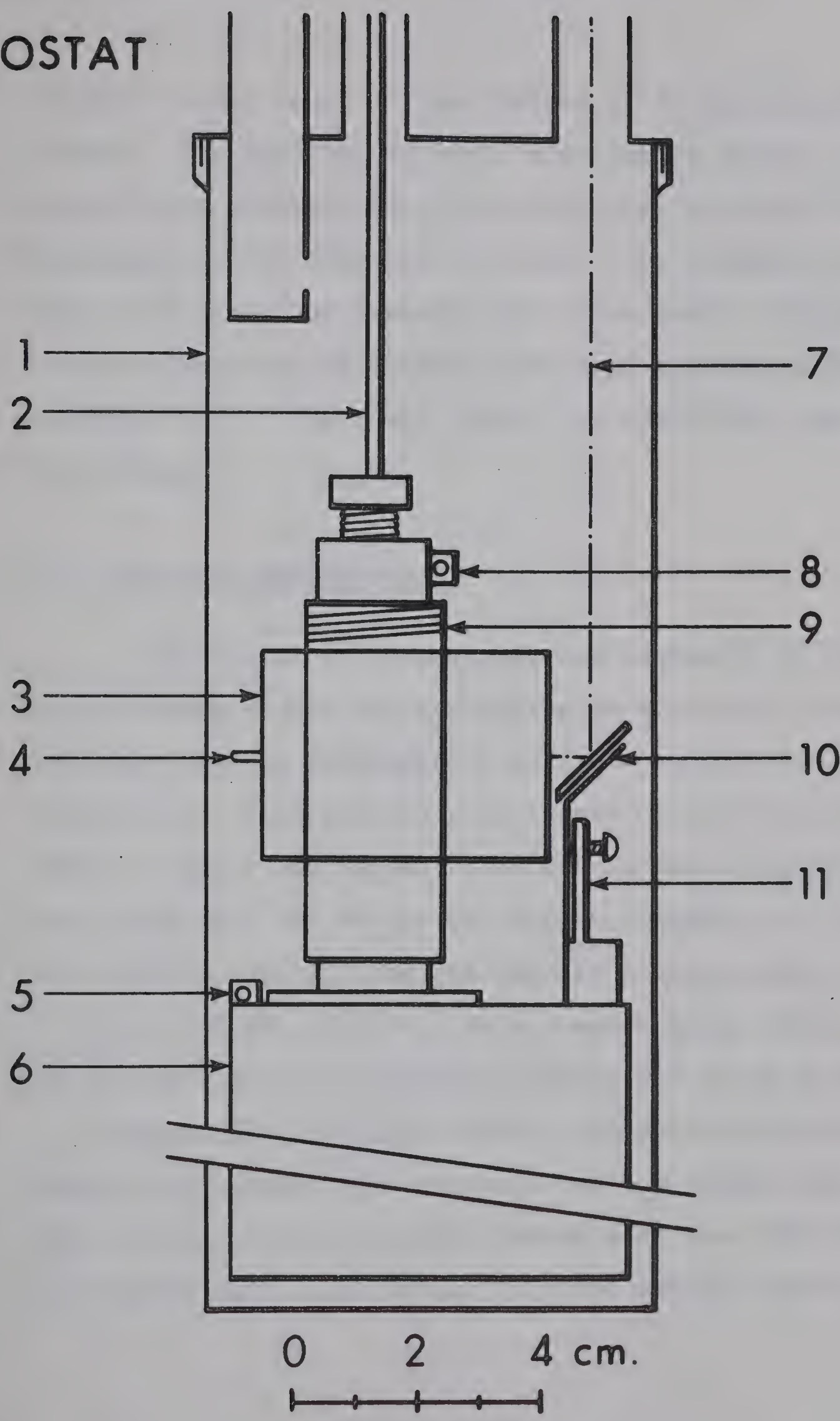
Shortly after completing the measurements on longitudinal sound velocity I had the unfortunate experience of observing pressure oscillation in the helium gas above the liquid level of the dewar similar to the oscillation in the familiar dipstick level indicator. They increased the evaporation rate from the previous $140 \text{ cm}^3/\text{hr}$ to about $2500 \text{ cm}^3/\text{hr}$ and prevented further experiments. I have tried to suppress these oscillations by a styrofoam plug about half way between the liquid helium surface and the top of the dewar, by filling the brass head of the cryostat with styrofoam or aluminum foil, by connecting a 10 litre ballast volume to the dewar, by disconnecting the dewar from the recovery line and venting it to atmospheric pressure, and by using a

FIGURE 9

Cryostat

1. Copper can, enclosing high vacuum
2. Vacuum jacketed high pressure capillary
3. High pressure sample chamber
4. Connector to sound transducer
5. Germanium thermometer
6. Pot, filled with pumped liquid helium
7. Laser beam
8. Allen-Bradley thermometer
9. Manganin heater
10. Mirror
11. Adjustable mirror support

CRYOSTAT



slightly longer dewar (78 cm instead of 73 cm), but with little success. The oscillation would sometime be absent only to appear again spontaneously after the next filling of the dewar. The inside of the dewar is 9 cm and it is connected to a brass head of 12 cm inside diameter and 13 cm length through a Corning flange (Pyrex conical pipe system, Corning Glass works, Corning N. Y.). The round copper can inside the dewar measures 7.5 x 26 cm.

3.12 The high pressure cell

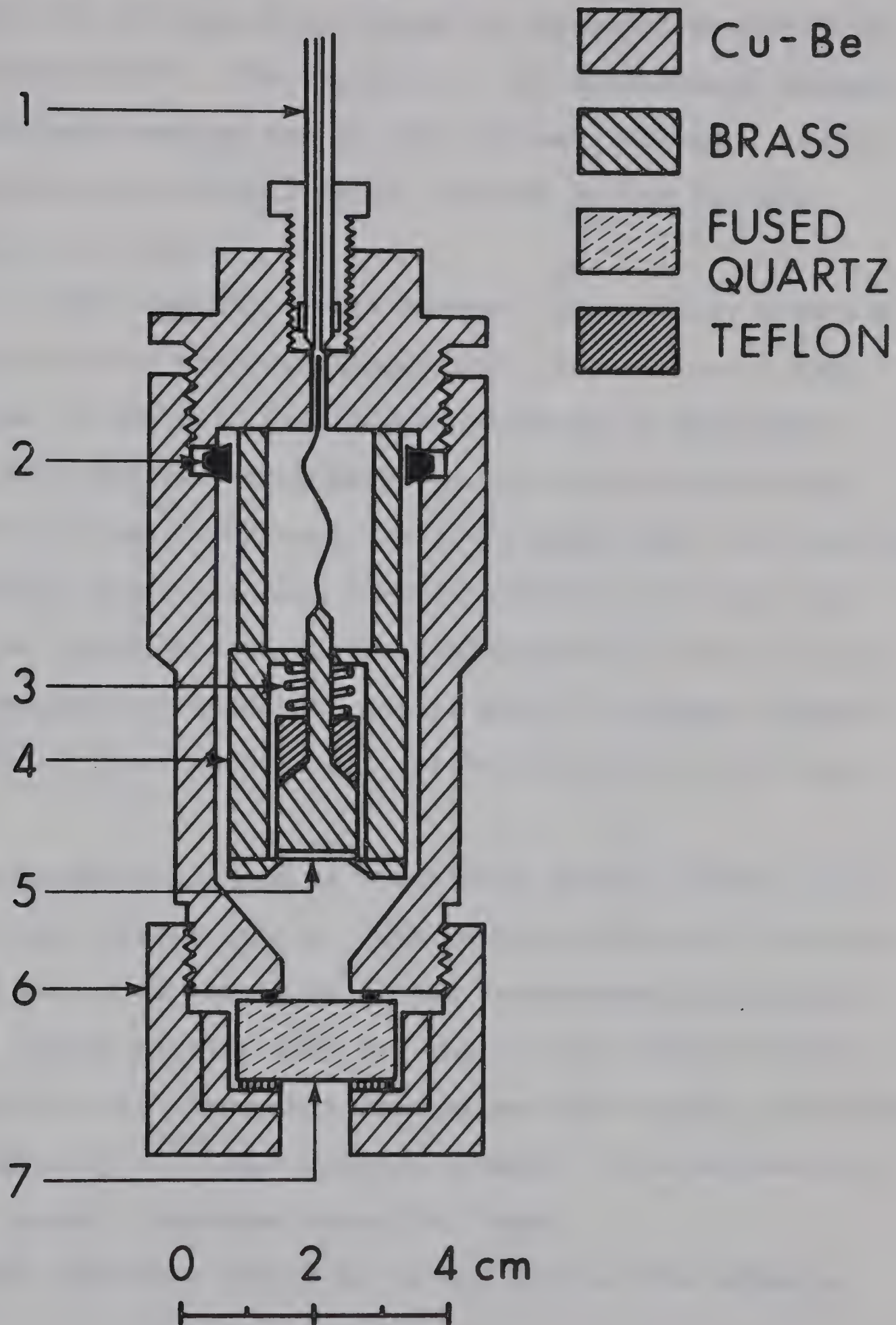
The aim of the experiment was initially to measure not the velocity but the absorption of sound and I spent therefore much time in developing a suitable support for the quartz transducers. With this support I have observed up to 72 sound echos in liquid helium and up to 200 in solid helium. In the first bomb that had an optical window (figure 10) I retained this support and did some preliminary measurements at a pressure of 58 and 128 bar with it. This chamber hangs freely from the pressure capillary inside a copper can which is submerged in a pumped bath of liquid helium. Crystals were grown by cooling the chamber with exchange gas and keeping the capillary from blocking with a manganin heater wire that runs inside it. Not surprisingly, the success rate for making single crystals

FIGURE 10

Sample chamber 1

1. High pressure capillary
2. Lens ring seal
3. Spring
4. Sound transducer assembly
5. Quartz transducer
6. Indium O-ring
7. Quartz window

SAMPLE CHAMBER 1



was quite low and led me to design an improved version which is described below. The crystals in the preliminary chamber were observed from the top of the cryostat through a window in the bottom of the cell using a system of two mirrors attached to the cell.

In the improved sample chamber (figure 11), crystals were grown with a vertical temperature gradient and I made the bottom of the cell from copper which has a high heat conductivity and can carry away the heat of solidification to the helium pot. The cell itself is made from a 2% beryllium copper alloy which has high tensile strength, low heat conductivity (compared with copper) which makes it easy to produce a temperature gradient, and is easy to machine, polish and solder. After machining it is hardened for 1 1/2 hrs at 315° C.

The special shape of the bottom should induce nucleation at the coldest spot A. One of the nuclei will then outgrow the others as the solid liquid interfaces moves up and act as a single crystal seed for the larger crystal higher up. I have however no proof that this arrangement really increases the probability of single crystal growth. It is around 50% with the growth technique described later.

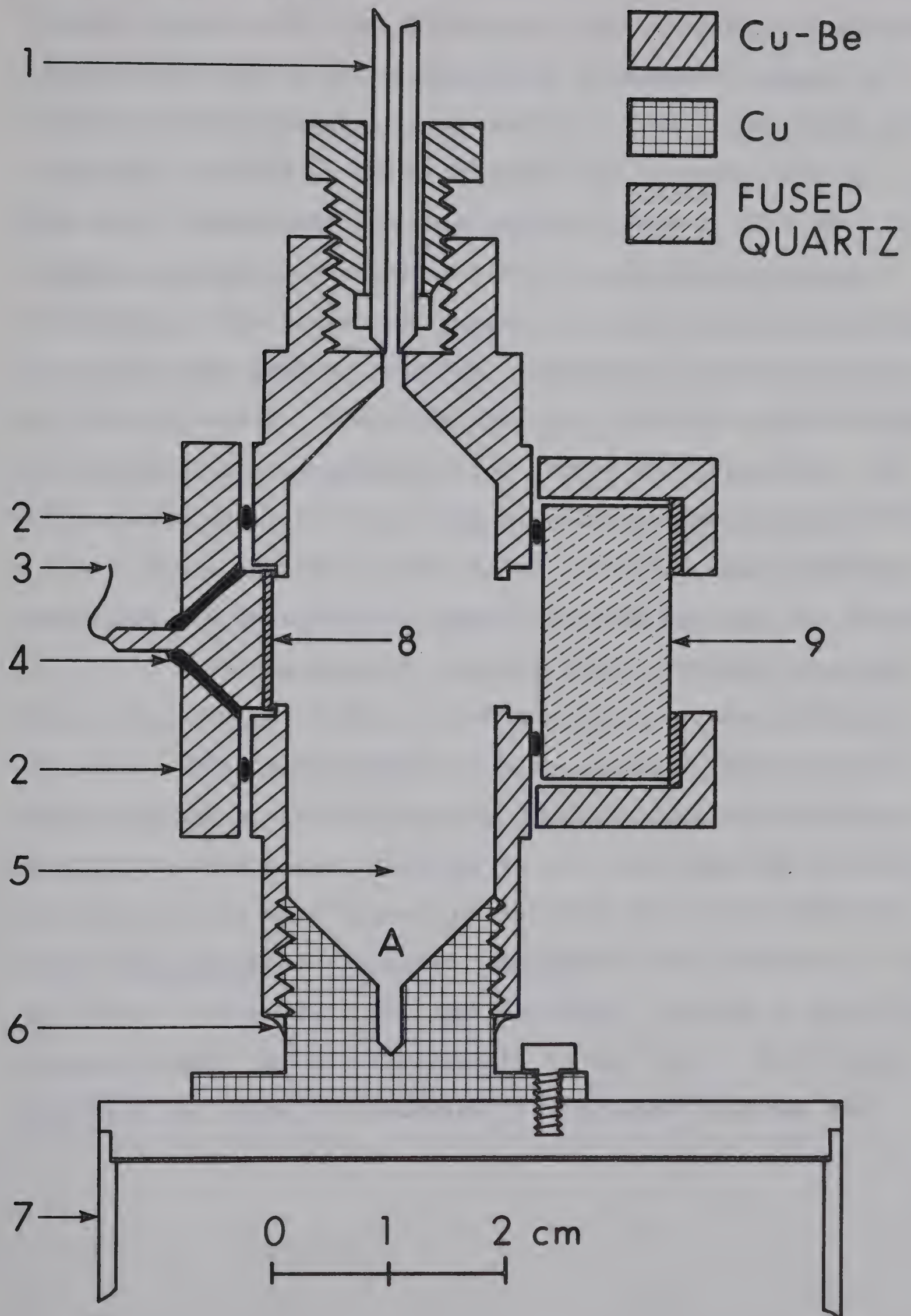
No obstacles should be in the path of the growing

FIGURE 11

Sample chamber 2

1. High pressure capillary
2. Indium O-ring
3. Electrical connection to backside of sound transducer
4. Stycast epoxy for electrical insulation
5. Solid helium
6. Soft solder
7. Helium pot
8. Sound transducer
9. Window

SAMPLE CHAMBER 2



crystal and Dr. J.E. Vos (Delft) has told us that he sometimes observed pinning of grain boundaries to discontinuities in the wall of the container. My cell is a tube with window and transducer mounted in holes drilled from the side into it. The sound transducers are thin quartz plates of 12.5 mm diameter plated on both sides with a layer of aluminum as electrodes. The transducer serves also as a mirror to reflect the light beam that is used for orientation determination out of the cell again. Therefore the cell requires only one window which facilitates corrections for stress birefringence, and this window is at the same time a reflector for the sound beam.

The advantage is that light and sound beam coincide in direction and position and sample the same part of the crystal.

I used the greased indium O-ring technique described by Vos and Kingma (1967) to seal the fused silica window to the bomb. The O-rings had initially a square cross section of 0.7 mm and an inside diameter of 15 mm. After compression the thickness was approximately 0.1 mm. The sealing surface on the bomb was hand lapped and polished to a mirror finish. This seal withstands repeated temperature and pressure cycling but fails eventually. The same technique is used to seal the backing plates for the transducers to the cell. The center piece of the plate is electrically insulated from the cell

and in contact with one electrode of the transducer. The other electrode facing the helium is grounded to the bomb. This centerpiece is epoxied into place with Stycast 2850 GT (Emerson & Cumming Inc., Canton, Mass.). The tapering should prevent back reflection of sound. The surface against which the transducer is pressed with two washer springs is lapped and polished until a check for flatness with an interferometer plate in sodium light shows less than one fringe over the whole surface. This is more than adequate for a sound wave length of approximately 0.1 mm.

The parallelism between window and transducer is not very critical for velocity measurements. Coarse adjustment was achieved by shining a laser beam onto the transducer and compressing the indium O-ring until the reflection from the transducer coincides with the reflection from the inside face of the window. With careful tightening of the screws interference fringes are observed and circularized. I estimate window and transducer to be parallel within about 10^{-3} radians.

3.13 Temperature measurement and control

I determined the temperature of the helium pot by measuring the resistance of a germanium thermometer (Solitron Devices, Riviera Beach, Fla.) with an isolating potential

FIGURE 12

Electronic temperature regulator

R1 Allen-Bradley thermometer, 3.5 k at $T = 2.5$ K

R2 Manganin heater

R3 Dummy heater

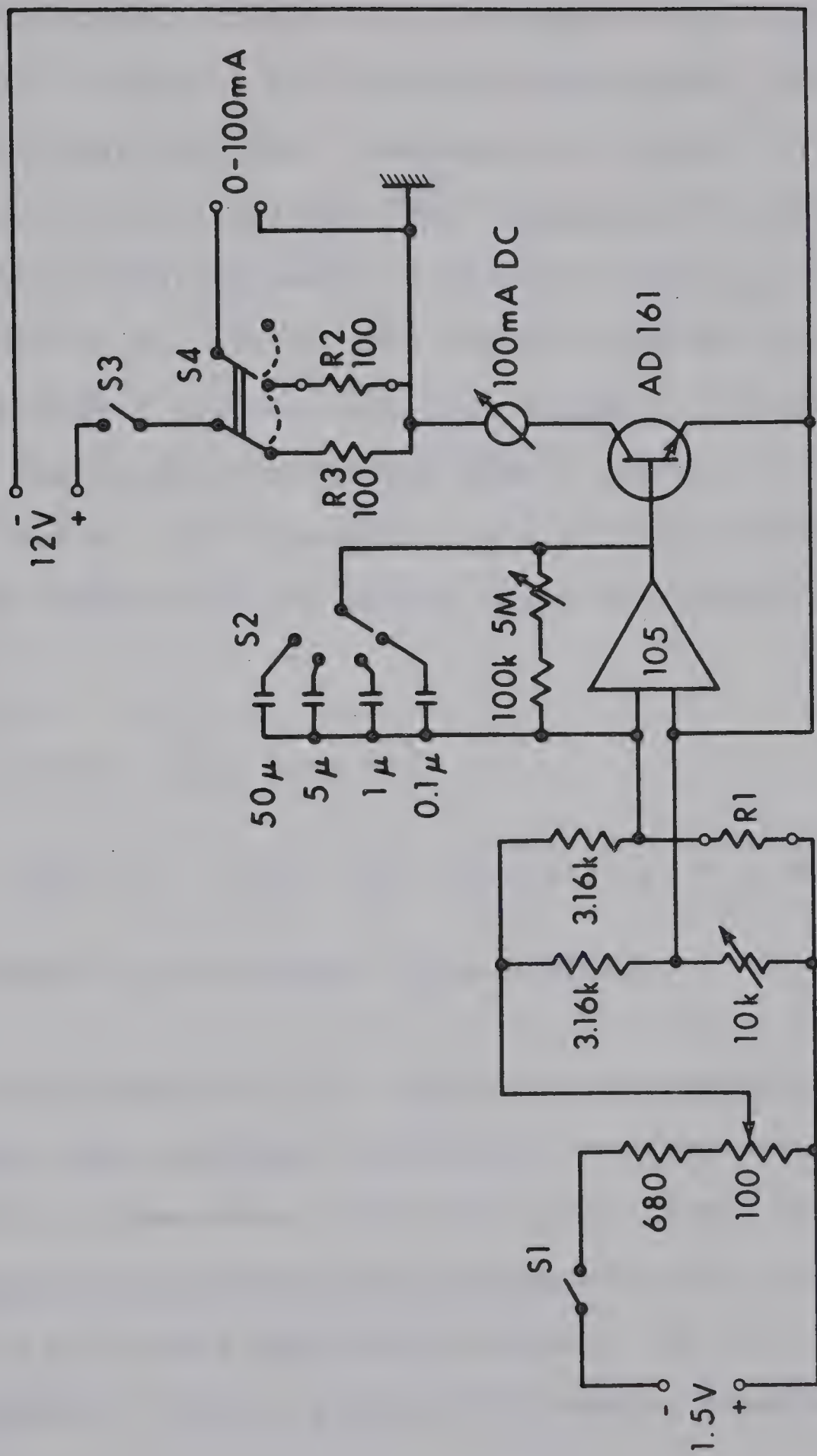
S1 Thermometer current on/off

S2 Time constant selector

S3 Heater current on/off

S4 left side: measure R1, manual heater current regulation
right side: automatic heater current regulation

105 Operational amplifier, model 105 (Analog Devices)



comparator circuit (Dauphinee and Mooser (1955), Dauphinee and Woods (1955), Dauphinee and Preston-Thomas (1958)). The resistance at 2 K is about 1000 Ohm, the measuring current 10^{-6} Amp. and the precision about 0.1 mK. The thermometer is calibrated against the vapour pressure of He^4 using the T_{58} scale (Brickwedde et al. (1960)). For unknown reasons, but most likely because I did not wait long enough for thermal equilibrium, the calibration points show a scatter of ± 5 mK from a smooth curve. For interpolation a polynom of degree 6 is fitted by computer to the points using the method of least squares:

$$\log T = \sum_{i=0}^6 A_i (\log R)^i \quad 3.1$$

$$A_0 = -28.798, A_1 = 41.815, A_2 = -20.512, A_3 = 3.2818,$$

$$A_4 = 0.42763, A_5 = -0.19410, A_6 = 0.016811.$$

The temperature at the top of the pressure cell is found from the resistance of an Allen-Bradley radio resistor with a room temperature resistance of 100 Ohm. It is calibrated against the germanium thermometer using exchange gas to establish thermal equilibrium between the two thermometers. This thermometer serves also as the sensing element in an

electronic circuit that keeps the top temperature constant and above the melting temperature to keep the pressure capillary from blocking and provides the necessary temperature gradient for crystal growth. It forms one arm of a Wheatstone bridge. The out of balance dc-signal is amplified and integrated by an operational amplifier with a time constant that can be selected between 0.01 and 250 sec. and then amplified further by a power amplifier which controls the current through a 100 Ohm manganin heater. This feedback loop regulates the top temperature around 2 K to within a few mK when cooling the bottom of the cell to 1.3 K and has a drift under stable conditions of less than 1 mK over a period of 8 hrs. Used together with a dummy heater and a meter for the heater current it also serves as a thermometer. I would like to thank Dr. J.S. Rogers for help in the design of it.

It turned out that too much heat is flowing down the capillary (stainless steel, OD = 2.5 mm) from room temperature. A copper wire clamped to it and anchored at the pot is enough however to reduce the top temperature.

3.14 High pressure gas handling system.

Mezhov-Deglin (1965), who was the first to successfully grow single crystals of helium, stresses the importance of

purity of the initial gas and reports that best results are obtained by cleaning it with a leak that allows passage of superfluid helium only. On the other hand Ackerman and Guyer (1968) have observed second sound in crystals prepared from gas obtained from evaporating liquid helium. The sound velocity is probably much less affected by impurities than the sound absorption and it has to be only sufficiently high to allow the growth of single crystals.

The gas handling and cleaning system is shown in figure 13. The sample chamber is evacuated and flushed several times at room temperature with cleaned gas and then cooled with exchange gas under constant pressure of about 10 bar to 77 K. Then it is slowly pressurized to either 36 or 58 bar and cooled further to 4 K, thereby sucking gas through the U-tube that is dipped into a storage dewar. Cooling from 77 K to 4 K takes approximately one hour which should be sufficiently slow to liquify all helium that passes through the trap. A storage cylinder is used as ballast volume to maintain constant pressure during the growth as more helium passes into the cell. Pressure stability is therefore mainly determined by the amount of room temperature fluctuation and always less than 0.1 bar. I read the pressure on a Bourdon gage (Heise Bourdon Tube Co. Inc., Newton, Conn.) to ± 0.1 bar. (1 bar =

$$10^5 \text{ N/m}^2 = 0.98692 \text{ atm} = 1.01972 \text{ kg/cm}^2 = 10^6 \text{ dyn/cm}^2).$$

3.15 Crystal Growth

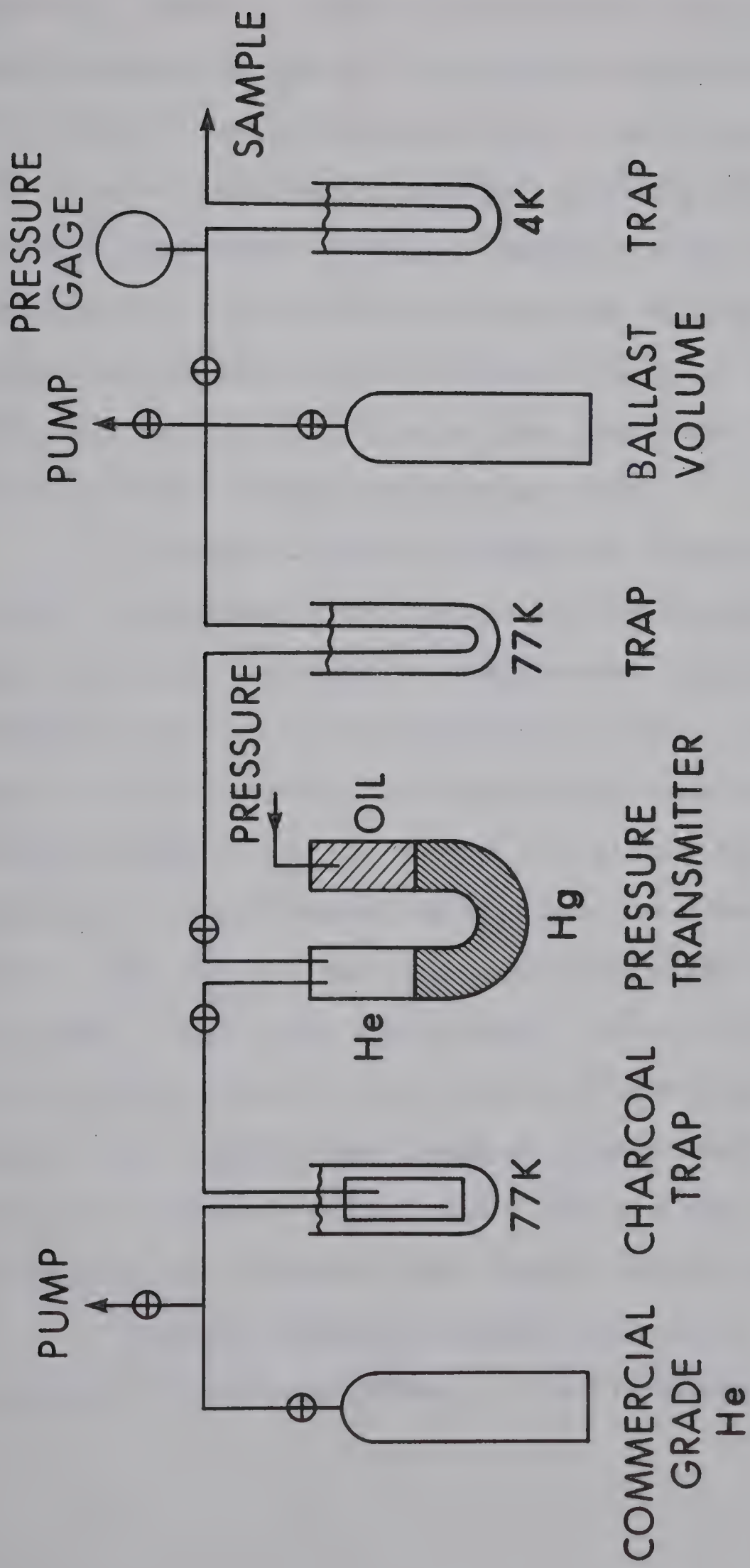
Crystals were grown at constant pressure and with a constant growth rate of 2 cm/hr using a technique described by Ackerman and Guyer (1968). I would like to thank Dr. Ackerman for telling me about it prior to publication. The main idea is to keep the fluid helium slightly above the melting temperature (about 20 mK) and to lower the temperature of the solid helium in such a way that the solid-liquid interface progresses upwards at constant velocity. Since the heat conductivity of the solid is several orders of magnitude higher than the liquid conductivity it can be assumed that all the heat of melting is carried away through the solid (the walls have a similar or smaller conductivity as solid He and are ignored). From the known temperature dependent conductivity (Bertman et al. 1966) the temperature at the bottom can be calculated as a function of time for a given growth rate.

Liquid helium I has a temperature conductivity $k/\rho.C$ (k = heat conductivity, C = heat capacity per gram) of about $10^{-4} \text{ cm}^2 \text{ sec}^{-1}$ so that it takes about 10^4 sec to reach thermal equilibrium in a volume of 1 cm^3 . Convective flow is absent because of the very small thermal expansion of liquid

FIGURE 13

High pressure gas handling system





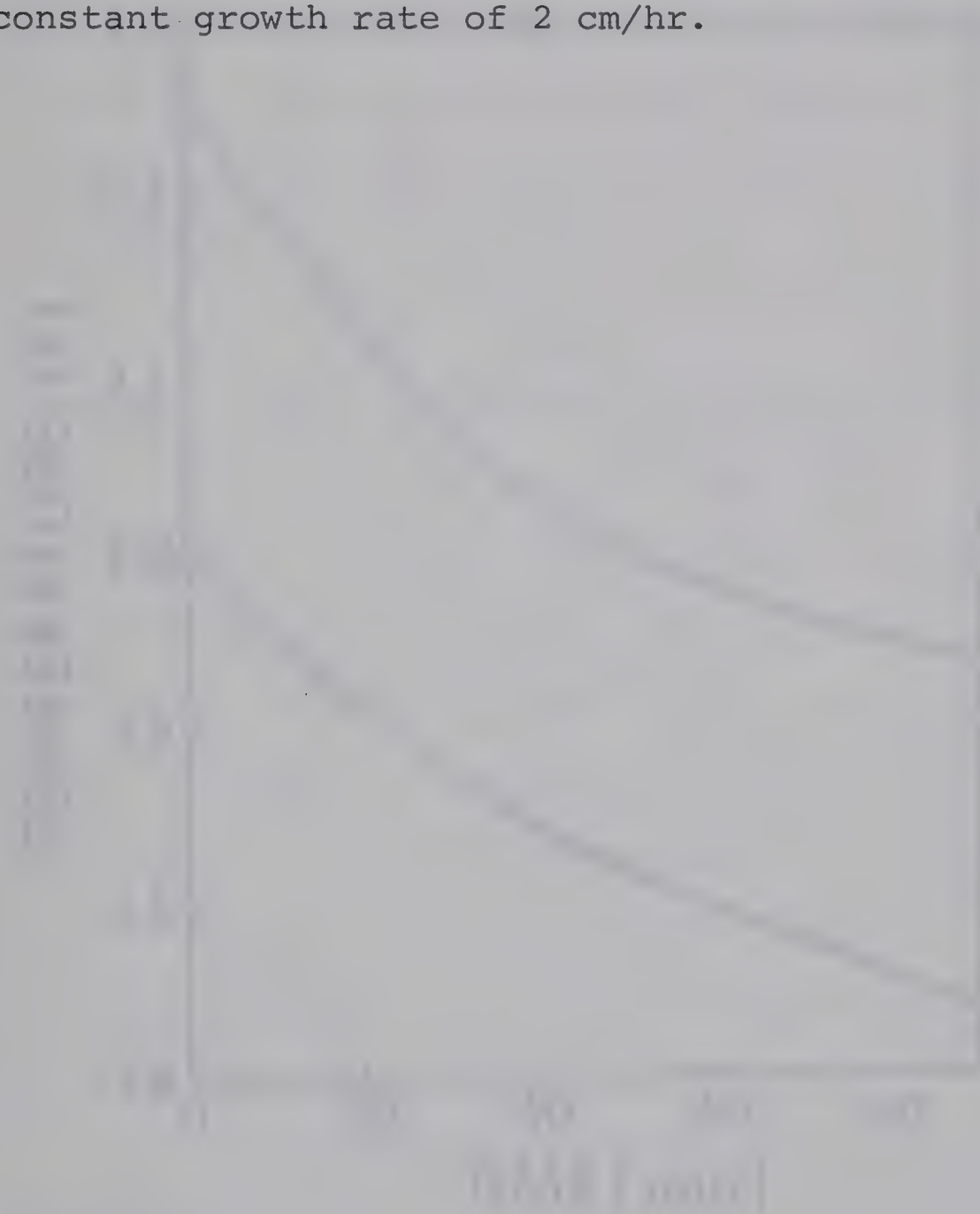
helium. Usually I made a new crystal after melting the previous and waiting for one or two hours for equilibrium. I have tried to observe the influence of that waiting time on crystal quality but find no conclusive results, probably because it depends also on many other factors. However after completing the experiments I calculated the average waiting time for the runs that yielded single crystals and find 90 min while the time for polycrystals was 65 min. Ackerman (1968) waits 6 to 10 hrs with a chamber of similar size.

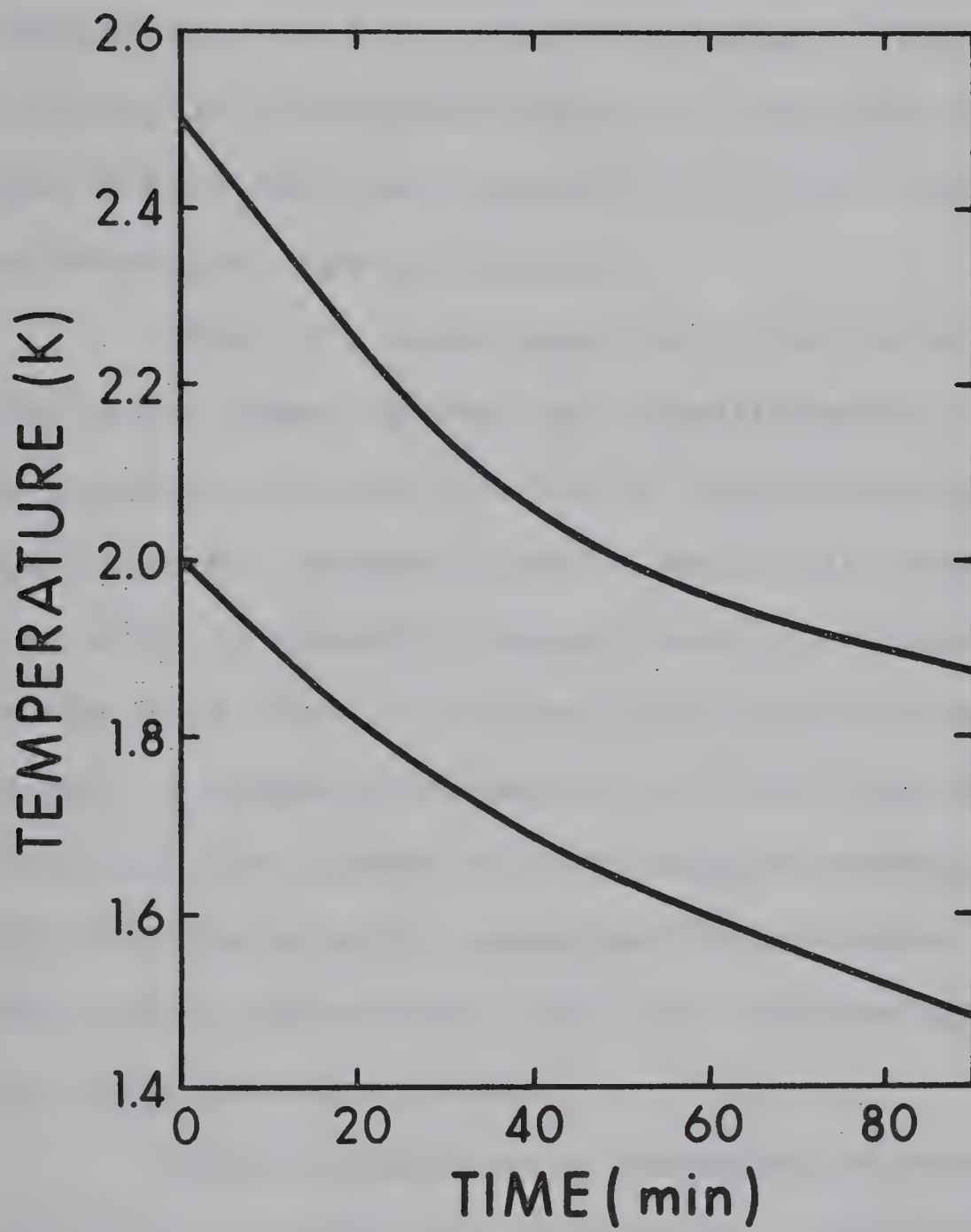
I keep the sound switched on before and during the growth to monitor the progress of the crystal. Since at 36 bar the sound velocity is temperature dependent near the melting line due to the vicinity of the λ -transition, this also allows to check for temperature equilibrium in the liquid. After a growth time of 60 min the liquid echo decreases in amplitude in a fluctuating way but the time delay remains the same. This shows that the pressure inside the cell has remained constant. After 100 min a small, fast echo from the solid is visible and grows at the expense of the liquid echo or, quite often, the liquid echo disappears completely before a new echo can be seen. After about 150 min the solid echo is stable in amplitude, or grows very slowly (figure 20).

Another indication shows that solid helium is in contact with the transducer: The transducer oscillates long

FIGURE 14

Temperature at bottom of sample chamber vs. time for a constant growth rate of 2 cm/hr.





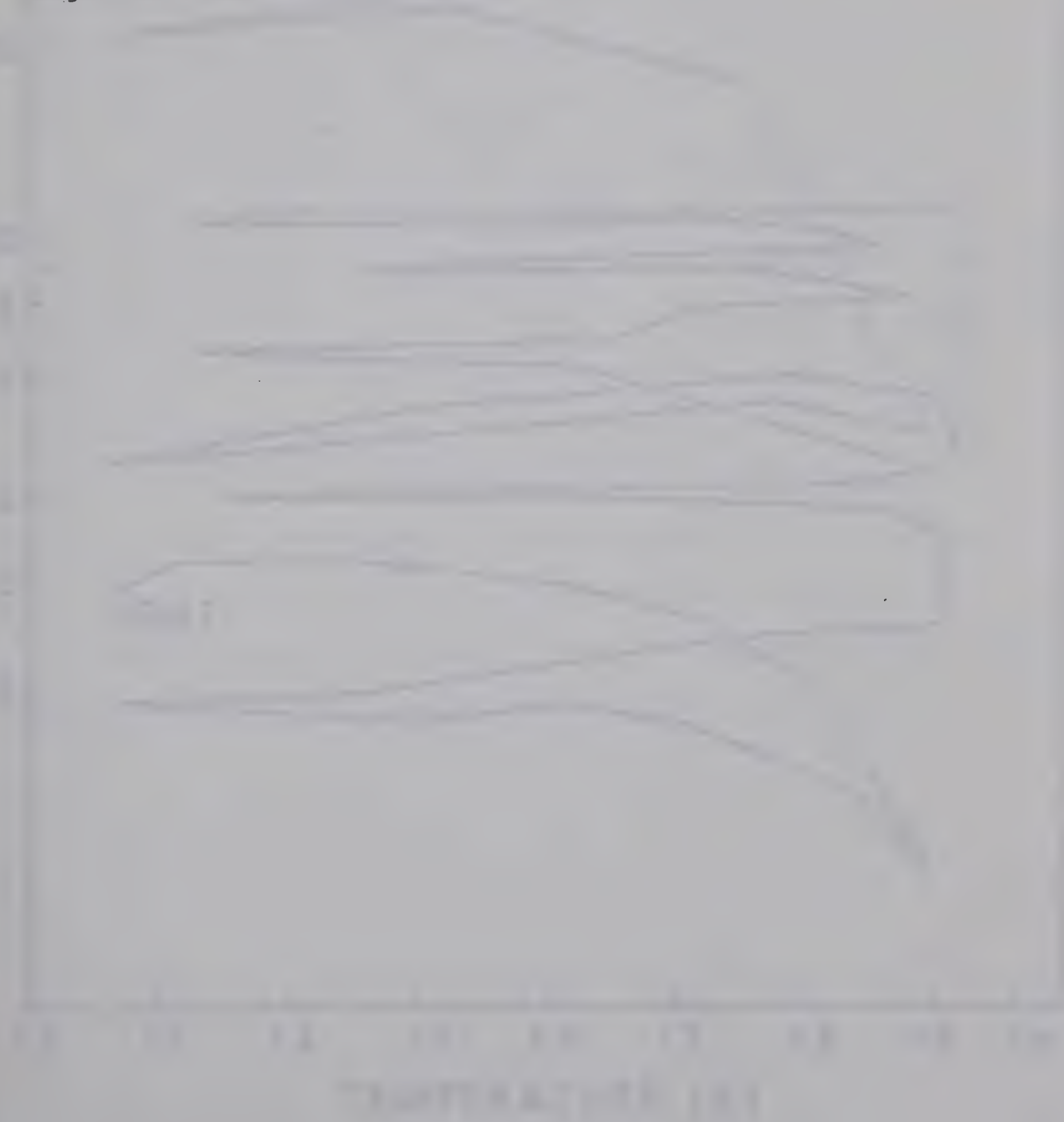
after the 2 μ sec electrical high frequency pulse is stopped because of the high Q-factor. The decay time depends on the acoustic impedance of the load and is about 53 μ sec for liquid and 35 ... 39 μ sec for solid helium, just about inversely proportional to the acoustic impedance. It should in principle be possible to measure the sound velocity at the surface via this effect and then compare it with the bulk sound velocity to determine crystal quality.

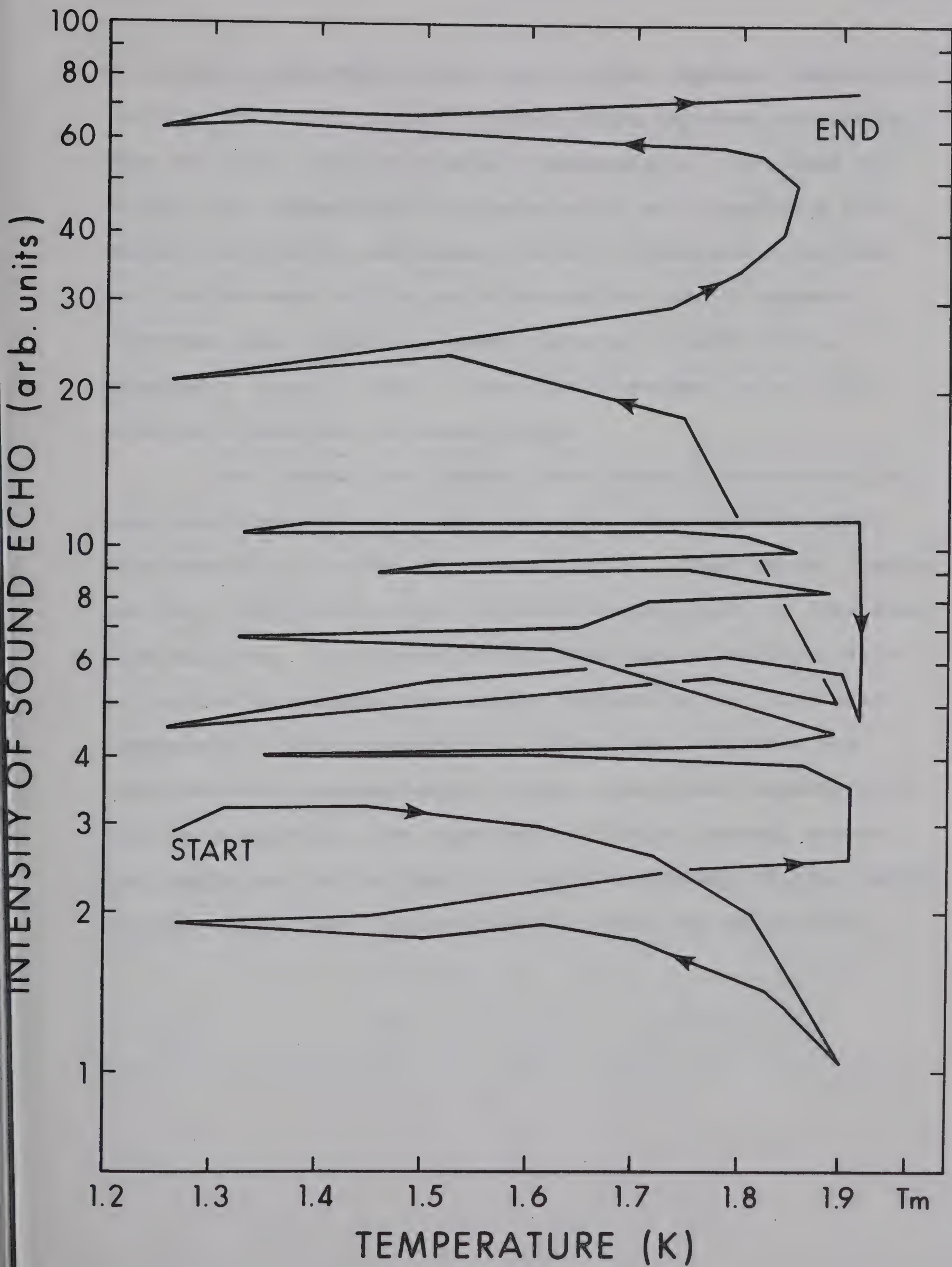
After the whole bomb is filled with solid, I reduce the heater power to zero and simultaneously raise the bottom temperature to within 0.2 K of the melting temperature to get equilibrium. Between 2 and 4 hrs after beginning of growth the velocity usually changes, mostly to higher values and seldom more than 1% in good crystals and then reaches a steady value. I assume that during this time recrystallization takes place and the growth of large single crystals which eventually fill the whole cell. Annealing for a longer time or closer to the melting temperature does not increase the echos any further and often decreases them.

I have occasionally attempted to measure the temperature dependence of the sound absorption. In figure 15 I plot the logarithm of the intensity of the first echo versus temperature. The experiment extended over 3 days. While this measurement

FIGURE 15

Intensity of longitudinal sound echo under repeated temperature cycling. The crystal was grown at a pressure of 36.2 bar, the sound frequency was 5 MHz, the total path length 4.57 cm.





is wildly irreproducible one can see that repeated temperature cycling from 1.9 K to 1.3 K and up again improves the crystal, more so than a stay at constant temperature. The cause may be that the temperature gradients which are invariably produced when cooling and warming offer a preferred direction for the movement of the grain boundaries, and it appears therefore that annealing under a gradient yields better crystals. I would like to thank Len Vienneau for an illuminating discussion on these points.

Lee, Heybey and Crepeau have recently undertaken the same measurements, at a lower density, with crystals grown from superfluid helium by pressurization. They report (Heybey and Lee (1967)) that single crystals can be grown in less than five minutes. The reason is that the heat of solidification is carried away much more rapidly because of the high heat conductivity of the superfluid. Since many crystals are required for a determination of the orientation dependence of the sound velocity, the importance of quick crystal growth can hardly be over estimated. The disadvantage of this method is that only a very limited density range can be studied.

3.2 Optics

3.2.1 Birefringence

The crystal structure of solid He^4 was determined with x-rays (Keesom and Taconis, (1938), Mills and Schuch, (1961), Mills and Schuch, (1962), Schuch and Mills, (1962), Schuch and Mills (1963) and with neutron scattering (Henshaw (1958), Lipschultz et al. (1967), Minkiewicz et al. (1968) Brun et al. (1968), to be hexagonal close packed over the greater part of the phase diagram.

Because of the hexagonal symmetry helium is uniaxially birefringent which means that the index of refraction is different for light polarized parallel ($= n_e'$) and perpendicular ($= n_o'$) to the optic axis. The optic axis of a plate is the projection of the c-axis on the plate (figure 16). Plane polarized light will be split into two components and after passage through the plate they will have a phase difference ϕ

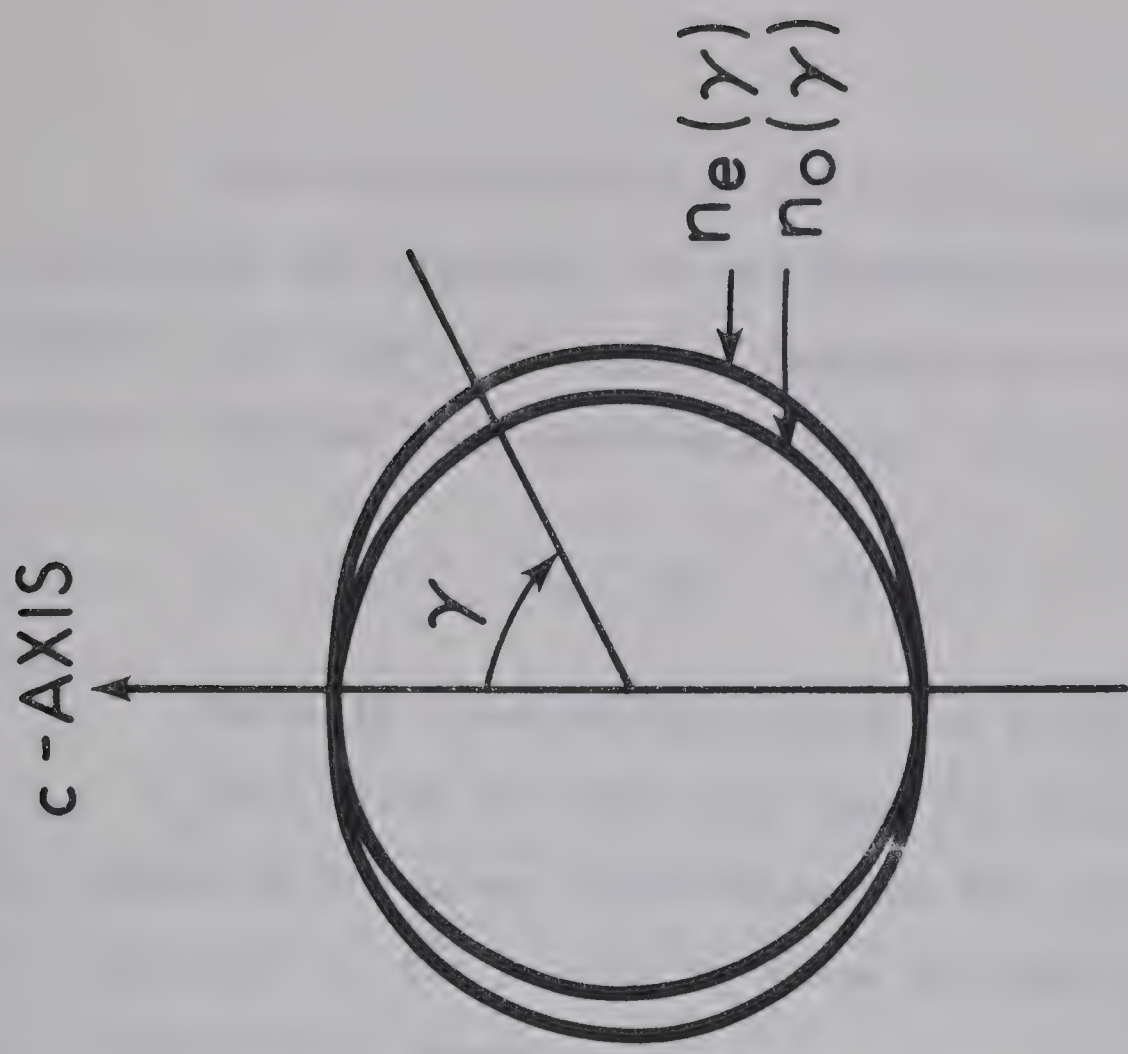
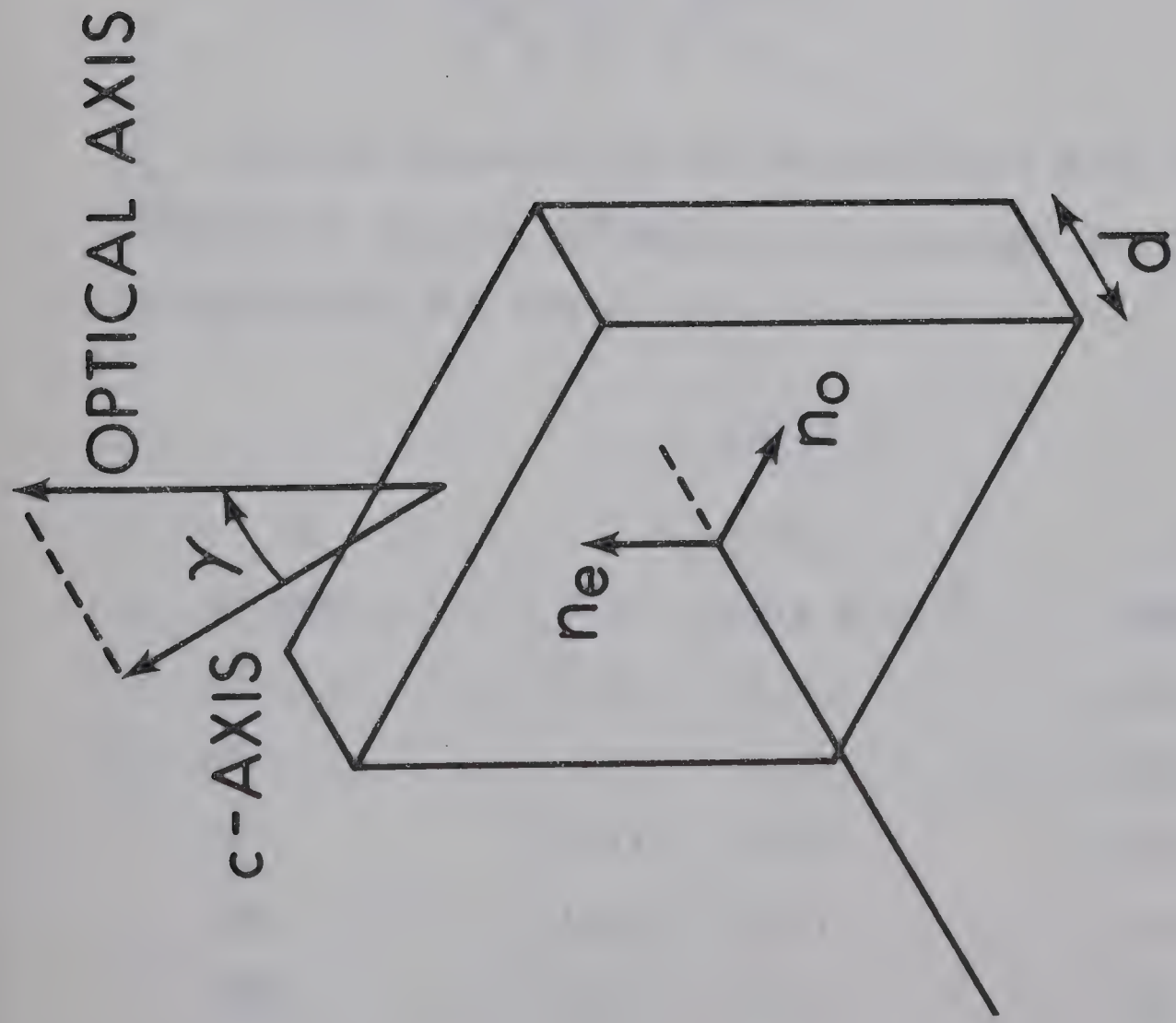
$$\phi = \frac{(n_e' - n_o') \cdot d}{\lambda} \quad 3.2$$

d is the thickness of the plate, λ the light wavelength. The resulting light is in general elliptically polarized. I will in the remainder of this chapter call any optical element that introduces a phase difference between two perpendicular components a phase plate and ϕ the retardation of the plate.

FIGURE 16

Birefringent plates





The difference in the refractive indices, $n'_e - n'_o$, depends on the direction of the lightbeam with respect to the crystal axis and in hexagonal crystals is a function of the angle γ between beam and c-axis only

$$n'_e - n'_o = (n_e - n_o) \cdot \sin^2 \gamma \quad 3.3$$

Strictly speaking this relation holds only for $|n_e - n_o| \ll 1$ which is certainly true for helium ($n_e - n_o \approx 10^{-6}$). By measuring the phase difference one can therefore determine the position of the c-axis in space and the angle γ if the birefringence is known:

$$\sin \gamma = \left(\frac{\phi \cdot \lambda}{(n_e - n_o) \cdot d} \right)^{\frac{1}{2}} \quad 3.4$$

$n_e - n_o$ was measured by Vos et al. (1967 b,c) for densities between 11 and 21 cm³/mole and by Heybey and Lee (1967) at 21 cm³/mole (see Table 1.).

TABLE 1

p	$n_e - n_o$	Ref.
25 atm	$2.6 \pm 0.1 \times 10^{-6}$	Heybey and Lee (1967)
26	2.8 ± 0.2	Vos et al. (1967 b)
30	2.76 ± 0.08	Vos et al. (1967 c)
72	2.91 ± 0.07	Vos et al. (1967 c)
140	3.42 ± 0.07	Vos et al. (1967 c)
1050	6.3 ± 0.5	Vos et al. (1967 c)

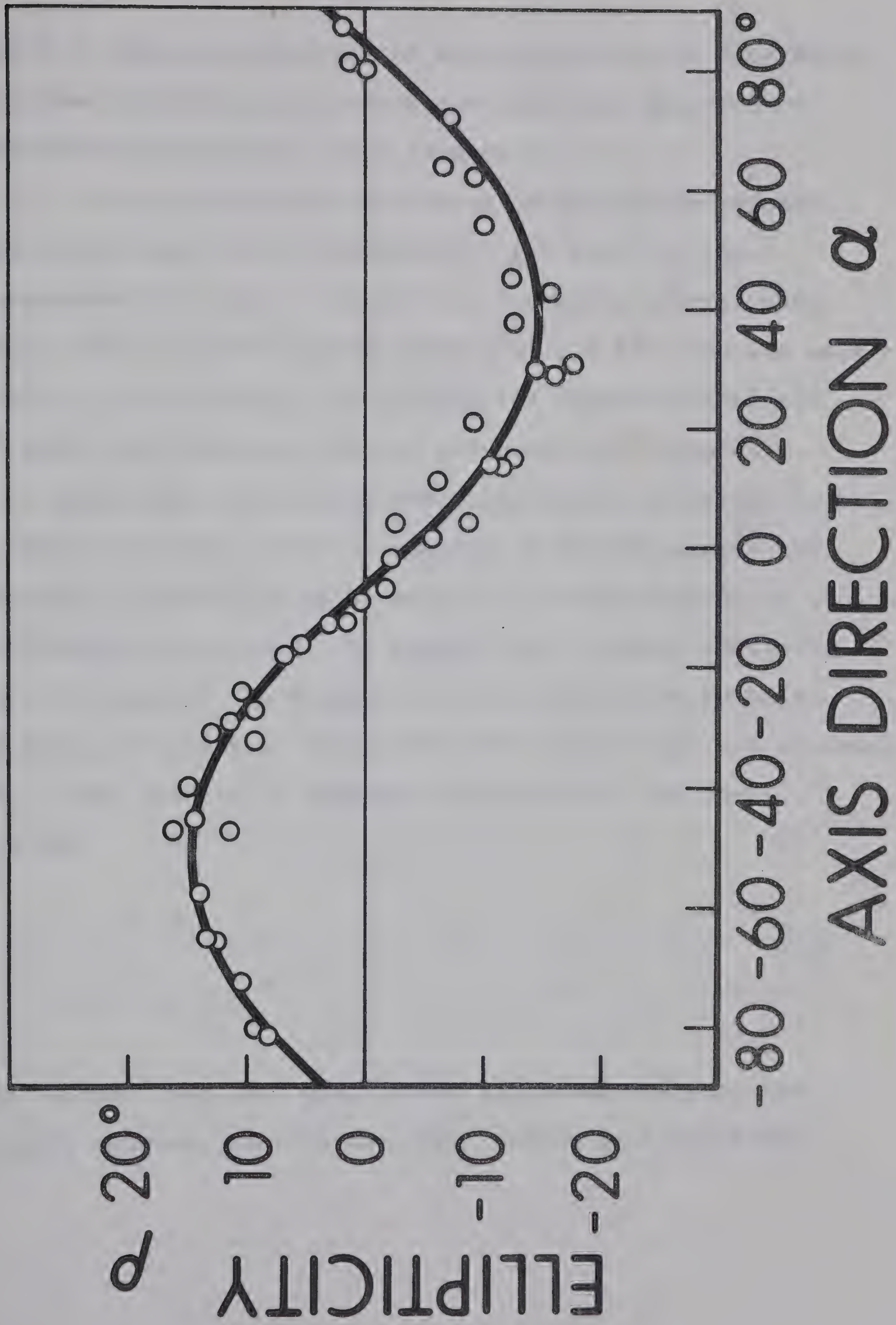
I want to emphasize at this point that it is a coincidence that we can use birefringence to orientate the crystals for ultrasonic work, since birefringence does not give us the position of the a-axes. Fortunately this is not required because of the cylindrical symmetry of the velocity surface in hexagonal materials. Cubic materials are neither birefringent nor do they have a simple velocity surface.

One can measure the retardation in principle with one of the many methods suggested in textbooks of optics. These methods become however inaccurate or unreliable in the presence of straylight of which we have plenty due to the two windows between the helium crystal and the analyzing equipment. I use therefore a similar procedure as Vos et al (1967 b). A plane polarized beam of arbitrary polarization vector is sent through the crystal. The resulting light is elliptically polarized. With a quarter wave plate and an analyzer I then determine the two parameters that characterize it, namely the direction α of the major axis of the ellipse (measured from some arbitrary zero direction fixed to the laboratory frame) and the ratio $\tan \rho$ of the minor and major axis. I plot these parameters for about 25 different directions of the initial polarization vector, each approximately 15° apart. The way α and ρ change with initial polarization obviously

FIGURE 17

Ellipticity and axis direction of elliptically polarized light.





depend on the properties of the plate, that is its retardation ϕ and the direction G of its optical axis and they can be inferred from the $\rho(\alpha)$ - plot (figure 7).

I now return to a more detailed description of the individual steps in this procedure. The first is the measurement of ρ and α . To do this I place a quarter wave plate, which is just a phase plate with $\phi = 90^\circ$ with its axis parallel to the axis of the ellipse and remove thereby the 90° phase shift between the two perpendicular components. After the quarter wave plate the elliptically polarized light is plane polarized. With an analyzer I then determine the direction of polarization by setting it perpendicular to it for complete extinction. Of course I do not know initially where the axis of the ellipse is and have to find by trial and error the position of quarter wave plate ($=m_1$) and analyzer ($=n_1$), that results in complete extinction of the light. I then get

$$\alpha = m_1$$

3.5

$$\rho = m_1 - n_1$$

This assumes that both quarterwave plate and analyzer are properly mounted, that is the zero reading on their scale

coincides exactly with their optical axis, but usually this is not so. Fortunately I get complete extinction for two different but symmetric settings of plate (m_1, m_2) and analyzer (n_1, n_2) and can use them to calculate and eliminate that error

$$\alpha = \frac{1}{2} (n_1 + n_2)$$

3.6

$$\rho = \frac{1}{2} (n_1 - n_2)$$

The next step is the calculation of the retardation ϕ and the axis direction G of the phase plate from the $\rho(\alpha)$ -plot. For this I make use of formulas given in Born (1965, p. 27) that relate the shape and position of an ellipse to the phase difference and amplitude of two perpendicular oscillations and find for $\rho(\alpha)$

$$\sin^2 2\rho(\alpha, \phi, G) = \frac{\sin^2 \phi \cdot \tan^2 2(\alpha - G)}{\cos^2 \phi + \tan^2 2(\alpha - G)} \quad 3.7$$

One can see that $\rho = 0$ for $\alpha = G$ and G can therefore be read directly from the plot. To find the retardation ϕ we note that

$$\sin^2 2\rho = \sin^2 \phi \quad \text{for} \quad \alpha = G + \frac{\pi}{4}$$

or

$$\phi = 2\rho \left(\alpha = G + \frac{\pi}{4} \right) \quad 3.8$$

A better way is to use the computer and find the parameters ϕ and G in equation 3.7 that give the best fit to the measured curve $\rho(\alpha)$. The problem has no analytic solution like many non linear least square fits and requires an iterative procedure.

The optical observation in polarized light allows also to decide whether I have grown a single crystal or not. Unfortunately I am too far away from the crystal, and the various windows and mirrors distort the image so much that I could not see the crystal directly. However, if more than one crystal is present it is impossible to find a setting of quarter wave plate and analyzer that results in complete extinction of the beam. Extinction could only be accomplished for one crystal and this setting would not block light of another polarization. The sensitivity of the criterion is given by the amount of stray light which I estimate at a few percent, so that stray crystals which cover less than a few percent of the field of view will go undetected.

Another indication of single crystals is the fact

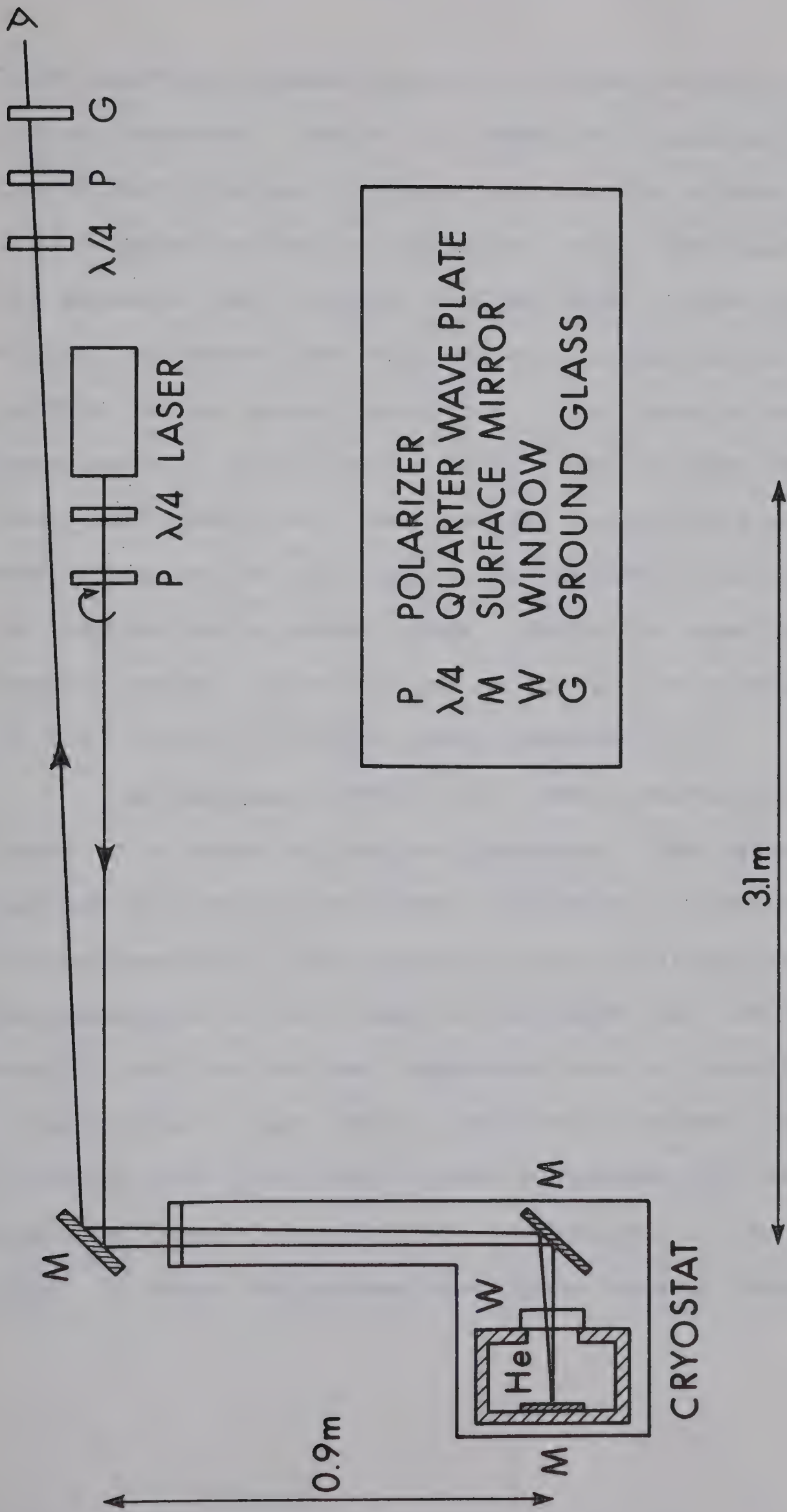
that the measured $\rho(\alpha)$ -curves obey the relationship 3.7 to within the accuracy of measurement of ρ and α . A large scatter is usually due to difficulties in locating the extinction setting and means therefore that more than one crystal is present. For single crystals the rms deviations from the curve are of the same order ($2 \dots 3^\circ$) as in the measurements with liquid helium in place of the solid.

3.2.2 Optical apparatus

Figure 18 is a diagram of the optical apparatus used to measure the retardation. The light of the Spectra Physics Laser (Mod. 130) is monochromatic with a wavelength of 632.8 nm, well collimated (beam spread $7 \cdot 10^{-4}$ rad) and plane polarized. The output power is 1 mW. Since the direction of polarization is fixed, a polarization rotator was built consisting of a quarter wave plate and a polarizer. The plate has its axis 45° from the polarization direction of the laser and produces therefore circular polarized light which is then plane polarized by a plastic sheet polarizer. The beam is then reflected into the cryostat by a mirror that can be rotated around a vertical axis and tilted around a horizontal axis with adjusting screws. The window is a glass disc of

FIGURE 18

Optics for the birefringence measurement (schematic)



12 mm aperture pressed against a rubber O-ring by the atmospheric pressure. Inside the cryostat is another mirror that can be turned around the same axis as the mirror on top and also adjusted around a horizontal axis. The beam then enters the pressure cell through a 12 mm thick window of fused silica, traverses the cell and gets reflected on the aluminized surface of the sound transducer. The incoming and outgoing beam are at a slight angle (5×10^{-3} rad) so that the outgoing beam just misses the laser and can be analyzed with a quarter wave plate and an analyzer. The extinction of the light beam is observed on a ground glass. Since the beam passes the crystal twice, its effective length in the crystal is doubled to 4.57 cm and so is the total phaseshift ϕ .

As mentioned before the simple mechanical arrangement leads to a number of optical problems. The reflection at the surface of a metallic mirror introduces a phase shift between the components of the electric vector that are parallel and perpendicular to the plane of incidence and the reflection coefficient for the two components are not exactly the same. I have tried to use totally reflecting prisms instead, because although they give also a phase difference for the two components at least the reflection coefficient is the same for both. I found the prisms unsuitable however because it was

difficult to keep the lower prism at constant and uniform temperature and it showed stress birefringence varying with time and temperature due to nonuniform thermal expansion of the glass.

If we are only interested in the state of polarization of a light beam and not its direction we can represent a mirror through a phase plate. Its axis is in the plane of incidence and its retardation is equal to the phase difference ϕ for reflection of parallel and perpendicular component and can be calculated from electromagnetic theory. The reason is that it does not matter for a mathematical description of the beam by which mechanism the shift has been produced in an element. (I have assumed here that the difference in reflection coefficient between the two components can be neglected. It is 7% for aluminum mirrors and its influence will be discussed later).

The problem is now how to measure the birefringence of a plate that can only be observed through a series of phase plates, two of it being the "mirror"-plates and one the high pressure window which might show stress induced birefringence.

Vos et al. (1967 b) have solved that problem when only one plate is present, namely the birefringent window. The solution is based on a matrix calculus invented by Jones

(1941 a,b,c) in which optical elements are represented by matrices and a series of elements by matrix products. It involves measuring the retardation ψ and the axis direction p of the combination of helium crystal and window and the retardation β and axis direction b of the empty cell. The retardation ϕ and axis direction g of the helium crystal alone is then

$$\cos \frac{1}{2}\phi = \cos 2(b-p) \cdot \sin \frac{1}{2}\psi \cdot \sin \frac{1}{2}\beta + \cos \frac{1}{2}\psi \cdot \cos \frac{1}{2}\beta$$

3.9

$$\sin 2(b-g) = \sin \frac{1}{2}\psi \cdot \sin 2(b-p) / \sin \frac{1}{2}\phi$$

This solution is easily adapted to the case of compound windows. Jones (1941 b) shows that a series of phase plates can be represented mathematically by one single phase plate and a rotation of the coordinate system. The rotation affects only the axis direction g of the crystal, in which we are not interested anyway, but otherwise the same formula as for the single window case apply, only β and b are now the retardation and axis direction of the whole optical system but without the helium crystal, or with liquid helium which is not birefringent.

3.2.3 Errors in the orientation measurement

The assumption made above that for metallic reflection the reflection coefficient is identical for components parallel and perpendicular to the incident plane needs some justification. It is very difficult to treat the whole optical system mathematically without making that assumption and I will therefore only examine what happens to the $\rho(\alpha)$ -curve of a single metallic mirror and an angle of incidence of 45° . Then I will verify experimentally that equation 3.9 can indeed be used for a train of mirrors. For an aluminum mirror at 45° incidence the retardation is 168° and the ratio of the reflection coefficients is 0.927.

The axis direction of the equivalent phase plate remains unchanged, since this involves only the reflection of one component, and the reflection coefficient for the other does not matter. If both incident components are equal, that is for $\alpha = G + 45^\circ$ and one of them is reduced by 7% more than the other through the reflection, this is equivalent to a rotation of the coordinate system by an amount $(\tan^{-1} 0.927) - 45^\circ$, in other words a distortion of the α -axis by a maximum of 2° . This is within the accuracy of measuring α .

For the experimental verification I put a mica phase plate at room temperature in place of the helium crystal and

measure its phase difference through the cryostat. Giving it 3 different orientations gave the same results within 1° and agreed with a direct measurement to within 1° . The retardation of that plate was 28° . With a 67° -plate, consistency was again 1° and the deviation from the direct measurement 2° . The total retardation β of the empty cryostat was 32° at room temperature.

During the actual run β changed to 80° and the empty cryostat had to be measured at frequent intervals. This could be due to formation of an oxide layer on the mirror or a change of the complex refractive index of the bottom mirror with temperature, and an uncertainty of 5° for ϕ is probably more realistic. The corresponding error in the orientation γ is greatest for $\beta = 0^\circ$ and $\beta = 90^\circ$ since $d\gamma/d\phi$ is infinite there. This is an unfortunate aspect of the birefringence method since these are just the direction of prime interest. Around $\gamma = 10^\circ$ and $\gamma = 80^\circ$ the uncertainty is of the order of $\pm 10^\circ$, going down to $\pm 5^\circ$ at $\gamma = 45^\circ$.

The error due to the uncertainty of crystal thickness is negligible compared with this, but the uncertainty in the birefringence $n_e - n_o$ of about 3% contributes 1° at $\gamma = 45^\circ$, going up to 7° at $\gamma = 70^\circ$.

3.3 Ultrasonics

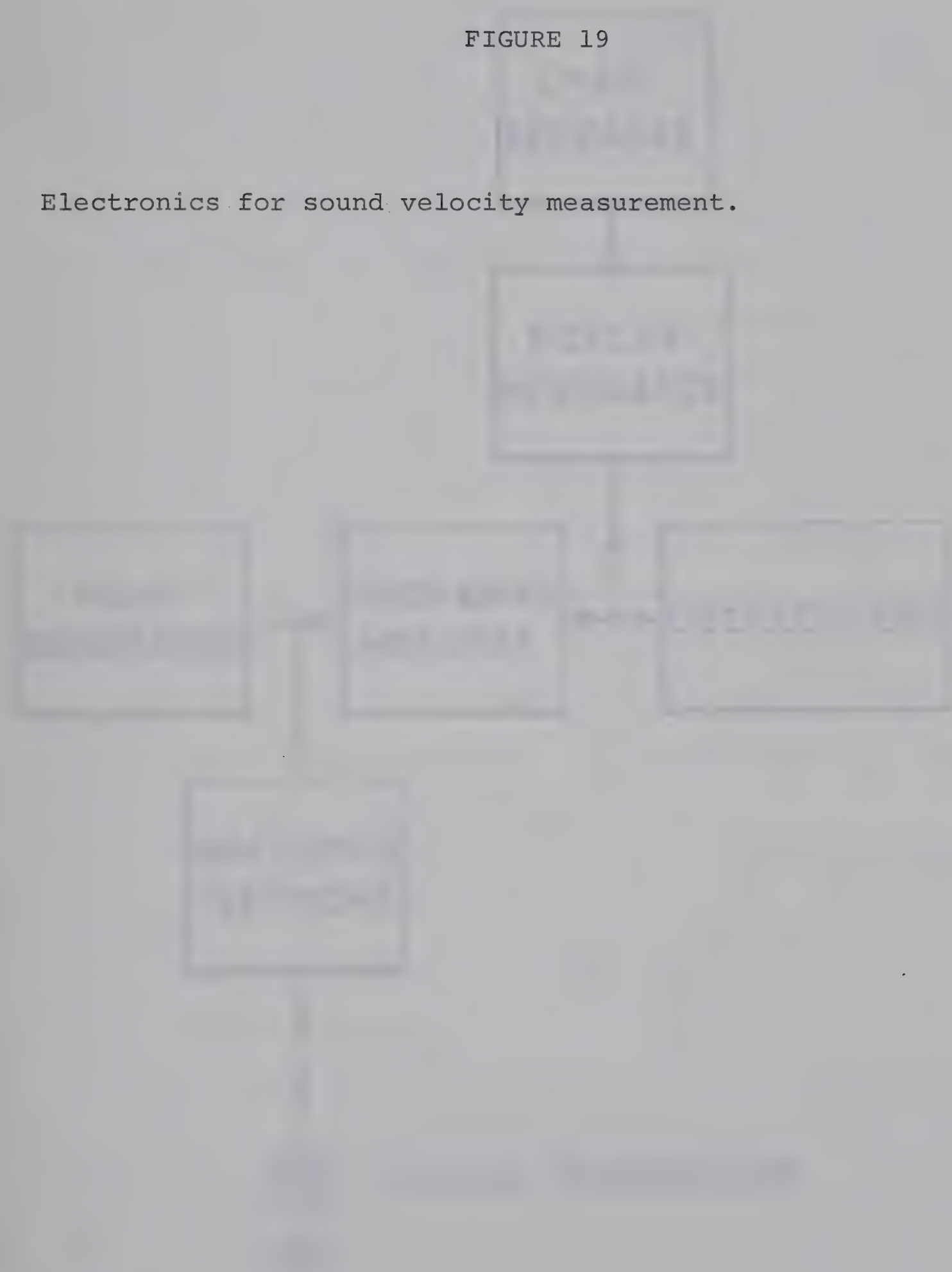
3.3.1 Electronics

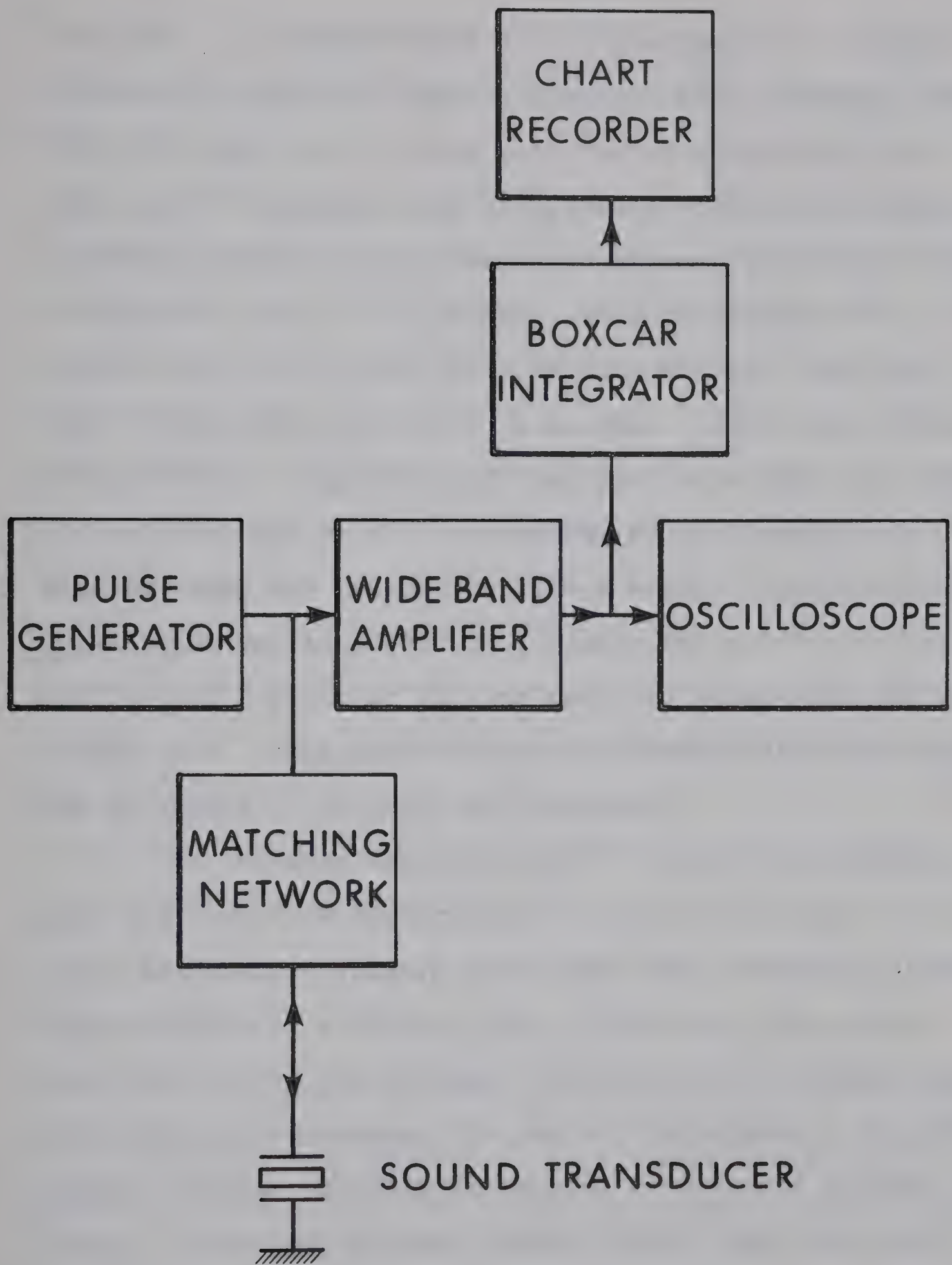
The sound velocity was measured with the pulse echo method. A high frequency pulse of 10 MHz and 150 V_{pp} amplitude is applied to a piezoelectric quartz crystal of 12 mm diameter for 2 μ sec with a pulse repetition frequency of 100 Hz. The transducers for longitudinal sound are x-cuts, for transverse I use AC-cut plates. The transducers resonate mechanically at that frequency and send a sound pulse through the helium which is reflected, travels back and is picked up again by the same transducer which converts it into an electrical signal. The time delay between the initial pulse and the echos is measured with the calibrated delayed sweep of an oscilloscope. The total path length is obtained from a flight time measurement in liquid helium and the known sound velocity of liquid helium (Vignos and H. Fairbank 1966). I have also determined this velocity at 4.13 K in the pressure range from 20 to 50 bar by measuring the cell dimensions at room temperature with a micrometer and get values which are higher by about 0.2%, which is well within the combined errors.

Figure 19 is a schematic diagram of the circuitry. All components except the matching network are commercially

FIGURE 19

Electronics for sound velocity measurement.





available. As pulsed oscillator I used part of a Sperry Ultrasonic Comparator (Sperry Products Inc., Danbury, Conn.). The pulse amplifier of that unit failed repeatedly and I replaced it therefore with an Arenberg wideband amplifier (Arenberg Ultrasonic Laboratory, Jamaica Plain, Mass.) with a bandwidth from 0.7 to 70 MHz. This corresponds to a rise time of about 0.02 μ sec which is much smaller than the rise time of the pulse generator (0.1 μ sec). After amplification the pulses are rectified and displayed on a Tektronix Model 556 oscilloscope which is triggered by the Sperry unit. Its delayed sweep was calibrated with a crystal controlled counter (Transistor Specialities Inc., Plainview, L.I.) of a rated accuracy of 3 parts in 10^7 and found to agree with the dial to within 0.1%. This calibration was repeated after one year and no change in accuracy was observed.

To increase the accuracy of the time measurement I read the time from the trigger to the leading edge of as many echos as possible (always more than two) and made a linear least square fit through a plot of time vs. echo number. The slope then gives the averaged time between two echos while the intercept represents the sum of the delays in the electronic circuits probably associated with finite trigger rise times. A similar although smaller effect was also seen by Vignos and H. Fairbank (1966) who attribute it to a delay in the conversion of mechanical into electric signal. It is of

the order of 1 or 2 μsec in our case, depending on the time base setting of the oscilloscope and can therefore not be neglected.

The accuracy of the time measurement is limited to 0.1 μsec by the risetime of the pulses and to 0.1% by the resolution of the dial of the calibrated sweep. Since the velocity data used to calculate v are accurate to 0.3% I estimate the absolute error in v to be about 0.5%. Using the same equipment, the resolution of the time measurement can be increased by displaying with high time resolution (0.05 $\mu\text{sec}/\text{cm}$) a portion of an unrectified echo with fixed delay and observing the phase shift of the echo. The jitter in the delayed sweep of 0.01% sets the limit for the sensitivity. I found it convenient to record the shape and amplitude of the echos during crystal growth. This was done with a boxcar integrator (Princeton Applied Research, Princeton, N.J.) and a chart recorder (figure 20).

3.32 Matching

The impedance of the quartz transducer at resonance is of the order of 1 MOhm in parallel with the electrode capacitance C of 10 pF, while the impedances of amplifier and

oscillator are around 50 Ohms. The capacitance represents a short circuit to the high frequency pulse and a much higher oscillator amplitude is required than if C were absent. The usual procedure is to put an inductance in parallel and tune the resulting LC-circuit to resonate at the mechanical resonance of the transducer, but this has the disadvantage to require critical tuning, which may not survive during cooling of the apparatus and more seriously, it works only for one frequency. A solution which solves both this problem and the mismatch between oscillator and transducer is found from transmission line theory (Skillig (1951), p. 337 ff). This theory says that a transmission line can be used as an impedance transformer if its length is comparable to the wavelength of the electromagnetic wave that it transmits. At 10 MHz the wave length is about 20 m, and since the coax cable between equipment and transducer is 3 m that is the case. The complex input impedance Z_L of a cable with cable impedance Z_0 and length a for a load Z_L and a wave vector k is given as

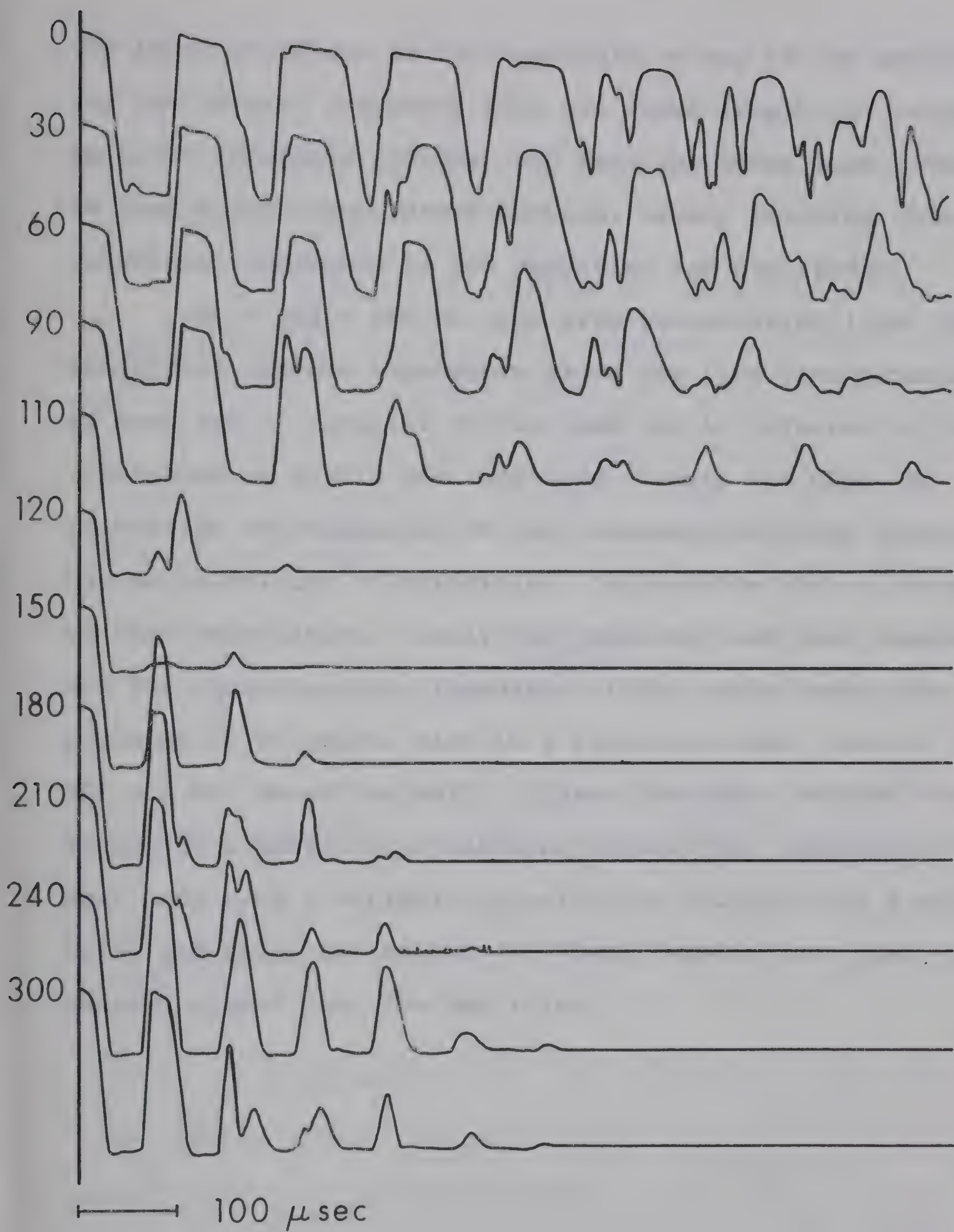
$$Z_i = Z_0 \left(1 - \frac{Z_0 - Z_L}{Z_0 + Z_L} e^{-2ika} \right) / \left(1 + \frac{Z_0 - Z_L}{Z_0 + Z_L} e^{-2ika} \right)$$

Various graphical ways exist to evaluate this expression (Smith (1944)). The first thing to do is to calculate

FIGURE 20

Sound echos in liquid and solid helium during crystal growth

The elapsed time since the start of growth is given in minutes beside each chart recorder trace. Between 0 and 90 min the echos correspond to propagation in liquid helium. After 10 min. a small echo from solid helium is observed and grows to reach a maximum amplitude at 240 min. In order to observe the small echos in solid helium the amplifier gain was set very high. The smaller sound absorption in liquid helium then yields echos so large that the amplifier saturates and they appear with a clipped off top and constant amplitude on the recorder trace. The irregular shape of the multiple echos is not well understood but may be due to resonance and interference effects in the amplifier.



the input impedance of the coax cable on top of the cryostat for the desired frequency from its known length and characteristic impedance (50 Ohm) and from the known load. The rest is then a room temperature problem, namely matching this calculated impedance to the amplifier and oscillator.

This again can be done with transmission lines by connecting various impedances along the line from generator to load and in parallel to the load and is referred to in the literature as double stub matching. Again the place of connection and magnitude of the necessary matching impedances can be calculated in principle. In practice the parameters of that calculation, namely the generator and load impedance and the characteristic impedance of the cable inside the cryostat (# 39 copper wire in a stainless steel tube of 0.8 mm ID) are not known too well. I have therefore adapted the basic layout of a double stub matching network and terminated the stub ends with a variable capacitor or inductor and find by trial and error the setting of these terminations that yield maximum signal into the amplifier.

4. RESULTS

4.1 Sound velocity in hcp He⁴ as a function of crystal orientation.

The velocity of longitudinal sound for different orientations was measured for pressures of 36, 58 and 128 bar. Table 2 gives total path length $2x1$, birefringence $n_e - n_o$ (Vos et al. 1967 c), molar volume V and melting temperature T_m (Grilly and Mills, (1959), (1962)) for these experiments.

TABLE 2

p (bar)	2x1 (cm)	$n_e - n_o$ ($\times 10^{-6}$)	V (cm ³ /mole)	T_m K
36.0 \pm 0.1	4.57 \pm 0.01	2.77 \pm 0.08	20.32 \pm 0.01	1.949 \pm 0.005
58.0 \pm 0.1	4.09 \pm 0.01	2.85 \pm 0.08	19.28 \pm 0.01	2.524 \pm 0.005
128.0 \pm 0.1	7.17 \pm 0.02	3.35 \pm 0.08	17.33 \pm 0.01	3.924 \pm 0.005

The first experiments at 58 and 128 bar were done with the preliminary bomb. Only two points were measured at 128 bar, both giving the same orientation $\gamma = 46^\circ$ and velocity $v_1 = 748\text{m/sec}$. At 58 bar a total of 60 crystals were grown (figure 21). The large scatter in the data, which is outside

the estimated error in velocity and orientation is probably due to an unsatisfactory optical arrangement that could not detect polycrystals. The light beam has to pass 3 mirrors between laser and helium crystal and it is likely that it is cut off at the edges and does not cover the whole cross section sampled by the sound beam. The criterion of total extinction to establish whether a single or polycrystal is present then loses its power and the data suggest that it fails frequently in this arrangement. If another criterion is chosen for the quality of the crystals namely the number of echos that could be detected, the picture improves somewhat. (Black dots in Figure 21 are samples that showed more than 6 echos). In any case it is clear that the two points at 128 bar have to be regarded with caution.

I designed therefore another sample container with a copper bottom that should provide a better nucleation point than the quartz window of the preliminary cell and had a horizontal optical path which reduced the number of mirrors to 2, and thereby increased the success rate for single crystals from 5% to 50%. A further improvement would be to have windows in the side of the cryostat and eliminate the mirrors altogether. This is also the set-up chosen by Lee's group (Lee et al. (1969)), and it allows direct visual in-

FIGURE 21

Longitudinal sound velocity in hcp He^4 , $V = 19.28 \text{ cm}^3/\text{mole}$.

Full circles are from crystals with more than 6 echos.



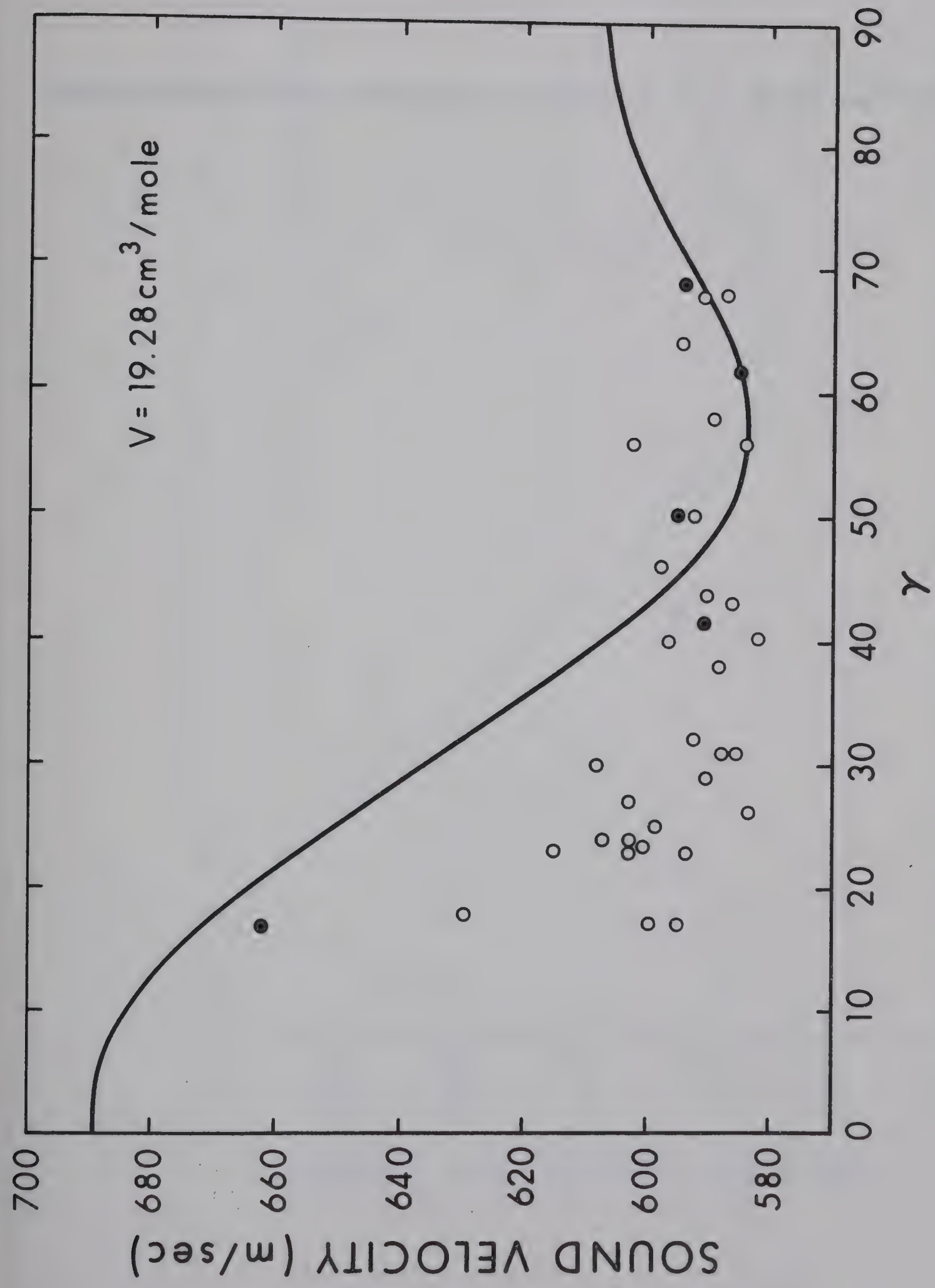


FIGURE 22

Longitudinal sound velocity in hcp He^4 , $v = 20.32 \text{ cm}^3/\text{mole}$.



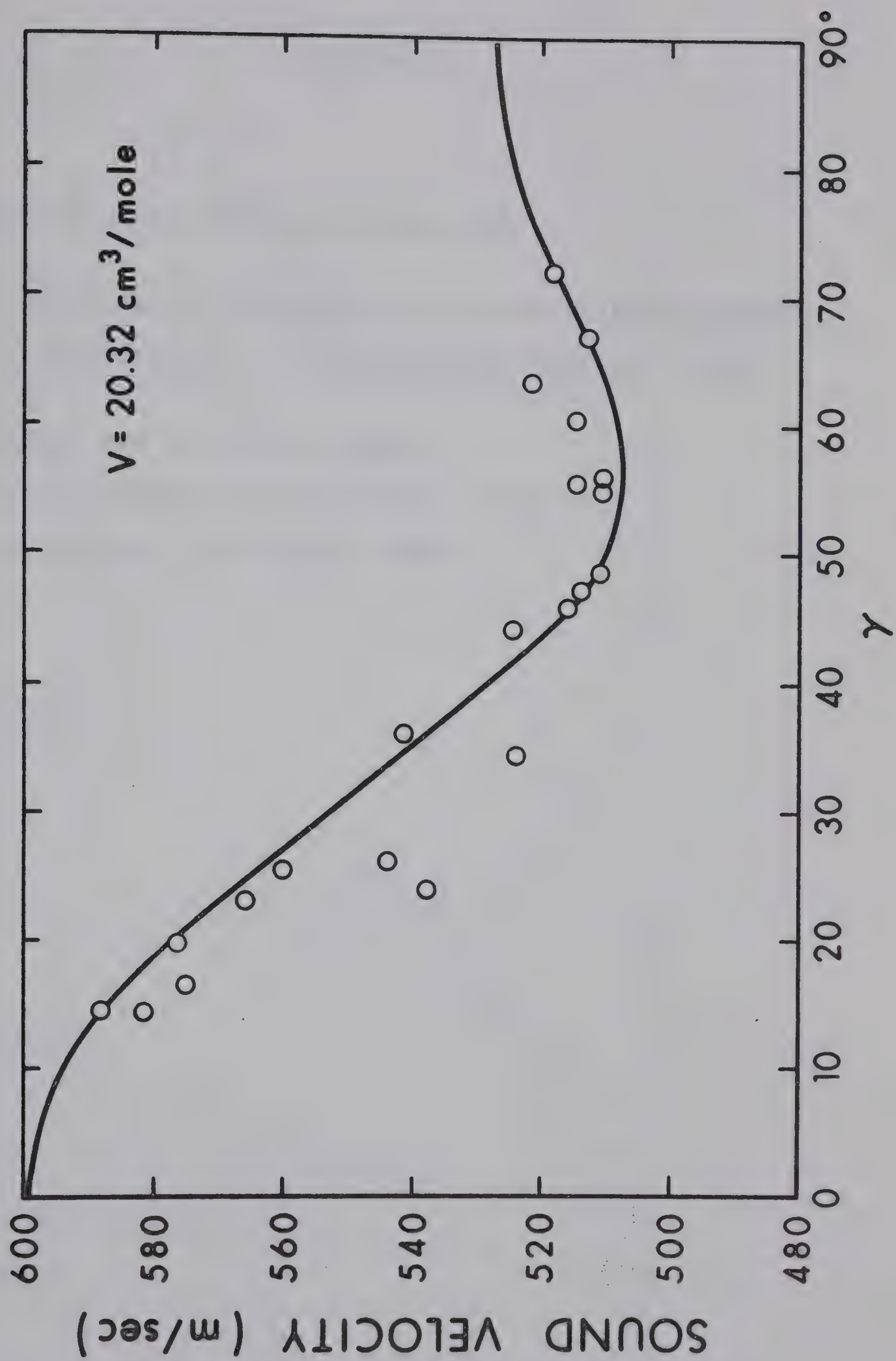


FIGURE 23

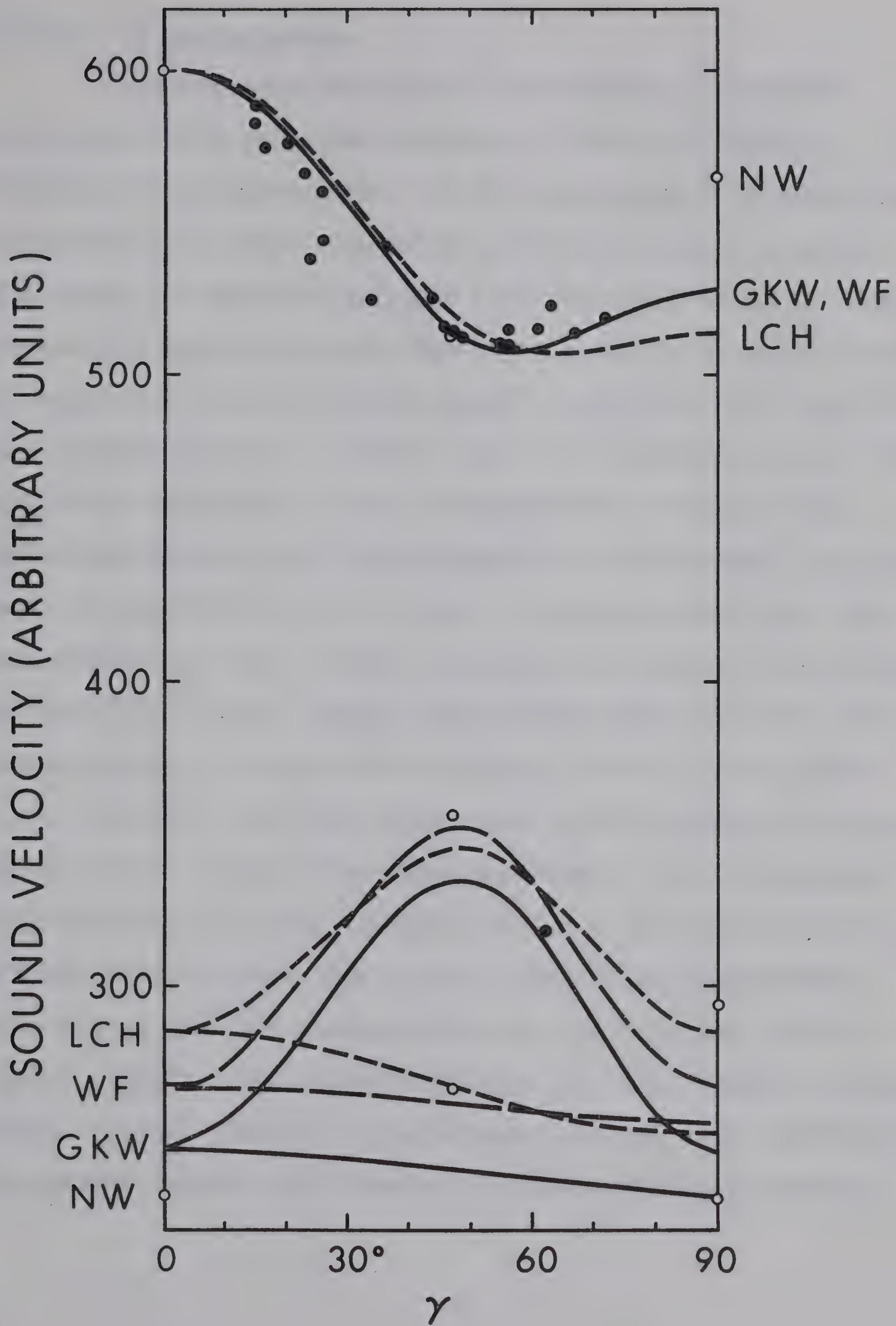
Anisotropy of sound velocity in hcp He^4 .

All velocities are multiplied with a normalization factor to give a longitudinal velocity of 600 m/sec at $\gamma = 0$.

NW Nosanow and Werthamer (1965)

GKW Gillis, Koehler and Werthamer (1968)

LCH Lee, Crepeau and Heybey (1969)



spection of the crystals.

With this new container I have grown 42 crystals (figure 22) at a pressure of 36 bar. For 25 of these I determined the orientation. Of the remaining 17 crystals, 10 showed only one sound echo of an intensity that was smaller by a factor 10 or more compared with the other samples. Three samples had small spurious echos with a delay of about 80% of the delay for the first echo, which I interpret as a reflection from a grain boundary. Since there is a discontinuity in the wall of the container at the corresponding distance (the window hole pierces through the wall) it may be that crystal growth is disturbed at this point. Three samples were lost through melting when I tried to anneal them very close to the melting temperature. Three more samples were lost for other reasons, such as running out of liquid helium in the dewar.

When it turned out that some of the remaining 25 points showed scatter larger than expected from an error analysis, their growth record was re-examined and I found that one had drifted 1% in velocity during the orientation measurement. Three others had the lowest number of echos of all the 25 samples, namely 3 and I rejected them so that finally 21 points remain. These criteria are arbitrary and are only justified because the scatter gets smaller as the demands on crystal

quality are raised.

The measured anisotropy of the longitudinal sound velocity can be compared with Lees measurements at a smaller density (Lee et al., 1969) (Figure 24) and with two theoretical calculations (Nosanow and Werthamer (1965), Gillis et al. (1968)). As a guide to the eye, I have drawn a line in Figure 22 which represents the calculations of Gillis et al. for a molar volume of $19.2 \text{ cm}^3/\text{mole}$, but multiplied all their velocities with 0.915 to get a best fit to the measured points. Figure 23 includes in addition the results of Lee et al. and of Nosanow and Werthamer, all multiplied by a scale factor to give a velocity of 600m/sec for $\gamma = 0$. I have thereby assumed that the anisotropy is the same for different molar volumes. Within the limited accuracy of this measurement there is quantitative agreement between all four results, with the measurements being slightly in favour of the calculations of Gillis et al. Also shown in figure 23 are transverse velocities, multiplied by the same scale factors. Our results, calculated from the elastic constants obtained in section 4.3 are between the experimental results of Lee et al. (1969) and the theoretical results of Gillis et al. (1968) and have qualitatively the same dependence on the angle γ . For clarity, the data of Nosanow and Werthamer are shown for the directions

[0001], $[01\bar{1}0]$ and $[01\bar{1}1]$ only ($\gamma = 0^\circ, 90^\circ$ and $46^\circ 41'$).

I have measured the transverse velocity and orientation in one sample at 36.0 bar and get 319 m/sec at $\gamma = 62^\circ$. With the scale factor chosen for a best fit to the longitudinal velocity, this point agrees well with the theoretical and scaled down velocity of Gillis et al. (1968) and also with the velocity calculated from our elastic constants.

To my knowledge this is the first observation of transverse sound in a He^4 crystal that was not prepared from the superfluid. Growing crystals from superfluid helium is thought to be the easiest method and to give the best single crystals and from my experience it is more difficult to observe transverse sound than longitudinal. This may be the reason for the lack of observations of transverse sound above 29 bar. Lipshultz and Lee (1965) have measured transverse velocities in unoriented samples around 25 atm and obtain values between 230 m/sec and 315m/sec and Lee et al. (1969) finds 225m/sec for the smallest and 309m/sec for the biggest velocity in oriented crystals at the same pressure.

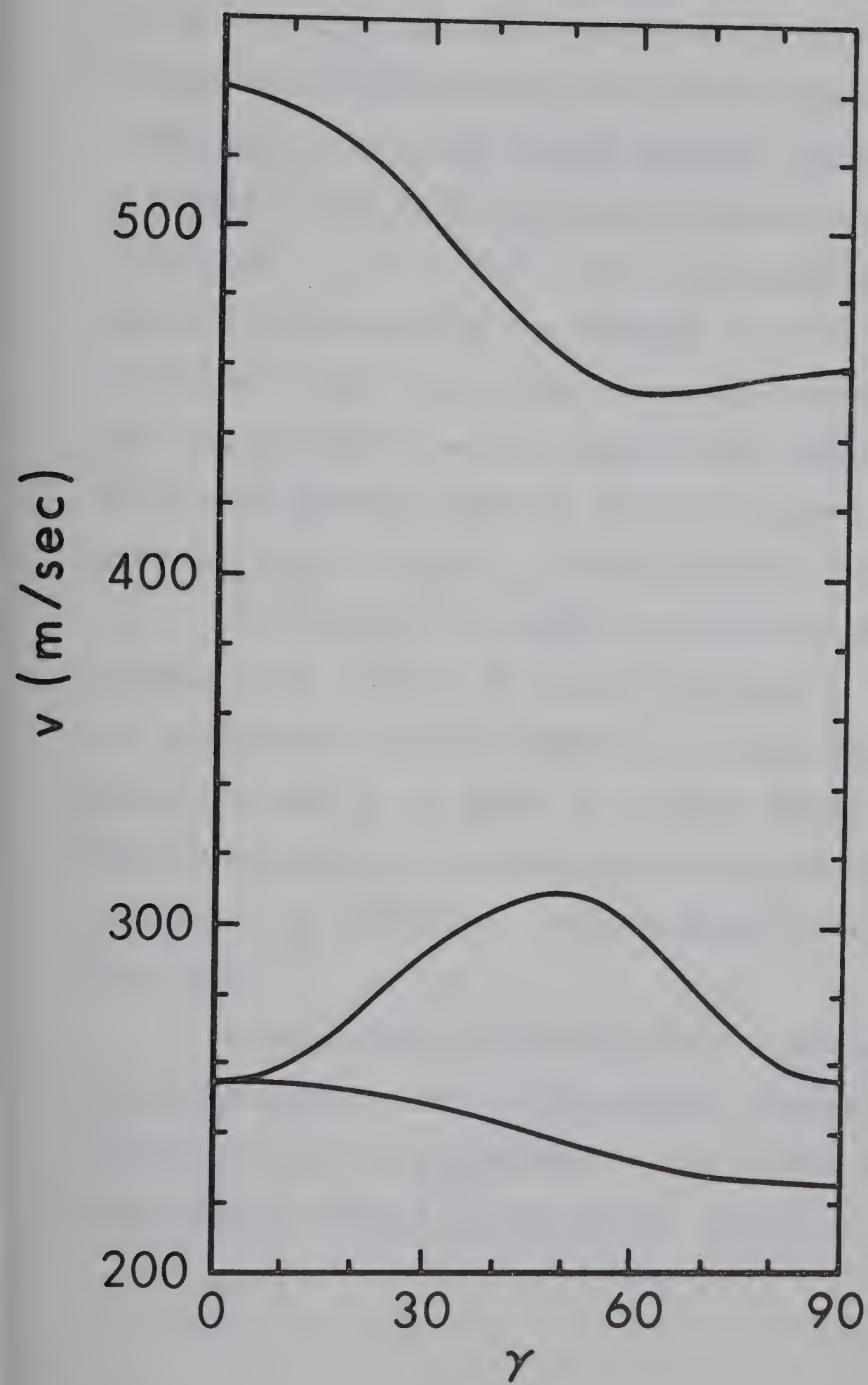
To answer the question whether the observed anisotropy in hcp He^4 is in any way unusual, I have calculated the velocity surface of all 16 hexagonal crystals for which the elastic constants are available (Landolt-Börnstein, (1966)). It turns

FIGURE 24

Sound velocity in hcp He^4 , according to Lee et al. (1969)

$v = 20.97 \text{ cm}^3/\text{mole}$.





out that there is some correlation between the ratio of the crystallographic axes c/a (Crystal Data, 1963) and the shape of the velocity surface. This ratio is obtained from x-ray or neutron diffraction and is 1.63 for hcp He⁴, nearly identical to the ratio for close packed spheres, $c/a = (83)^{\frac{1}{2}} = 1.63299$. In crystals that have the same c/a as helium, such as Co (1.62), Mg (1.62) or Ice (1.63), the anisotropy is qualitatively the same with the highest velocity occurring in the direction of the c -axis and a minimum around 55° . This is also the case for a simple theoretical model of a hexagonal solid with harmonic springs between nearest neighbours, for which $c_{11}:c_{12}:c_{13}:c_{33}:c_{44} = 29:11:8:32:8$ (Leibfried, (1955)).

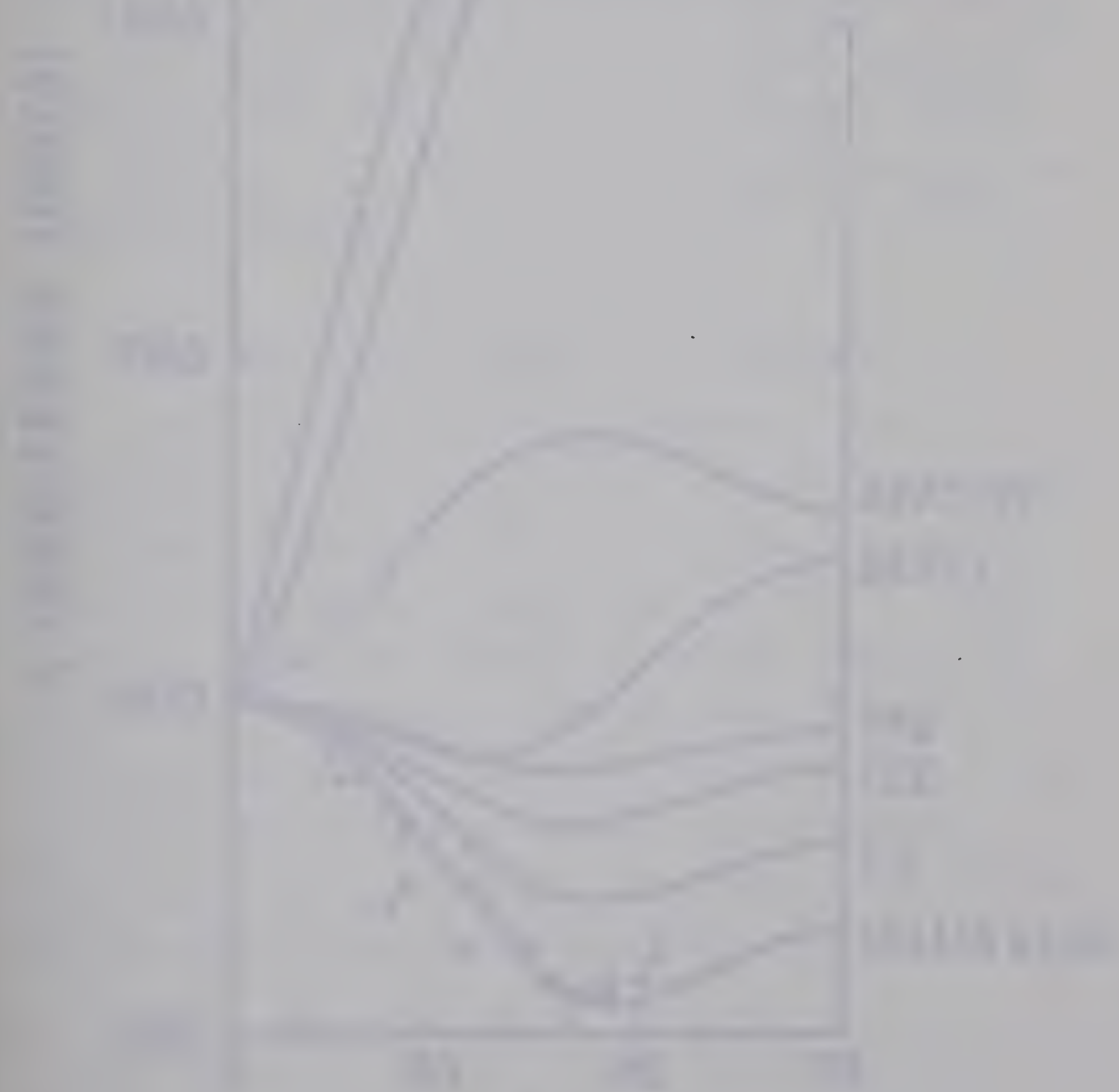
In crystals for which c/a deviates much from 1.63, for example in Cd (1.88), Zn (1.86), Apatite (0.73) or Beryl (1.00), the anisotropy is quite different (figure 25) and it appears therefore that it is given to a large extent by the shape of the elementary cell and not so much by the exact nature of the interparticle potential. Helium seems to be no exception to that rule.

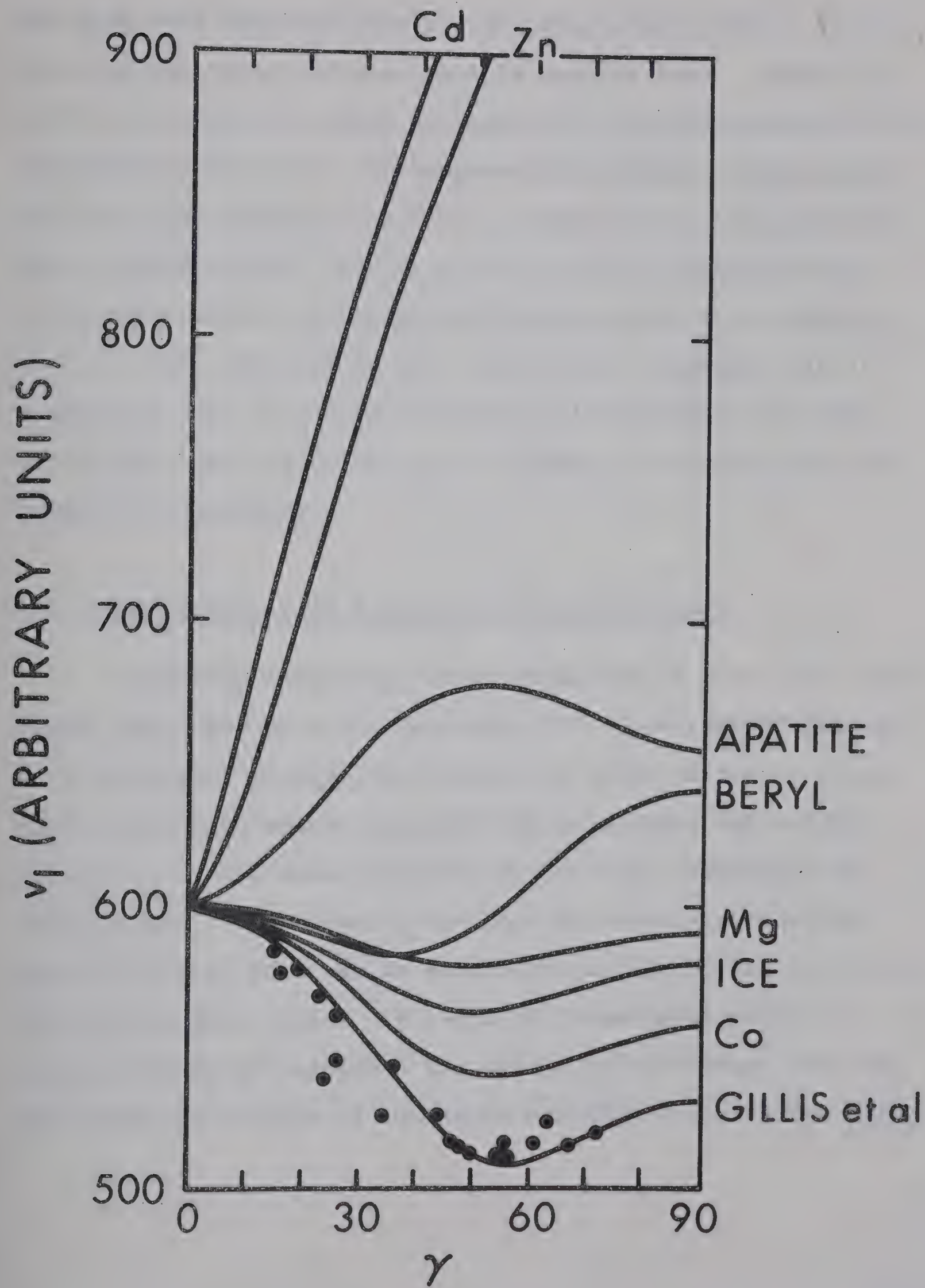
I conclude this section with a comment on growth in preferred directions. If the single crystals would grow or recrystallize from polycrystals in a random way, the number of measurements would be proportional to $\sin \gamma$, that is, we would

FIGURE 25

Longitudinal sound velocity in hexagonal crystals.

All velocities are multiplied with a normalization factor to give a longitudinal velocity at $\gamma = 0$ of 600m/sec.





see much more crystals with $\gamma = 90^\circ$ than with $\gamma = 0^\circ$. It is obvious from figure 22 that this is not the case. Growth in preferred directions might be induced by irregularities at the nucleation point or by the temperature gradient during growth and annealing which in our case is perpendicular to the direction of observation. If the c-axis would be preferentially along the gradient we again would measure much more crystals with $\gamma = 90^\circ$, which we do not. All we can therefore say at present is that we observe nonrandom distribution of orientation and that the c-axis is not likely to coincide with the temperature gradient.

4.2 Sound velocity as a function of molar volume

The compressibility of solid helium is about 10^3 times higher than that of sodium or about 10^5 times that of diamond. It is therefore possible to reduce the molar volume of helium appreciably with modest pressure and to measure the volume dependence of the sound velocity or of other properties of solid helium. The former is perhaps the most stringent experimental test that can be applied to lattice dynamics in the long wave length limit. It should be remembered that its primary aim is to calculate the energy of the solid, and that the volume derivative of the sound velocity involves the third

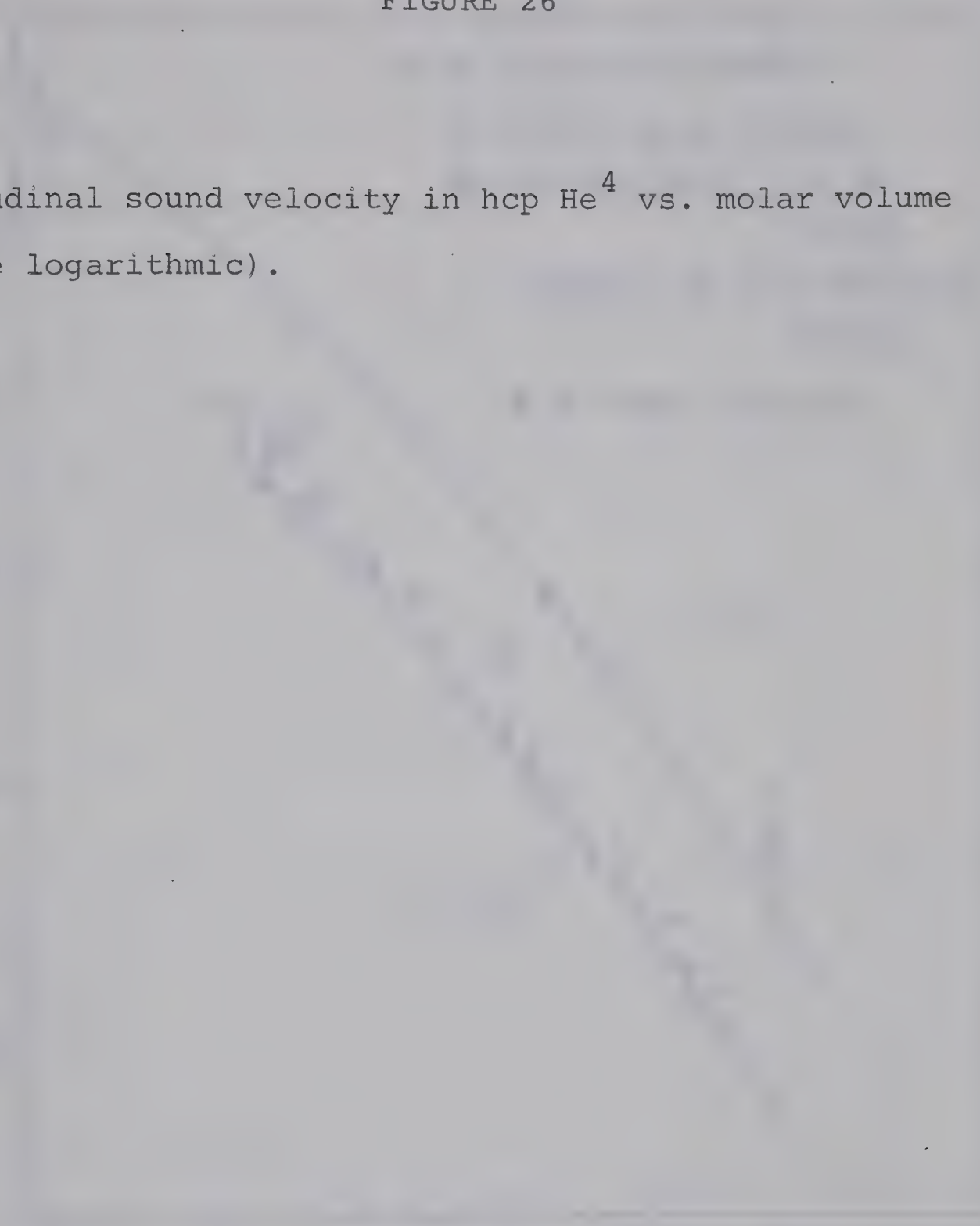
derivative of energy with respect to volume (the first gives the pressure, the second the compressibility).

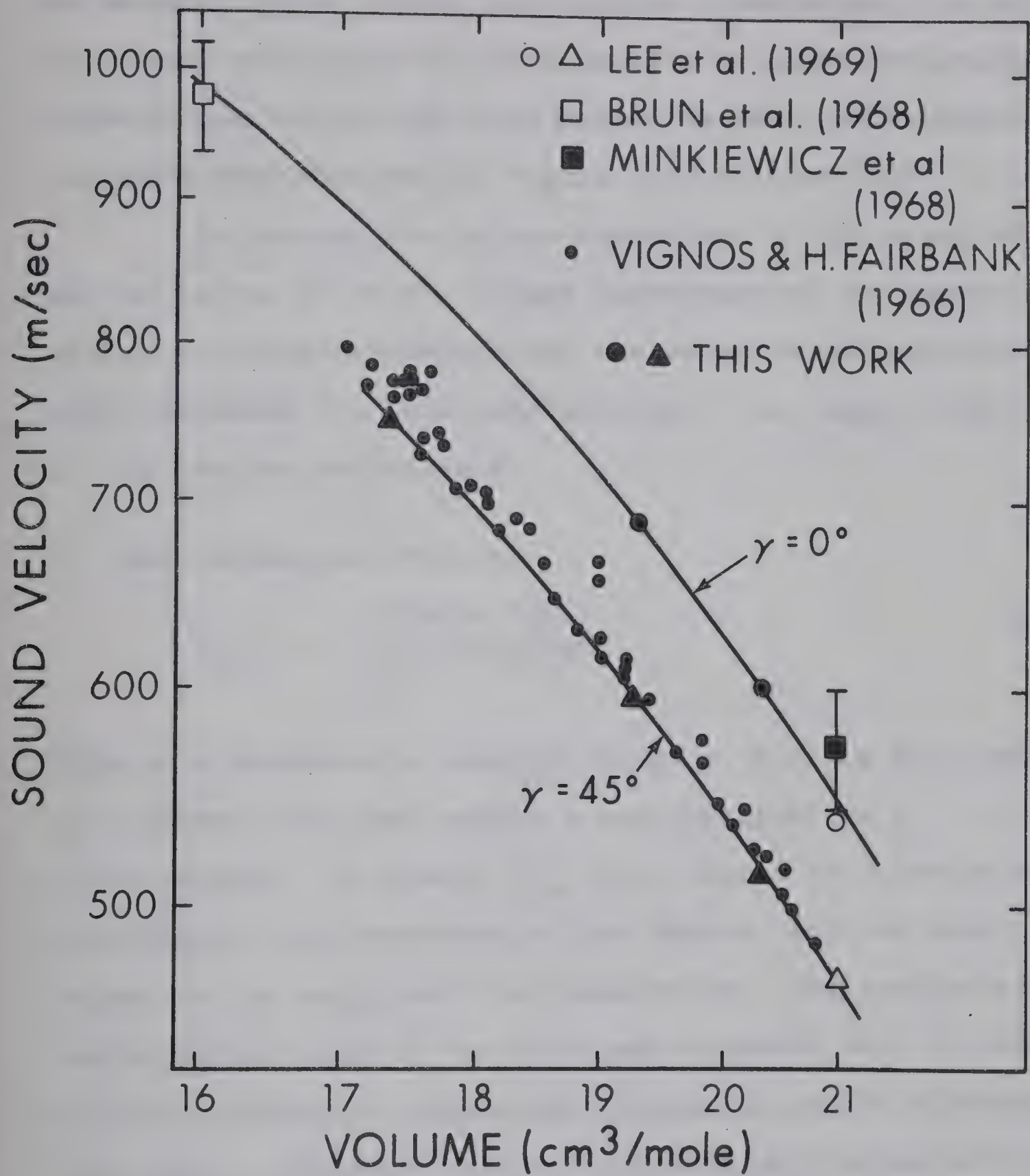
In figure 25 I compare the measured sound velocity along the c-axis ($\gamma = 0$) and at $\gamma = 45^\circ$ from the c-axis with values observed by Lee et al. (1969 b) at a molar volume of 20.97 cm^3 . Also shown are sound velocities calculated with equation 2.38 from the phonon spectrum of hcp single crystals. This was obtained from inelastic neutron scattering by Minkiewicz et al. (1968) at $V = 21.1 \text{ cm}^3/\text{mole}$ and by Brun et al. (1968) at $V = 16.0 \text{ cm}^3/\text{mole}$. The black dots represent measurements by Vignos and H. Fairbank (1966) on polycrystals or possibly single crystals of unknown orientation.

The different measurements agree within the error limits although the sound velocities of Lee et al. (1969) seem to be somewhat low. I have therefore calculated the Debye temperature from their elastic constants and obtain $\theta_0 = 2,58 \text{ K}$ which is also lower than Edwards and Pandorfs value of 26.1 K at that volume. The Bulk modulus K^{-1} obtained from equation (2.36) is also 10% lower than measured by Jarvis et al. (1968). The data of Vignos and H. Fairbank show a smaller anisotropy than our measurements. The explanation may be that the largest velocities occur in directions around the c-axis, and these directions have a small probability of occurring if

FIGURE 26

Longitudinal sound velocity in hcp He^4 vs. molar volume
(double logarithmic).





we assume crystal growth with random orientation. In addition the lower velocities are associated with large deviations between wave vector and beam direction and could therefore not have been observed by Vignos (see section 2.3).

To discuss the volume dependence of the sound velocity and to relate it to the volume dependence of the Debye temperature, the compressibility and the second sound velocity I will introduce the Grüneisen constant γ and begin with a review of its various definitions:

1) Mode Grüneisen constant

$$\gamma_{q,s} = - \frac{d \log \omega(q,s)}{d \log V} \quad 4.1$$

This is a microscopic quantity where $\omega(q,s)$ is the frequency of a phonon with wave vector q and polarization s . V is the molar volume. In general $\gamma_{q,s}$ will depend on orientation, polarization and frequency of the phonon, and the molar volume of the solid and the temperature. The various macroscopic definitions of the Grüneisen constant will be averages in which different frequencies, polarizations or orientations will have a different weight, depending on the macroscopic quantity.

Grüneisen's assumption was that in a lowest approxi-

mation all modes would have the same volume dependence, in which case the various definitions of γ will all give the same value. In a real solid, this need not be so, nor will the Grüneisen constants be independent of volume or temperature.

2) Grüneisen constant from sound velocity

In the long wave length limit, where there is no dispersion and

$$\omega(q,s) = q \cdot v_s \quad 4.2$$

we find

$$\gamma_s = - \frac{d \log v_s}{d \log V} + \frac{1}{3} \quad 4.3$$

where v_s is the sound velocity in direction q . γ_s depends on direction and polarization s ($= l, t_1, t_2$).

3) Grüneisen constant from Debye temperature

$$\gamma_D = - \frac{d \log \theta_0}{d \log V} \quad 4.4$$

θ_0 is the Debye temperature at absolute zero. This is the quantity usually referred to without specification in the solid helium literature. Expressing θ_0 in terms of sound

velocities

$$\theta_0 \propto V^{-\frac{1}{3}} \left(\sum_S v_S^{-3} \cdot d\Omega \right)^{-\frac{1}{3}} \quad 4.5$$

and differentiating with respect to $\log V$ we get

$$\gamma_D = \frac{\sum_S \int \gamma_S \cdot v_S^{-3} d\Omega}{\sum_S \int v_S^{-3} d\Omega} \quad 4.6$$

Under the assumption of elastic isotropy and for a typical case of $v_t = \frac{1}{2} v_l$ (v_l and v_t being the longitudinal and transverse velocities) one gets,

$$\gamma_D = (16\gamma_t + \gamma_l) / 17 \approx \gamma_t \quad 4.7$$

Since the transverse modes contribute much more to the Debye temperature than the longitudinal, the Debye Grüneisen constant will also reflect their dominance.

4) Grüneisen constant from compressibility:

$$\gamma_k = - \frac{d \log v_k}{d \log V} + \frac{1}{3} \quad 4.8$$

where v_k is a quantity with the dimension of a velocity defined as

$$v_k = (\rho \cdot K)^{-\frac{1}{2}} \quad 4.9$$

ρ is the density, K the compressibility at absolute zero. K can be expressed in terms of the elastic constants which in turn are obtained from the sound velocities. If we know their volume derivatives. γ_k can be calculated exactly. For the isotropic case

$$\gamma_k = (\gamma_l \cdot v_l^2 - \frac{4}{3}\gamma_t v_t^2) / (v_l^2 - \frac{4}{3}v_t^2) \quad 4.10$$

The above relations all concern the behaviour of long wave length phonons at 0 K and do not depend on any assumptions about the equation of state, while the next definition does.

5) Grüneisen constant from thermal expansion

$$\gamma_\alpha = - \frac{\alpha \cdot V}{K \cdot C_V} = \frac{V}{C_V} \cdot \left(\frac{dp}{dT} \right)_V \quad 4.11$$

It can be shown by thermodynamic arguments (Edwards and Pandorf, (1965)) that γ_α is independent of temperature and equal to γ_D if the specific heat can be written in the form $C_V(T,V) = f(T/\theta_0)$ where θ_0 is a function of V only.

6) Grüneisen constant from second sound

$$\gamma_{II} = - \frac{d \log v_{II}}{d \log V} + \frac{1}{3} \quad 4.12$$

Since the second sound velocity depends on the first

sound velocity (equation 2.39) in such a way that the transverse velocities are weighted even heavier than in the Debye temperature, we would expect that γ_{II} would be very close to γ_t , but nothing definite can be said before the anisotropic case is calculated.

The experimental information on Grüneisen parameters is collected in table 3. We note that both the compressibility and the Debye temperature give values for γ_D and γ_k that are lower at smaller molar volumes. This is in agreement with the volume dependence of the sound velocity which also decreases with smaller molar volume as can be seen from figure 26, and also with the neutron diffraction data at $16.03 \text{ cm}^3/\text{mole}$, which shows the decrease of the slope $d \log v / d \log V$.

The Grüneisen parameter for longitudinal sound that we observe is the same for the two directions of propagation that were investigated and is $\gamma_l = 3.0 \pm 0.1$ for a volume of 20 cm^3 . This is larger than the Debye Grüneisen parameter $\gamma_D = 2.6$ at this density. We can ask how large the transverse γ_t would have to be to give the correct Debye Grüneisen constant γ_D and I find, by trying different values of γ_t in equation 4.6 that $\gamma_t = 2.54$. I have assumed that γ_t is the same for both transverse branches and independent of orientation. Let

TABLE 3

Grüneisen constants of hcp He⁴.

Parameter		Density Range	Reference
$\gamma_{\text{longitudinal}}$ ($\gamma = 0^\circ$)	3.0 ± 0.1	19...21 cm ³	This work
$\gamma_{\text{transverse}}$ ($\gamma = 45^\circ$)	3.0 ± 0.1	19...21	This work
γ_D	2.6 ± 0.05	16.5...21	Edwards and Pandorf (1965)
γ_D	2.4	12...16	Dugdale and Franck (1964)
γ_D	2.5	12...20	Heltemes and Swenson (1962)
γ_D	$1.02 + 0.083.V$	13.7...20.5	Ahlers (1967)
γ_k	2.8...3.2	16.5...21	Edwards and Pandorf (1965)
γ_k	2.4	12...16	Dugdale and Franck (1964)
γ_k	3.06	17.5...21	Jarvis et al. (1968)
γ_k	1.6 - 2.0	6...12	Stewart (1963)
γ_α	2.5...2.9	17.5...21.0	Jarvis et al. (1968)
γ_{II}	2.9	17.5...20.5	Ackerman and Guyer (1968)

us now calculate the volume dependence of the compressibility, based on $\gamma_l = 3.0$ and $\gamma_t = 2.54$. To do this I calculate the sound velocities at two volumes V and $V + dV$, (using the anisotropy of Gillis model), from these the elastic constants and the compressibilities from equation 2.36 and finally v_k from equation 4.9 for both volumes. I obtain $\gamma_k = 3.2$ which compares well with values obtained from measured compressibilities at 20 cm^3 (table 3). The observed volume dependence of the longitudinal sound velocity is therefore consistent with calorimetric data.

The work of Jarvis et al. (1968) has shown that the assumption that solid helium obeys a reduced equation of state, that is $C_V(T,V) = f(T/\theta_0(V))$, is not justified and therefore no simple comparison can be made with the parameter γ_α , derived from thermal expansion measurements. It is also not clear why the parameter from the second sound velocity, $\gamma_{II} = 2.9$, differs so much from γ_t , but more detailed work on second sound, both experimental and theoretical, is needed to discuss this point further.

We finally compare the volume dependence of the longitudinal sound velocity with theoretical calculations of Nosanow and Werthamer (1965) (NW) and of Gillis, Koehler and Werthamer (1968) (GKW). For simplicity, figure 27 shows only the

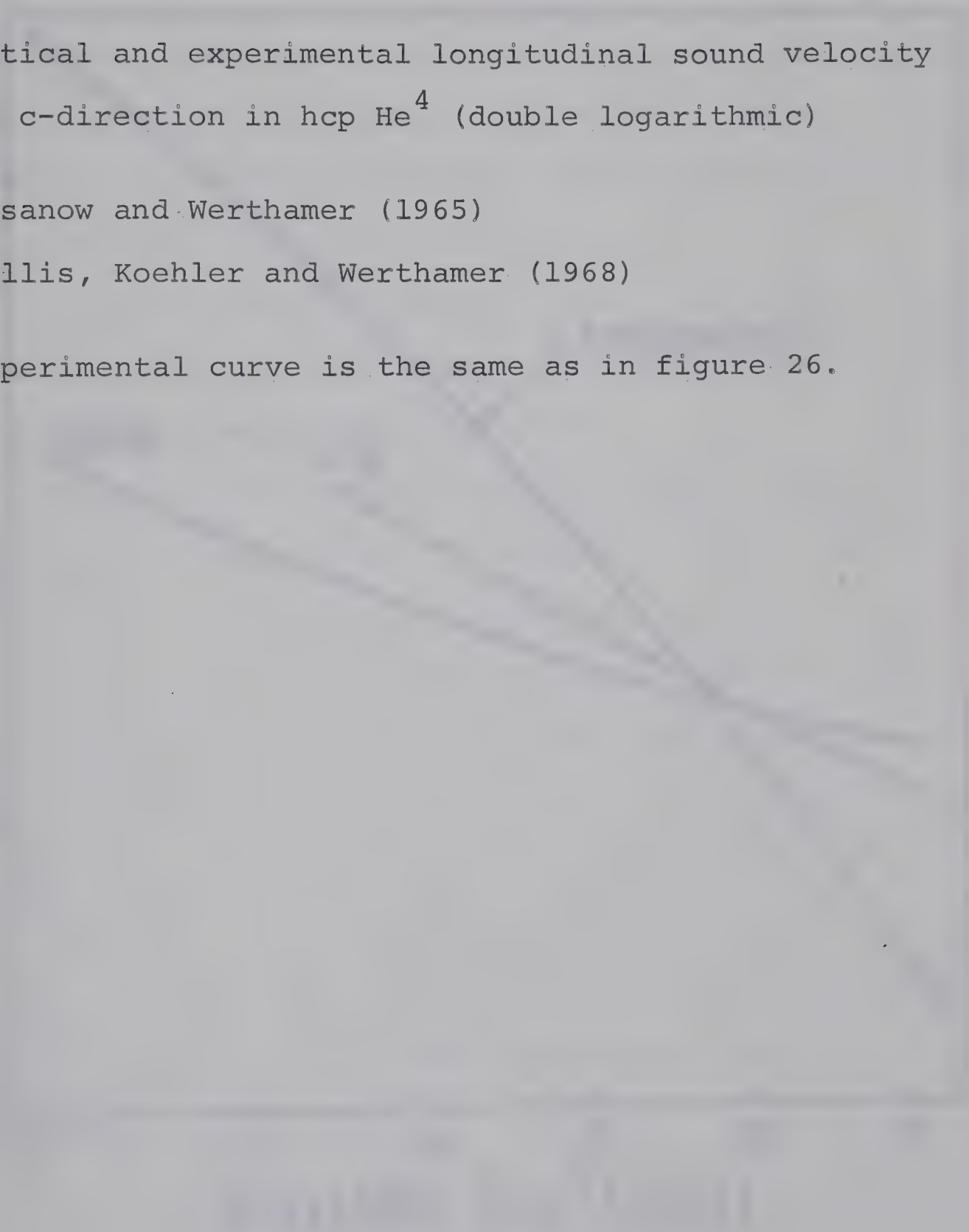
FIGURE 27

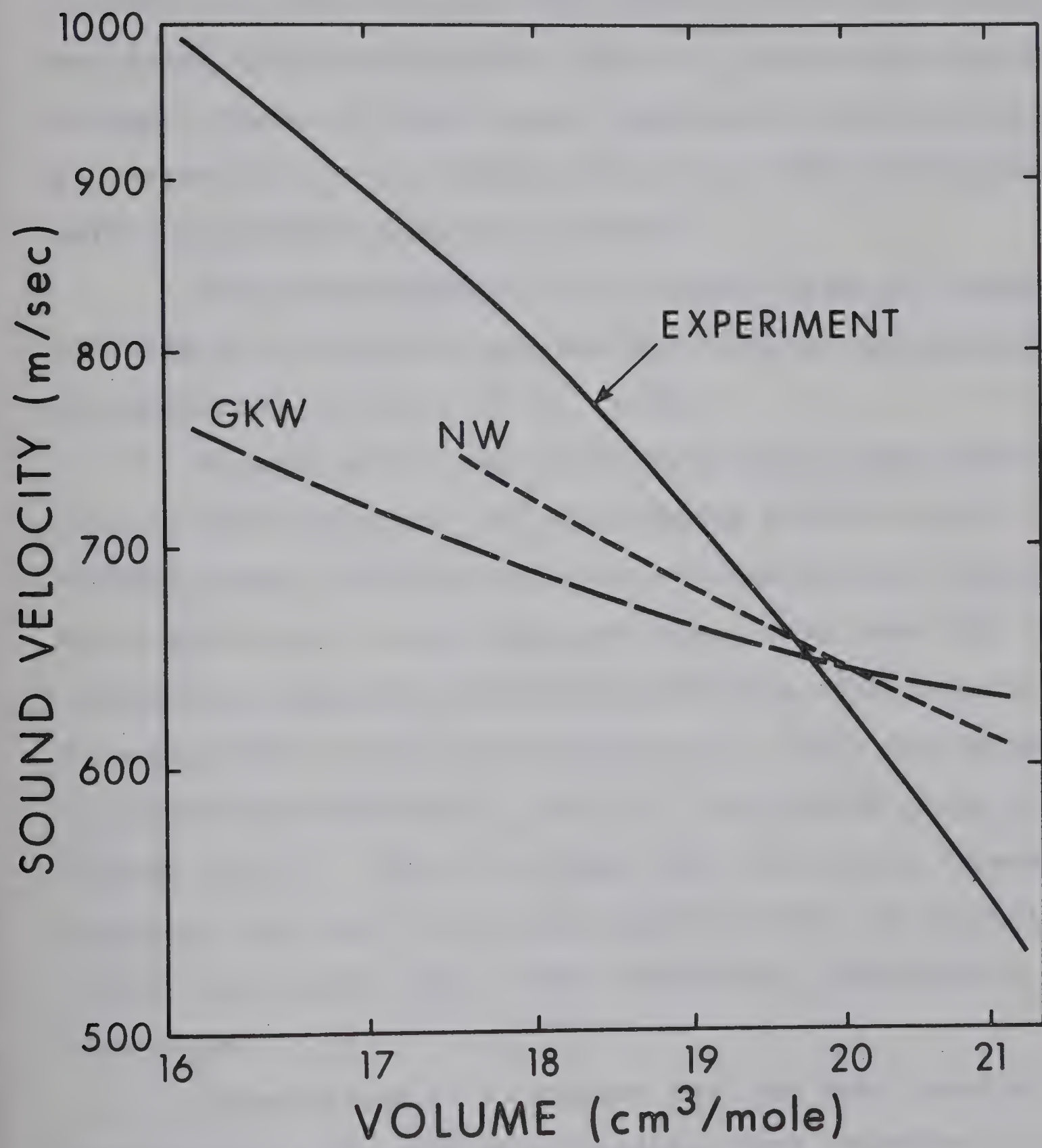
Theoretical and experimental longitudinal sound velocity
in the c-direction in hcp He^4 (double logarithmic)

NW Nosanow and Werthamer (1965)

GKW Gillis, Koehler and Werthamer (1968)

The experimental curve is the same as in figure 26.





velocities in the direction of the c-axis. We see that both theories agree well with the observation at a molar volume of 20 cm^3 , but also that the volume dependence is not satisfactory and leads to discrepancies of 20% in v_1 at high and low molar volume. Stated in other words, the theories predict Grüneisen parameters of $\gamma_1 \approx 0.7$ (GKW) and $\gamma_1 \approx 1.0$ (NW) in disagreement with our observed value of $\gamma_1 = 3.0$.

Which approximation in the theory is mainly responsible for this is not clear at present and different possibilities are discussed by Gillis et al. (1968):

In both calculations 3-particle short range correlations were neglected. We would expect that at smaller volumes, where the motion of the particles is more restricted, these would play a more important role. They have been included in a calculation of sound velocities at different densities for bcc He^3 by de Wette et al. (1967) and change the Grüneisen parameter γ_1 from 1.0 (only 2-body terms included) to 1.3. They also found that the cluster expansion converges less well for the hcp phase so that the inclusion of 3-body terms might lead to more significant improvements in this phase.

Nevertheless it is thought that the main cause of the discrepancy is the particular analytic form (equation 2.13) of

the correlation function f , which has the advantage of producing a quickly converging cluster expansion. A better correlation function would improve the theory at small volumes and at the same time lead to a better convergence, which is needed for the hcp phase. Work in progress on this problem has been reported at the Aspen Quantum Crystal Conference (1967) by Horner and Guyer and Nosanow.

Another approximation to be checked is the interparticle potential which may not be well represented by a Lennard-Jones potential (Munn and Smith, (1965)). However since the large zero point motion produces an average over this potential its detailed behaviour is probably of minor importance.

4.3 The elastic constants of solid helium

Of the five elastic constants of a hexagonal crystal, only four (c_{11} , c_{13} , c_{33} , c_{44}) determine the longitudinal sound velocity; c_{12} can only be determined from the pure transverse mode. Of these four constants only two can be obtained directly from the present set of measurements with sufficient accuracy: c_{11} from the longitudinal velocity in the basal plane and c_{33} from the longitudinal velocity in the c -direction.

To determine the remaining constants we may use the longitudinal velocity at $\gamma = 45^\circ$, published data for the compressibility and a relation between four of the elastic constants that holds for all hexagonal crystals provided they do not change their shape under hydrostatic pressure.

Solid helium satisfies this condition very well at least up to a pressure of 1100 bar and probably beyond as can be seen from the observed variation of the ratio c/a of the crystallographic axes with pressure (table 4). The most accurate determination of c/a comes from birefringence measurements because these are sensitive to deviations from the ratio for close packed spheres, $c/a = 1.63299$, while neutron and x-ray diffraction experiments measure c and a separately. The c/a ratios calculated by Vos et al. (1967 b, 1967 c) using the theory of Kronig and Sonnen (1958) change only by 3 parts in 10^4 for a volume change from 12.5 to 20.6 cm^3/mole . This implies that the linear compressibility (the relative decrease in the length of a line when the crystal is subject to hydrostatic pressure) must be the same in the c -direction and in the a -direction in solid helium. The expression for the linear compressibility in a hexagonal crystal is (Nye (1964), p.146)

TABLE 4

Ratio of the crystallographic axes c/a for hcp He^4

Pressure (atm)	Volume (cm^3/mole)	c/a	Method *	Reference
26	20.9	1.632 ± 0.005	B	Vos et al. (1967 b)
30	20.6	1.6320	B	Vos et al. (1967 c)
72	18.8	1.6323	B	Vos et al. (1967 c)
140	17.0	1.6324	B	Vos et al. (1967 c)
1050	12.5	1.6324	B	Vos et al. (1967 c)
29.7	20.66	1.628 ± 0.009	X	Mills and Schuch (1962)
129	17.4	1.627	X	Schuch and Mills (1963)
129	17.4	1.597 ± 0.005	X	Quoted by Keller (1969)
66	18.51	1.63 ± 0.03	N	Henshaw (1958)
66	18.51	1.612 ± 0.004	N	Recalculation by Donohue (1959)
25	21.1	1.638 ± 0.003	N	Minkiewicz et al. (1968)
227	16.03	1.6288 ± 0.001	N	Brun et al. (1968)

* B Birefringence

X X-ray diffraction

N Neutron diffraction

$$\beta(\gamma) = \frac{(c_{33} - c_{13}) - (c_{33} + c_{13} - c_{11} - c_{12}) \cdot \cos^2 \gamma}{(c_{11} + c_{12})c_{33} - 2c_{13}^2} \quad 4.13$$

where γ is the angle between c-axis and the direction of the line. The condition $\beta(0) = \beta(90^\circ)$ leads to

$$c_{33} + c_{13} - c_{11} - c_{12} = 0 \quad 4.14$$

and the volume compressibility K_0 becomes now

$$K_0 = 3 / (c_{33} + 2c_{13}) \quad 4.15$$

From published values for K and the previously determined constants c_{11} and c_{33} we obtain c_{13} from equation 4.15 and then c_{12} from equation 4.14. The three constants c_{11} , c_{13} and c_{33} together with the longitudinal velocity at $\gamma = 45^\circ$ finally yield c_{44} from equation 2.33.

Values for the isothermal compressibility in the density range of interest have been published by Edwards and Pandorf (1965) and by Jarvis et al. (1968). Since the temperature dependence of Edwards and Pandorf's isothermal compressibilities is in conflict with the measurements of Jarvis et al. and also with our measurements on the temperature dependence of the sound velocity, we consider Jarvis data more reliable. We find by interpolation of their measurements to

the densities of our measurements for the compressibility at 0 K, $K_0 = 0.309 \times 10^{-8} \text{ cm}^2/\text{dyn}$ at $V = 20.32 \text{ cm}^3/\text{mole}$ and $0.218 \times 10^{-8} \text{ cm}^2/\text{dyn}$ at $19.28 \text{ cm}^3/\text{mole}$. The corresponding velocities at $\gamma = 45^\circ$ are 517 m/sec and 596 m/sec, respectively. A correction would have to be applied to all velocities to get the elastic constants at 0 K because of the variation of the velocities with temperature. This correction of about 0.2% however is small compared with the errors in v_1 and is therefore ignored. The full set of elastic constants obtained in this way is shown as a function of molar volume in figure 28. Table 5 gives numerical values together with constants directly determined by Lee et al. (1969) from their measurements of longitudinal and transverse velocities. Also shown are elastic constants obtained with equation 2.33 from published theoretical sound velocities. We estimate the accuracy of our constants to be $\pm 4\%$.

These constants can now be used to calculate the velocities of the transverse modes and the velocity of second sound from equation 2.33 and 2.39 (Table 6). The one measurement of the transverse velocity at $20.32 \text{ cm}^3/\text{mole}$ is 2.5% lower than the value of 327 m/sec calculated from the elastic constants, which we consider satisfactory agreement.

Interpolating second sound velocities reported by

FIGURE 28

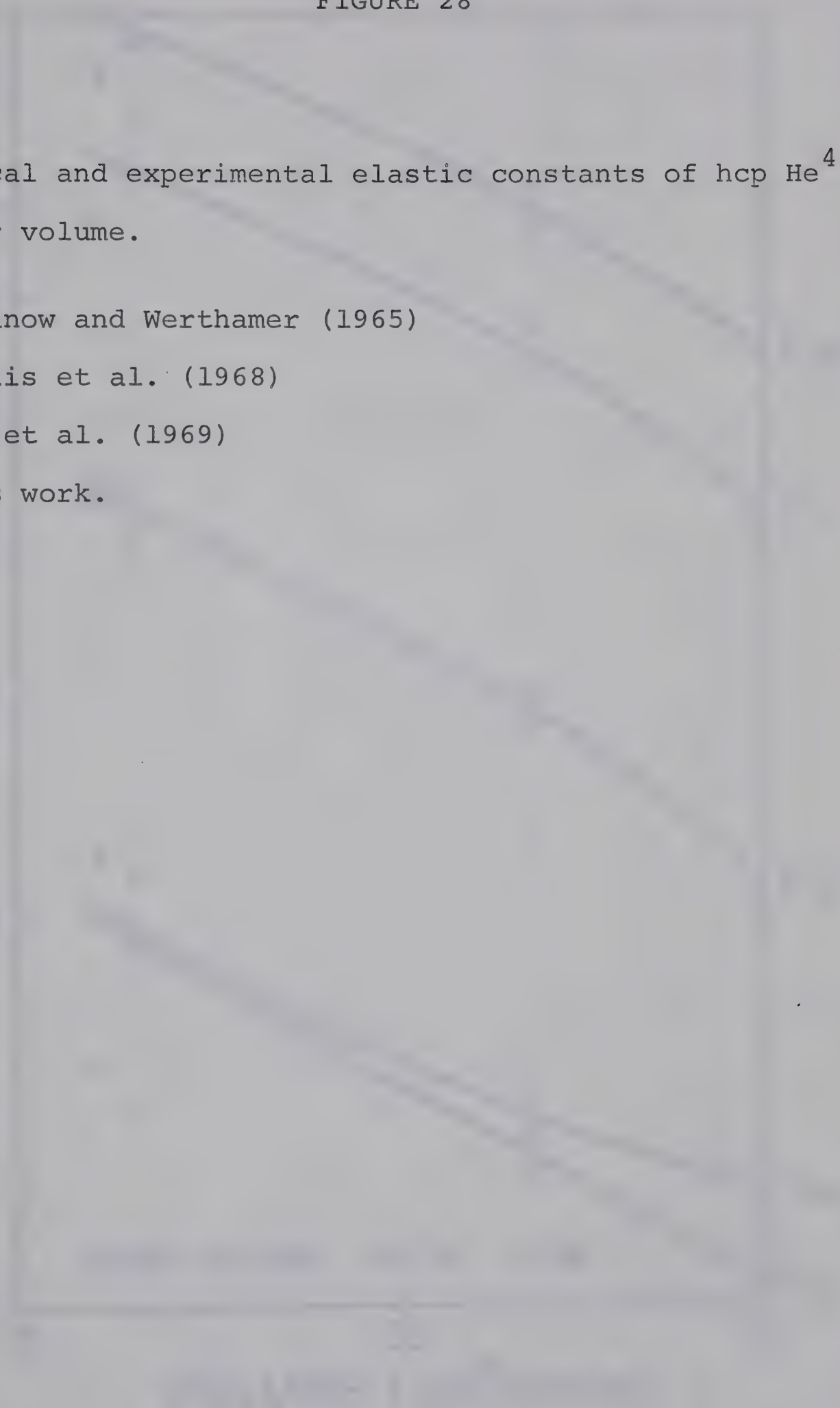
Theoretical and experimental elastic constants of hcp He^4
vs. molar volume.

NW Nosanow and Werthamer (1965)

GKW Gillis et al. (1968)

LCH Lee et al. (1969)

FW This work.



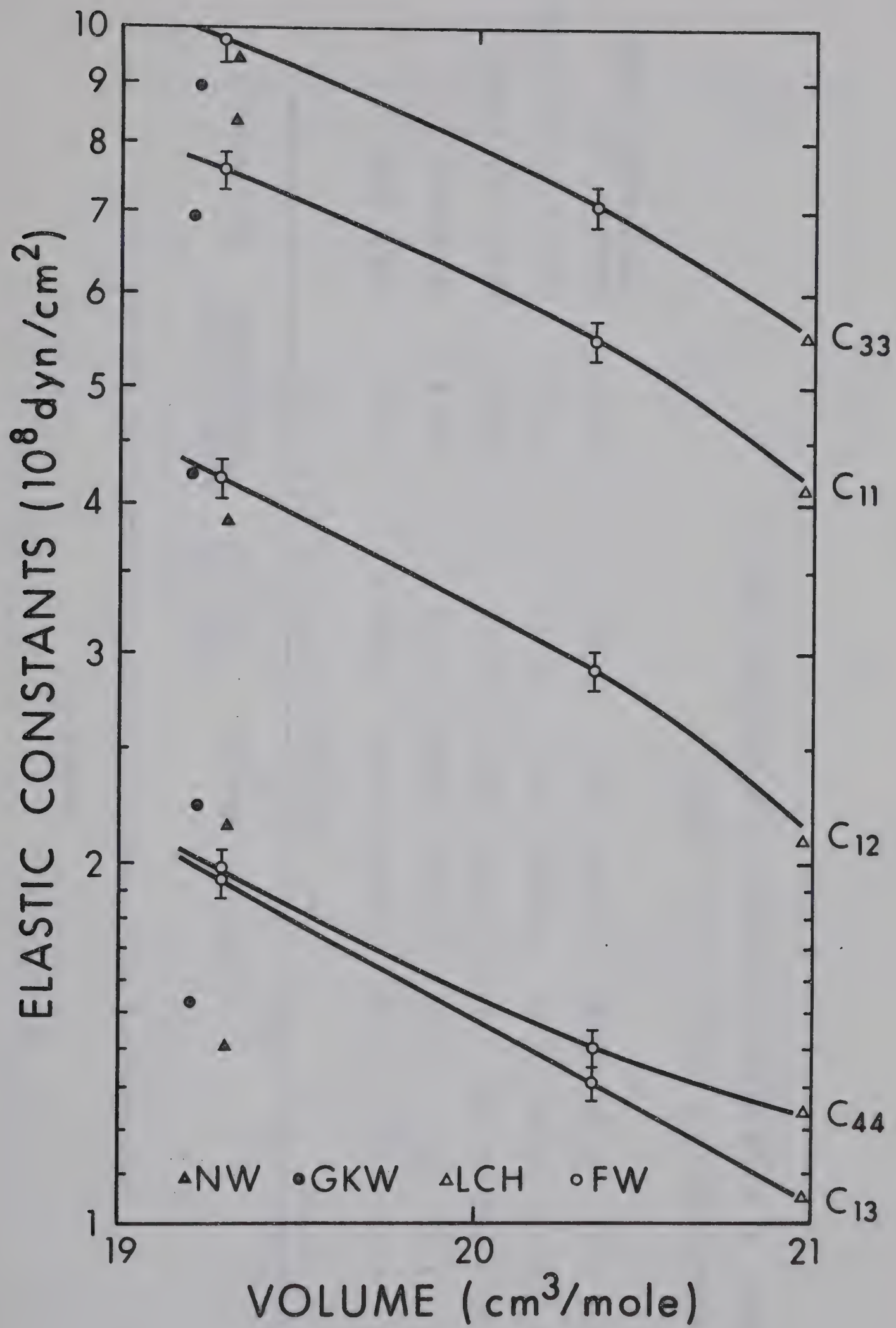


TABLE 5

Experimental and theoretical elastic constants of hcp He⁴

C ₁₁	C ₁₂	C ₁₃	C ₃₃	C ₄₄	Density		Volume V	Compress- ibility K ₀	Elastic Debye Temperature Θ ₀	Reference
					ρ	g/cm ³	cm ³ /mole	10 ⁻⁸ cm ² /dyn	K	
5.5	2.9	1.31	7.1	1.40	0.1970	20.32	0.308 *	28.8	This work	
7.6	4.2	1.98	9.8	1.96	0.2076	19.28	0.218 *	33.2	This work	
4.049	2.119	1.048	5.530	1.244	0.1909	20.97	0.408	25.8	Lee et al. (1969)	
6.94	4.23	2.23	8.94	1.52	0.2083	19.2	0.327	29.8	Gillis et al. (1968)	
8.36	3.84	2.14	9.44	1.40	0.2072	19.3	0.212	32.8	Nosanow and Werthamer (1965)	

* From measurements of Jarvis et al. (1969)

All other K₀ from elastic constants and equation 2.36.

TABLE 6

Longitudinal, transverse and second sound
velocity for different orientations γ

$$V = 20.32 \text{ cm}^3/\text{mole}$$

γ	v_l	v_{t1}	v_{t2}	v_{II}
0°	600 m/sec	267 m/sec	267 m/sec	157 m/sec
10	595	267	275	159
20	579	266	296	163
30	554	264	322	166
40	528	263	345	167
50	510	261	352	167
60	508	259	335	165
70	517	258	305	162
80	525	257	278	157
90	528	256	267	154

$$V = 19.28 \text{ cm}^3/\text{mole}$$

γ	v_l	v_{t1}	v_{t2}	v_{II}
0°	687 m/sec	307 m/sec	307 m/sec	180 m/sec
10	681	306	316	183
20	663	305	338	187
30	637	302	367	190
40	608	299	391	190
50	588	295	398	188
60	585	292	380	186
70	593	289	348	182
80	602	287	319	177
90	605	287	307	174

Ackerman and Guyer (1968), we find 130 m/sec at $20.32 \text{ cm}^3/\text{mole}$ and 170 m/sec at $19.28 \text{ cm}^3/\text{mole}$. It is not clear at present why the measured velocities are smaller than the values shown in table 6, but it should be remembered that equation 2.39 assumed elastic isotropy which is certainly not the case in solid helium. Qualitative agreement exists between the angular variation of the second sound velocity observed by Ackerman and Guyer (1968) and our data.

I have also calculated the Debye temperature at 0 K, θ_0 , by numerical integration of equation 2.35 and obtain $\theta_0 = 28.8 \pm 0.6 \text{ K}$ at $20.32 \text{ cm}^3/\text{mole}$ and $\theta_0 = 33.2 \pm 0.6 \text{ K}$ at $19.28 \text{ cm}^3/\text{mole}$ in good agreement with calorimetric values of 28.3 K and 32.5 K, respectively, reported by Edwards and Pandorf (1965).

It is remarkable that one of the Cauchy relations, $c_{44} = c_{13}$, (equation 2.40) is satisfied very well, especially at the higher densities. This is the relation that depends on the assumption of central forces. The other, $c_{11} = 3c_{12}$, which requires in addition that each atom is a center of inversion symmetry, does not hold however, as is expected in a hcp lattice.

4.4 Sound velocity as a function of temperature

Using the high resolution method for measuring small velocity changes described in section 3.31 we have measured the temperature dependence of the sound velocity at a volume of $20.42 \text{ cm}^3/\text{mole}$ ($p = 34.2 \text{ bar}$) between 0.7 K and the melting temperature of 1.9 K . We used a He^3 cryostat of conventional design and a high pressure cell similar to sample chamber 1 described in section 3.12, except that the quartz window was replaced by a polished bottom of high conductivity copper to improve crystal growth. Blocking of the high pressure line during crystal growth was prevented with a heater wire inside the line. The heater current was switched off during the velocity measurements, which therefore give values at constant volume. The data can be fitted to an equation

$$v_1(T) = 587 \times (1 - (1.23 \times 10^{-4}) \times T^{4.3}) \quad 4.16$$

(T in K, v_1 in m/sec)

The high absolute value of the velocity indicates that the propagation direction was close to the c-axis and the sample was probably a single crystal.

No theoretical estimates exist at present for the variation of the sound velocity with temperature and we there-

fore discuss the temperature dependence of the compressibility velocity $v_k(T)$ (equation 4.9) which should give an idea of the order of magnitude of the variation of the longitudinal velocity.

The temperature dependence of the isothermal compressibility $K_T(T)$ was found by Jarvis et al. (1968) who measured $(\partial p/\partial T)$ with a strain gage technique for different pressures and obtained K_T at the melting temperature from the work of Grilly and Mills (1962). $K_T(T)$ can then be obtained from numerical integration of the thermodynamic relations

$$\left(\frac{\partial K_T}{\partial T}\right)_p = -\left(\frac{\partial \alpha_p}{\partial p}\right)_T$$

where

4.17

$$\alpha_p = \frac{1}{V} \left(\frac{\partial V}{\partial T}\right)_p = K_T \left(\frac{\partial p}{\partial T}\right)_V$$

$K_T(T)$ has also been calculated from the specific heat by Edwards and Pandorf who assumed that solid helium obeys a reduced equation of state. With this assumption they get

$$K_T^{-1}(T) - K_T^{-1}(0) = \frac{\gamma_D}{V} ((\gamma_D + 1)(U - U_0) - \gamma_D T C_V) \quad 4.18$$

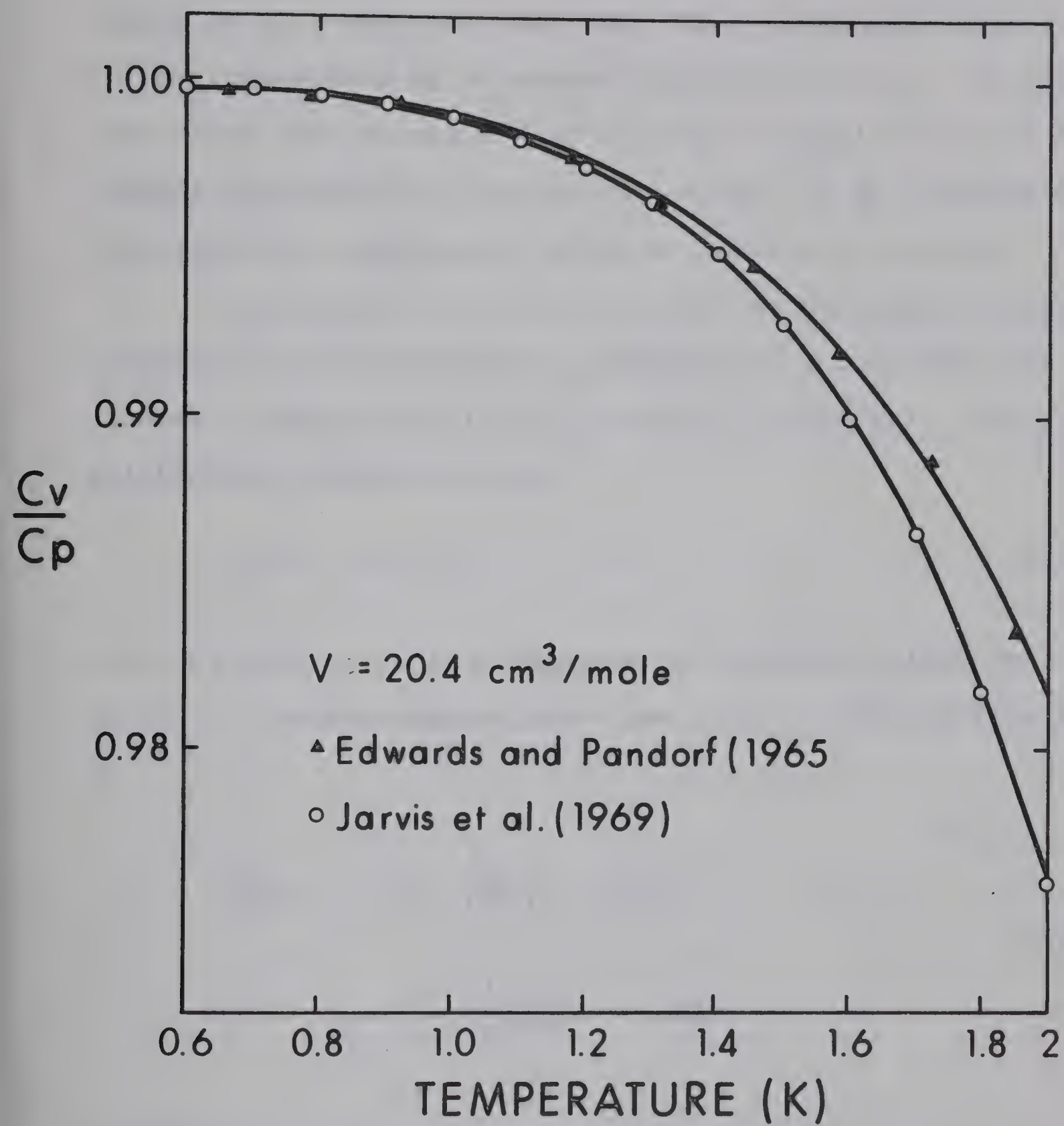
$U - U_0$ is the temperature dependent part of the internal energy and is obtained from the specific heat C_V . The

FIGURE 29

Ratio of specific heat at constant volume, C_V , to specific heat at constant pressure, C_p , vs. temperature.

$V = 20.4 \text{ cm}^3/\text{mole}$.





temperature variation of K_T calculated in this way is only about half as large as the more directly obtained value of Jarvis et al., who also show that their compressibilities can not be represented by a reduced equation of state. We therefore think that equation 4.18 is wrong if applied to hcp He⁴. Edwards compressibility would also result in an increase of velocity with temperature, while we observe a decrease.

At nonzero temperature we have to distinguish between isothermal compressibility K_T (temperature T constant) and adiabatic compressibility K_S (entropy S constant). The relationship between them is

$$K_S/K_T = C_V/C_P \quad 4.19$$

where C_V and C_P are heat capacity at constant volume resp. pressure. Thermodynamics gives the ratio of the specific heats as

$$\begin{aligned} \frac{C_P}{C_V} - 1 &= \frac{T}{C_V} \left(\frac{\partial p}{\partial T} \right)_V \cdot \left(\frac{\partial V}{\partial T} \right)_P \\ &= \frac{T}{C_V} \cdot \left(\frac{\partial p}{\partial T} \right)_V^2 \cdot V \cdot K_T \end{aligned} \quad 4.20$$

so that

$$K_S = K_T \left(1 - \frac{TVK_T}{C_V} \left(\frac{\partial p}{\partial T} \right)_V^2 \right) \quad 4.21$$

This equation now includes only quantities that are directly accessible to measurement. $(C_p/C_v)-1$ is given in Jarvis (1968) paper. For a reduced equation of state we would get

$$K_S = K_T (1 - \gamma_D^2 T C_v K_T/V) \quad 4.22$$

We see that $K_S - K_T$ is proportional to T^4 in this approximation (figure 29).

At a molar volume of 20.4 cm^3 , $K_T(T)$ increases by about 3% between $T = 0$ and the melting temperature of 1.9 K and $K_T(T)$ is larger by about 2.4% than $K_S(T)$ at this temperature.

Whether the sound velocities are given by the adiabatic or isothermal compressibility (or rather: elastic constants) depends on the frequency (Bhatia, (1967), p. 268). For low frequencies the wave length is sufficiently large that the compressed (or heated) and rarefied (or cooled) regions in a sound train are far enough apart that no heat conduction occurs between them. The compression is therefore adiabatic. If the frequency is higher than a characteristic frequency

$$\omega_c = C_v \cdot v_1^2/\kappa \quad 4.23$$

(κ is the heat conductivity; factors of the order unity are

ignored) this is no longer the case and the isothermal constants determine the longitudinal velocity. The transverse velocity is obtained in any case from the isothermal constants since no volume change is involved in their propagation.

In the intermediate region the velocity v_k is

$$v_k^2 = (\rho \cdot K_s)^{-1} \frac{\omega^2 + \omega_c^2}{(K_T/K_s) \cdot \omega^2 + \omega_c^2} \quad 4.24$$

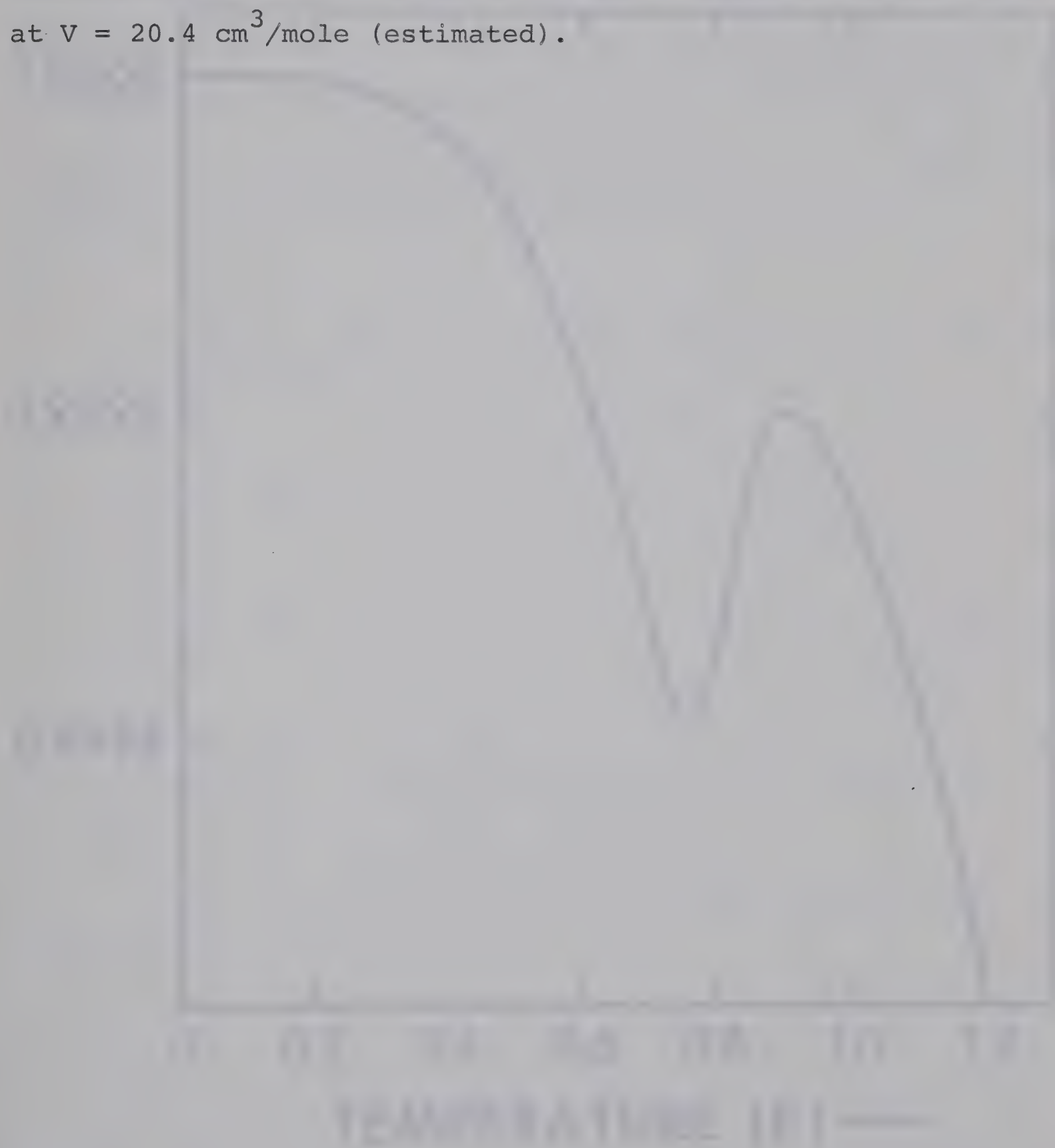
The expression for ω_c is equivalent to

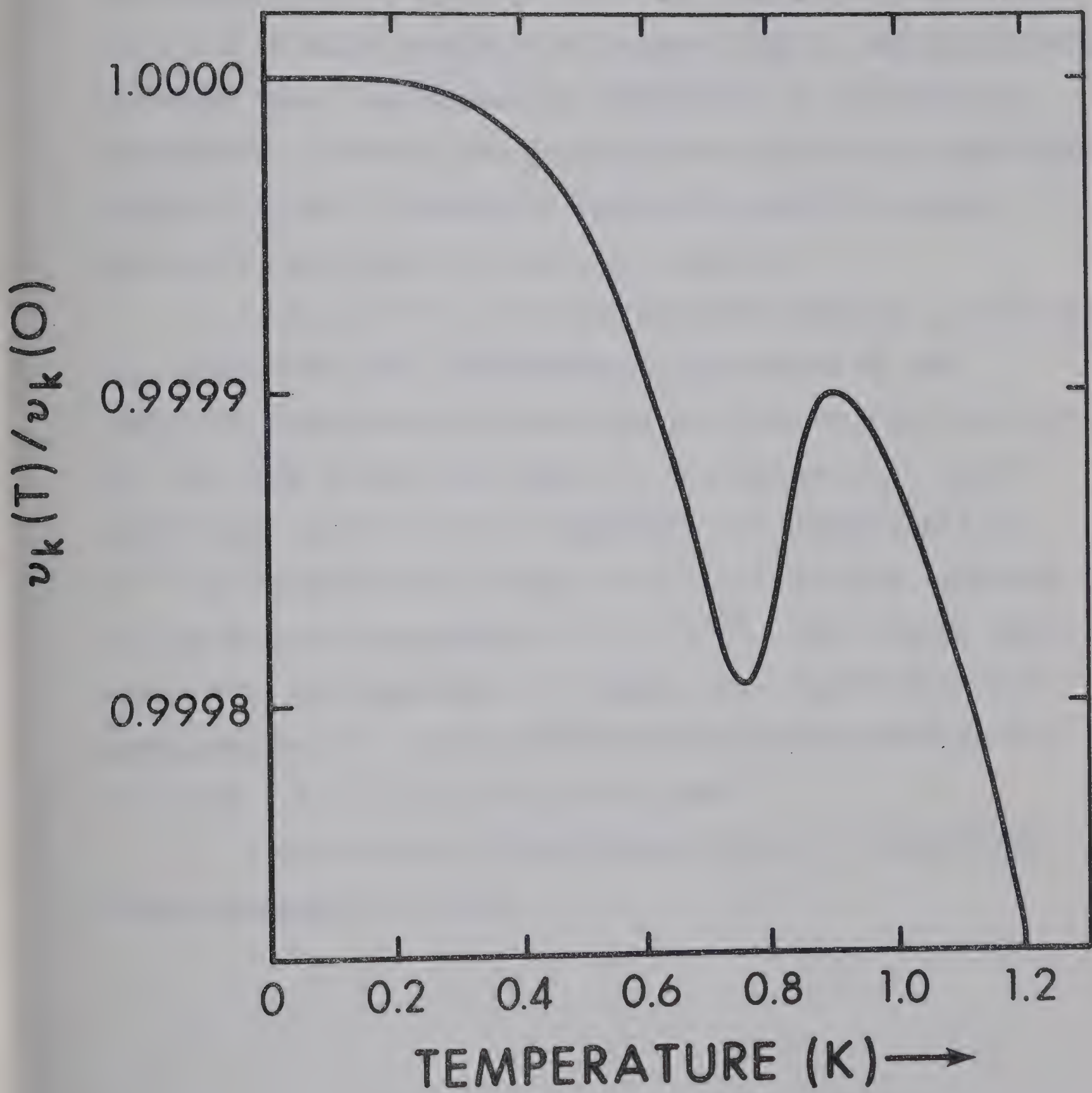
$$\omega_c = \tau_0^{-1} = v_l / \lambda \quad 4.25$$

where τ_0 and λ are the relaxation time and mean free path for umklapp processes. Values for λ have been calculated by Mezhev-Deglin (1965) from his thermal conductivity measurements, they depend on temperature as $T^{-1/2}$ in the temperature range that we have investigated. In our case the sound velocity was measured at a frequency of 5 MHz which is smaller than ω_c down to about 0.8 K. At this temperature we would therefore expect a velocity change of the order of $\frac{1}{2}(C_v(0.8K)/(C_p(0.8K) - 1)) \approx 10^{-4}$. Unfortunately this is just at the limit of resolution of our velocity measurement but should be easily observable with more sophisticated equipment (Abraham et al. (1969)). Associated with the velocity change is a peak in

FIGURE 30

Temperature dependence of the sound velocity in solid helium
at $V = 20.4 \text{ cm}^3/\text{mole}$ (estimated).





sound absorption (Guyer (1966)).

Due to the uncertainty of our knowledge of the relaxation time τ_0 and also because we have neglected factors of the order unity in equation 4.23, the transition temperature of 0.8 K is quite tentative at present, and in addition nothing is known about the temperature dependence of the transverse velocities. However, the general behaviour of the longitudinal velocity V_1 as a function of temperature should be quite similar to the one of V_k shown in figure 30.

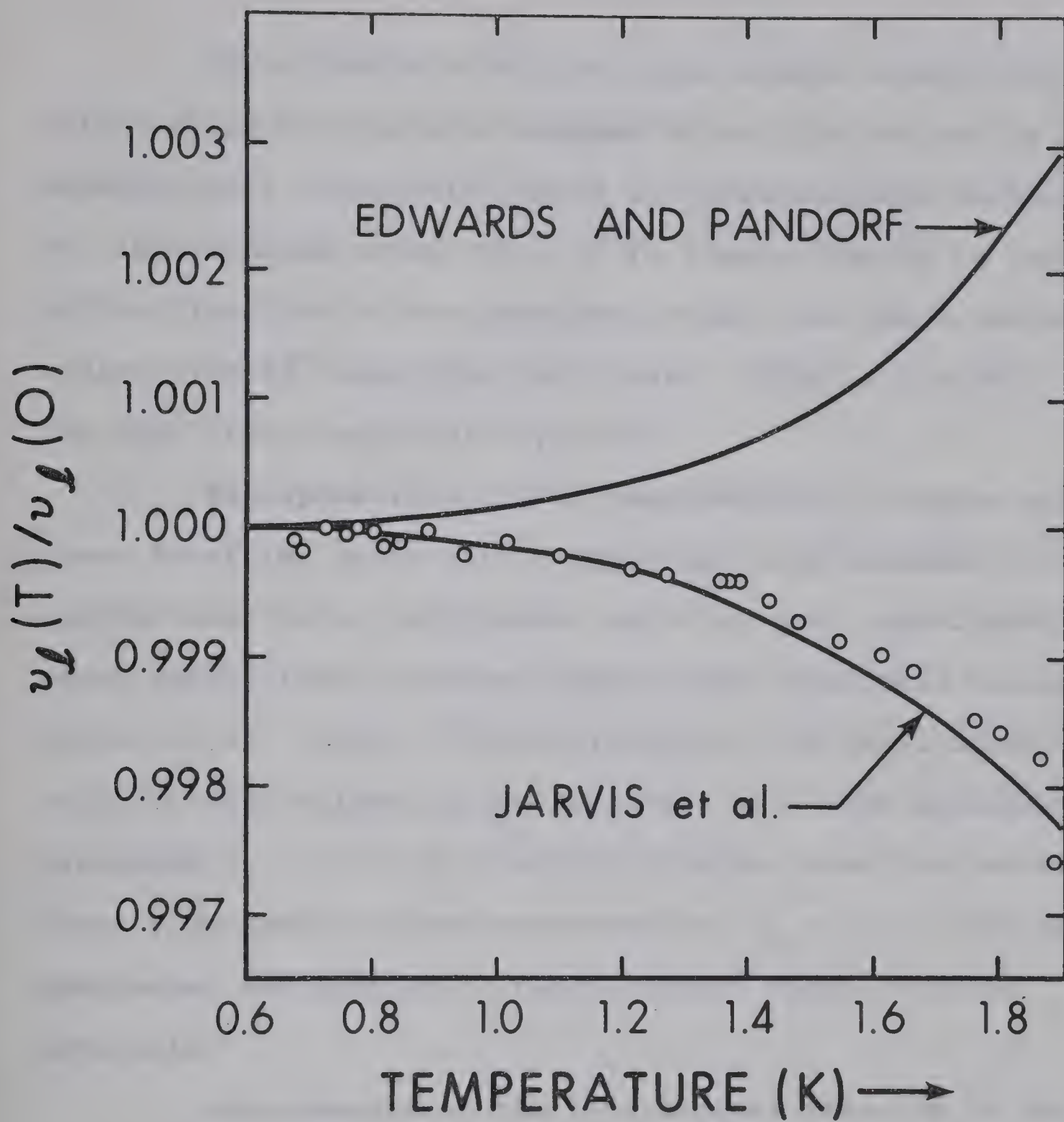
In figure 31 we show our measured velocity v_1 and also v_k , calculated from the temperature dependence of the adiabatic compressibility obtained from the data of Jarvis et al. and from Edwards and Pandorf. The change $\Delta v_k = v_k(T) - v_k(0)$ from Jarvis et al. is approximately proportional to $T^{4.4}$ in the temperature range $T = 1...2$ K, in good agreement of the observed dependence of $\Delta v_1 \sim T^{4.3}$. For a Debye solid, where $\Theta(T)$ is independant of temperature, Δv_k would be proportional to T^4 . In hcp He⁴ this approximation applies for $T \lesssim 0.02 \cdot \Theta_0$ or $T \lesssim 0.6$ K in our case.

I would like to thank Richard Hewko for performing the measurement of $v_1(T)$.

FIGURE 31

Longitudinal sound velocity in hcp He^4 vs. temperature.
 $V = 20.42 \text{ cm}^3/\text{mole}$. The solid lines represent the temperature dependence of the velocity calculated from the temperature dependence of the adiabatic compressibility based on measurements of Edwards and Pandorf (1965) and Jarvis et al. (1969).





5. CONCLUSIONS

It is possible to grow large single crystals of solid helium at pressures between 30 and 130 bar and to measure their orientation using the birefringence technique. The longitudinal sound velocity in these crystals is largest in the direction of the hexagonal c-axis and has a minimum in a direction 55° away from the c-axis. This is typical for many other hexagonal crystals.

Extrapolations of the measurements to higher and lower densities agree with sound velocities obtained from neutron scattering experiments and also with unpublished sound velocities in crystals grown from superfluid helium by Lee et al. (1968). The variation of the longitudinal velocity with volume can be expressed by a mode Grüneisen parameter $\gamma_1 = 3.0 \pm 0.1$, which is higher than the value found from specific heat measurements, $\gamma_D = 2.6$. This is not unexpected and similar to the situation found in other materials.

Measurements of the longitudinal velocity in the c-direction, in the basal plane and in an intermediate direction are sufficient in solid helium to determine all five elastic constants if the compressibility is known. The Debye temperatures calculated from these elastic constants were found to

agree with the calorimetric Debye temperatures within the combined errors of the two measurements.

For a molar volume $20.42 \text{ cm}^3/\text{mole}$ the longitudinal velocity decreases by 0.25% between $T = 0.6 \text{ K}$ and the melting temperature of 1.9 K , which is consistent with the increase of the compressibility with temperature, observed in strain gage experiments.

All these results lead to the conclusion that from an experimental point of view solid helium is not different from any other solid in its elastic behaviour.

The measurements allow for the first time a detailed comparison of the predictions of the theory of quantum crystals with experiment. At our densities, good agreement between the magnitude and the anisotropy of the longitudinal velocity is found, but present theory predicts a much weaker volume dependence than found experimentally.

BIBLIOGRAPHY

- Abel, W.R., Anderson, A.C., and Wheatly, J.C., (1961),
Phys. Rev. Letters 7, 299.
- Abraham, B.M., Eckstein, Y., and Ketterson, J.B., and
Vignos, J.H., (1969), Cryogenics 9, 274.
- Ackerman, C.C., Bertman, B., Fairbank, H.A., and Guyer R.A.
(1966), Phys. Rev. Letters 16, 789.
- Ackerman, C.C., (1967), Ph.D. thesis, Duke University, Durham,
North Carolina.
- Ackerman, C.C., and Guyer, R.A., (1968), Ann. Phys.
(N.Y.) 50, 128.
- Ahlers, G., (1966), Phys. Letters 22, 404.
- Ahlers, G., (1967), Phys. Letters 24A, 152.
- Alers, G.A., (1965), Physical Acoustics, W.P. Mason, edit.,
Vol. 111B, p.1. Academic Press, New York.
- Bertman, B., Fairbank, H.A., White, C.W., and Crooks, M.J.
(1966), Phys. Rev. 142, 74.
- Bhatia, A.B., (1967), Ultrasonic Absorption, Clarendon
Press, Oxford.
- Boccara, N., and Sarma, G., (1965), Physics 1, 219.
- Born, M., and Huang, K., (1962), Dynamical Theory of Crystal
Lattices, Clarendon Press, Oxford.

- Born, M., and Wolf, E., (1965), Optics, Pergamon Press, Oxford.
- Brickwedde, F.G., van Dijk, H., Durieux, M., Clement, J.R., and Logan, J.K., (1960), J. Res. NBS 64A, 1.
- Brueckner, K.A., and Froberg, J., (1965), Progr. Theoret. Phys. (Kyoto), Suppl.
- Brun, T.O., Sinha, S.K., Swenson, C.C., and Tilford, C.R., (1968) Proceedings of the I.A.E.A. Symposium on Inelastic Neutron Scattering, Copenhagen, p. 339.
- Choquard, P., The Anharmonic Crystal, (1967), Benjamin, New York.
- Crepeau, R., Heybey, O., and Lee, D.M., (1969) Bull. Am. Phys. Soc. 14, 95.
- Crystal Data, (1963), ACA Monograph 5, J.D.H., Donnay, edit., American Crystallographic Association.
- Dauphinee, T.M., and Moser, E., (1955), Rev. Sci. Inst. 26, 660.
- Dauphinee, T.M., and Woods, S.B., (1955), Rev. Sci. Inst. 26 693.
- Dauphinee, T.M., and Preston-Thomas, H., (1958), J.Sci. Inst. 35, 21.
- de Wette, R.W., Nosanow, L.H., and Werthamer, N.R., (1967) Phys. Rev. 162, 824.
- de Wette, F.W., and Nijboer, B.R.A., (1965), Phys. Letters 18, 19.
- Donohue, J., (1959), Phys. Rev. 114, 1009.
- Dugdale, J.S., and Franck, J.P., (1964) Phil. Trans. Roy. Soc. London A257, 1.

Edwards, D.O., and Pandorf, R.C., (1965), Phys. Rev. 140, A816.

Etters, R.D., (1968), Proc. Eleventh Int. Conf. Low Temp.

Phys. St. Andrews, Vol. 1, 440.

Falkoff, A.D., and Iverson, K.E., (1968), APL/360 Users Manual,
IBM Corporation.

Franck, J.P., (1964), Phys. Letters 11, 208.

Franck, J.P., (1968), Bull. Am. Phys. Soc. 13, 903.

Franck, J.P., and Wanner, R., (1969), Bull. Am. Phys. Soc.
14, 528.

Fredkin, D.R., and Werthamer, N.R., (1965), Phys. Rev.
138, A1527.

Gillis, N.S., and Werthamer, N.R., (1968), Phys. Rev.
167, 607.

Gillis, N.S., Koehler, T.R., and Werthamer, N.R., (1968),
Phys. Rev. 175, 1110.

Gold, L., (1950), Phys. Rev. 77, 390.

Green, R.E., and Henneke, E.G., (1967), J. Acoust. Soc.
Am. 41, 84.

Grilly, E.R., and Mills, R.L., (1959), Ann Phys. (N.Y.) 8, 1.

Grilly, E.R., and Mills, R.L., (1962), Ann. Phys. (N.Y.)
18, 250.

Guyer, R.A., (1966), Phys. Rev. 148, 789.

Hansen, J.P., and Levesque, D., (1968), Phys. Rev. 165, 293.

- Heltmes, E.C., and Swenson, C.A., (1962), Phys. Rev. 128, 1512.
- Henshaw, D.G., (1958), Phys. Rev. 109, 328.
- Hetherington, J.H., Mullin, W.J., and Nosanow, L.H., (1967),
Phys. Rev. 154, 175.
- Heybey, O.W., and Lee, D.M., (1967), Phys. Rev. Letters
19, 106.
- Heybey, O.W., and Lee, D.M., (1968), Bull. Am. Phys. Soc.
13, 112.
- Hooton, D. I., (1958), Phil. Mag. 3, 49.
- Horner, H., (1967), Z. Physik 205, 72.
- Huntington, H.B., (1958), Solid State Physics 7, 213.
- Iwamoto, F., and Namaizawa, H., (1966), Progr. Theoret. Phys.
(Kyoto) 37, 234.
- Jarvis, J.F., Ramm, D., and Meyer, H., (1968), Phys. Rev.
170, 320.
- Jastrow, R., (1955), Phys. Rev. 98, 1479.
- Jones R.C., (1941), J. Opt. Soc. Am. 31, 488, 493, 500.
- Keesom, W.H., and Taconis, K.W., (1938), Physica 5, 161.
- Keller, W., (1969), Helium-3 and Helium-4, Plenum Press, New York.
- Kittel, C., (1966), Introduction to Solid State Physics,
Wiley, New York.
- Koehler, T.R., (1967), Phys. Rev. Letters 18, 654.
- Koehler, T.R., (1968), Phys. Rev. 165, 942.

Kronig, R., and Sonnen, R.K.M., (1958), *Physica* 24, 432.

Landolt-Börnstein, New Series, (1966), Vol., III/1, Elastic, Piezoelectric and Related Constants of Crystals, R.F.S. Hearmon and K.H. Hellwege edit., Springer, Berlin.

Lee, D.M., Crepeau, R., and Heybey, O., (1969), Conference on Quantum Crystals, Aspen, Colorado, (unpublished).

Leibfried, G., (1955), Handbuch der Physik, S. Flugge edit., Vol. 7, pt. 1, p. 104., Springer, Berlin.

Leibfried, G., and Ludwig, W., (1961), *Solid State Physics* 12, 275.

Lipshultz, F.P., and Lee, D.M., (1965), *Phys. Rev. Letters* 14, 1017.

Lipshultz, F.P., Minkiewicz, V.J., Kitchens, T.A., Shirane, G., and Nathans, R., (1967), *Phys. Rev. Letters* 19, 1307.

London, F., (1954), Superfluids, Vol., 2, Wiley, New York.

Maradudin, A.A., Montroll, E.W., and Weiss, G.H., (1963), *Solid State Physics, Suppl.* 3, 1.

Mason, W.P., Edit., (1965), Physical Acoustics, Academic Press, New York.

Massey, W.E., and Woo, C.W., (1968), *Phys. Rev.* 169, 241.

McSkimin, H.J., (1955), *J. Appl. Phys.* 26, 406.

- Meissner, G., (1968), Phys. Rev. Letters 21, 435, Phys. Letters 27A, 261, Proc. Eleventh Int. Conf. Low Temp. Phys. St. Andrews, Vol. 1, 244.
- Mezhov-Deglin, L.P., (1965), Zh. Eksperim. i. Teor. Fiz. 49, 66, JETP 22, 47 (1966).
- Mills, R.L., and Schuch, A.F., (1961), Phys. Rev. Letters 6, 263.
- Mills, R.L., and Schuch, A.F., (1962), Proc. VIII Int. Conf. Low Temp. Phys., London, 423.
- Minkiewicz, V.J., Kitchens, T.A., Lipshultz, F.P., Nathans, R., and Shirane, G., (1968), Phys. Rev. 174, 267.
- Mullin, W.J., Nosanow, L.H., and Steinback, P.M., (1969), Phys. Rev. 188, 410.
- Munn, R.J., and Smith, F.J., (1965), J. Chem. Phys. 43, 998.
- Musgrave, M.J.P., (1954), Proc. Roy. Soc. A226, 339, 356.
- Nosanow, L.H., (1964), Phys. Rev. Letters 13, 270.
- Nosanow, L.H., and Werthamer, N.R., (1965), Phys. Rev. Letters 15, 618.
- Nosanow, L.H., (1966), Phys. Rev. 146, 120.
- Nye, J.F., (1964), Physical Properties of Crystals, Clarendon Press, Oxford.
- Pandorf, R.C., and Edwards, D.O., (1968), Phys. Rev. 169, 222.
- Ranninger, J., (1965), Phys. Rev. 140, A2031.

Schuch, A.F., and Mills, R.L., (1962), Phys. Rev. Letters
8, 469.

Schuch, A.F., and Mills, R.L., (1963), 6th Int. Congr. of the
Int. Union of Crystall., Rome, p. A21.

Skillig, H.H., (1951), Electric Transmission Lines, McGraw-Hill,
New York.

Smith, P.H., (1944), Electronics 17, No. 1, 130.

Stewart, J.W., (1963), Phys. Rev. 129, 1950.

Vignos, J.H., and Fairbank, H.A., (1961), Phys. Rev. Letters
6, 265.

Vignos, J.H., and Fairbank, H.A., (1966), Phys. Rev. 147, 185.

Vos, J.E., and Kingma, R., (1967a), Cryogenics 7, 50.

Vos, J.E., Blaisse, B.S., Boon, D.A.E., van Scherpenzeel, W.J.,
and Kingma, R., (1967b), Physica 37, 51.

Vos, J.E., Kingma, R., Van der Gaag, F.J., and Blaisse, B.S.,
(1967c), Phys. Letters 24A, 738.

Walker, E.J., (1959), Rev. Sci. Instr. 30, 834.

Wanner, R., and Franck, J.P., (1970), Phys. Rev. Letters
24, 365.

Wanner, R., (1970), to be published.

Werthamer, N.R., (1969), Am. J. Phys. 37, 763.

Wilks, J., (1967), The Properties of Liquid and Solid Helium,
Clarendon Press, Oxford.

Zener, C., (1936), Phys. Rev. 49, 122.

Ziman, J.M., (1965), Principles of the Theory of Solids,
University Press, Cambridge.

7. APPENDIX: COMPUTER PROGRAMS

All computations were done on a IBM/360 time sharing system using the language APL/360 (Falkoff and Iverson (1968)).

THE FUNCTIONS VL VT1 VT2 DELTAL DELTAT1 DELTAT2 DELL
CALCULATE QUANTITIES RELATED TO SOUND PROPAGATION IN
HEXAGONAL CRYSTALS FOR DIFFERENT PROPAGATION DIRECTIONS G.

G IS THE ANGLE IN DEGREE BETWEEN C-AXIS AND
WAVENORMAL.

C IS A VECTOR CONTAINING THE ELASTIC CONSTANTS IN
UNITS OF 10^8 DYN/CM², THE DENSITY IN UNITS OF G/CM³
AND THE ATOMIC WEIGHT.

C[1] ← C11

C[2] ← C12

C[3] ← C13

C[4] ← C33

C[5] ← C44

C[6] ← DENSITY

C[7] ← ATOMIC WEIGHT (REQUIRED FOR FUNCTION DEBH ONLY)

Z+G VL C LONGITUDINAL VELOCITY IN M/SEC

Z+G VT1 C 1. TRANSVERSE VELOCITY IN M/SEC

Z+G VT2 C 2. TRANSVERSE VELOCITY IN M/SEC

Z+G DELTAL C DEVIATION IN DEGREE OF LONGITUDINAL SOUND
BEAM FROM WAVENORMAL

Z+G DELTAT1 C DEVIATION OF TRANSVERSE SOUND BEAMS FROM
Z+G DELTAT2 C WAVENORMAL

Z+G DELL C DEVIATION IN DEGREES OF POLARIZATION VECTOR
FROM PURE POLARIZATION DIRECTION

G PH C IS AN AUXILLIARY FUNCTION USED IN VL VT1 VT2

Z+N HEXA C PRODUCES A TABLE OF THE ABOVE FUNCTIONS FOR
 $0 \leq G \leq 90$ WITH INCREMENTS OF N DEGREES FOR G

Z[;1] G

Z[;2] VL

Z[;3] VT1

Z[;4] VT2

Z[;5] DELTAL

Z[;6] DELTAT1

Z[;7] DELTAT2

Z[;8] DELL

Z+D DEBH C IS THE DEBYE TEMPERATURE AT ABSOLUTE ZERO.
D SPECIFIES THE NUMBER OF SECTIONS INTO WHICH
THE UNIT SPHERE IS DIVIDED FOR THE NUMERICAL
INTEGRATION. Z IS ACCURATE TO ABOUT 0.03
PERCENT FOR D+10.


```

      ∇VL[ ]∇
    ∇ Z←G VL C
[1]   G←OG÷180
[2]   Z←((C[1]+C[5])×(1OG)*2)+(C[4]+C[5])×(2OG)*2
[3]   Z←100×((Z+G PH C)÷2×C[6])*0.5
    ∇

      ∇VT1[ ]∇
    ∇ Z←G VT1 C
[1]   G←OG÷180
[2]   Z←100×(((0.5×(C[1]-C[2])×(1OG)*2)+C[5]×(2OG)*2)÷C[
      6])*0.5
    ∇

      ∇VT2[ ]∇
    ∇ Z←G VT2 C
[1]   G←OG÷180
[2]   Z←((C[1]+C[5])×(1OG)*2)+(C[4]+C[5])×(2OG)*2
[3]   Z←100×((Z-G PH C)÷2×C[6])*0.5
    ∇

      ∇PH[ ]∇
    ∇ Z←G PH C
[1]   Z←(((C[1]-C[5])*2)×(1OG)*4)+((C[4]-C[5])*2)×(2OG)*
      4
[2]   Z←(Z+2×((1OG)*2)×((2OG)*2)×((C[1]-C[5])×(C[5]-C[4]))+
      2×((C[3]+C[5])*2))*0.5
    ∇

      ∇DELTAL[ ]∇
    ∇ Z←G DELTAL C;H;M;N;A;E
[1]   H←(C[6]×((G VL C)÷100)*2)-C[5]
[2]   M←10OG÷180
[3]   N←20OG÷180
[4]   A←(H-(C[4]-C[5])×N*2)÷N×M×C[3]+C[5]
[5]   E←20÷(((10-3OA)*4)÷M*2)+(((20-3OA)*4)÷N*2))*
      0.5
[6]   Z←(H×30E)÷(C[6]×((G VL C)÷100)*2)
[7]   Z←(20-3OZ)×180÷01
    ∇

      ∇DELTAT1[ ]∇
    ∇ Z←G DELTAT1 C;E;H
[1]   E←2010OG÷180
[2]   H←(C[6]×((G VT1 C)÷100)*2)-C[5]
[3]   Z←(20-3O(H×30E)÷(C[6]×((G VT1 C)÷100)*2))×180÷01
    ∇

```


▽DELTA2[]▽

▽ Z←G DELTAT2 C;H;M;N;A;E

[1] H←(C[6]×((G VT2 C)÷100)*2)-C[5]

[2] M←100G÷180

[3] N←200G÷180

[4] A←(H-(C[4]-C[5])×N*2)÷N×M×C[3]+C[5]

[5] E← $\overline{20} \div (((10 \overline{30} A) * 4) \div M * 2) + (((20 \overline{30} A) * 4) \div N * 2)) * 0.5$

[6] Z←(H×30E)÷(C[6]×((G VT2 C)÷100)*2)

[7] Z←($\overline{30} Z$)×180÷01

▽

▽DELL[]▽

▽ Z←G DELL C;H;A;M;N

[1] H←(C[6]×((G VL C)÷100)*2)-C[5]

[2] M←100G÷180

[3] N←200G÷180

[4] A← $\overline{30} (H - (C[4] - C[5]) \times N * 2) \div M \times N \times C[3] + C[5]$

[5] Z←($\overline{20} ((10A) \times M) + (20A) \times N$)×180÷01

▽

▽HEXA[]▽

▽ Z←N HEXA C

[1] Z←((90÷N)+1),8)ρ0

[2] Z[;1]←0,(1(90÷N))×N

[3] Z[;2]←Z[;1] VL C

[4] Z[;3]←Z[;1] VT1 C

[5] Z[;4]←Z[;1] VT2 C

[6] Z[1;1]←1

[7] Z[;5]←Z[;1] DELTAL C

[8] Z[;6]←Z[;1] DELTAT1 C

[9] Z[;7]←Z[;1] DELTAT2 C

[10] Z[;8]←Z[;1] DELL C

[11] Z[1,((90÷N)+1); 5 6 7 8]←0

[12] Z[1;1]←0

▽

▽DEBH[]▽

▽ Z←D DEBH C;G;M

[1] Z←0

[2] M←1

[3] G←($\overline{45} \div D$)+M×90÷D

[4] Z←Z+(+/(G VL C),(G VT1 C),(G VT2 C))*-3)×100G÷180

[5] →((M←M+1)≤D)/3

[6] Z←0.36273433×(2×D×C[6]÷0Z×C[7])*÷3

▽

EXAMPLE

C←5.5 2.91 1.31 7.1 1.403 0.1970 4.003

10 VL C

594.7

10 VT1 C

266.6

10 VT2 C

274.7

10 DELTAL C

6.114

10 DELTAT1 C

-0.756

10 DELTAT2 C

17.64

10 DEEL C

5.126

20 DEBH C

28.77

5 HEXA C

0	600.3	266.9	266.9	0.0	0.0	0.0	0.0
5	598.9	266.8	268.9	3.1	-0.4	9.7	2.6
10	594.7	266.6	274.7	6.1	-0.8	17.6	5.1
15	587.9	266.2	283.9	9.0	-1.1	23.1	7.5
20	578.6	265.7	295.6	11.6	-1.4	26.0	9.5
25	567.3	265.0	308.7	13.8	-1.7	26.8	11.1
30	554.4	264.3	322.3	15.4	-1.9	25.5	12.1
35	541.0	263.5	335.1	15.9	-2.1	22.0	12.1
40	528.0	262.6	345.4	14.9	-2.2	16.0	10.9
45	517.0	261.7	351.7	11.7	-2.3	6.8	8.2
50	509.7	260.8	352.4	6.5	-2.3	4.8	4.5
55	506.9	259.9	346.6	0.8	-2.2	16.1	0.5
60	508.1	259.0	335.4	3.6	-2.0	24.5	2.5
65	511.9	258.3	320.7	5.8	-1.8	29.2	4.2
70	516.7	257.6	304.9	6.2	-1.5	30.6	4.7
75	521.3	257.1	289.9	5.4	-1.2	28.7	4.2
80	525.1	256.7	277.7	3.9	-0.8	23.1	3.1
85	527.5	256.5	269.7	2.1	-0.4	13.2	1.7
90	528.4	256.4	266.9	0.0	0.0	0.0	0.0

B29970